

DISSERTATION

CHARACTERIZATION OF THE FLOW CYTOMETRY MUTATION ASSAY AND
ITS USE IN NOVEL GENOTOXICITY STUDIES

Submitted by

Stephen Berkeley Keysar

Graduate Degree Program in Cell & Molecular Biology

In partial fulfillment of the requirements

For the Degree of Doctor of Philosophy

Colorado State University

Fort Collins, Colorado

Summer 2009

UMI Number: 3385170

All rights reserved

INFORMATION TO ALL USERS

The quality of this reproduction is dependent upon the quality of the copy submitted.

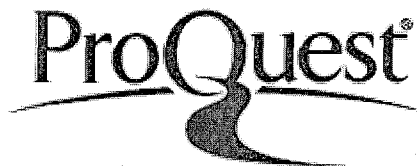
In the unlikely event that the author did not send a complete manuscript and there are missing pages, these will be noted. Also, if material had to be removed, a note will indicate the deletion.



UMI 3385170

Copyright 2009 by ProQuest LLC.

All rights reserved. This edition of the work is protected against unauthorized copying under Title 17, United States Code.



ProQuest LLC
789 East Eisenhower Parkway
P.O. Box 1346
Ann Arbor, MI 48106-1346

COLORADO STATE UNIVERSITY

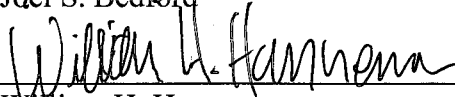
April 15, 2009

WE HEREBY RECOMMEND THAT THE DISSERTATION PREPARED UNDER OUR SUPERVISION BY STEPHEN B. KEYSAR ENTITLED *CHARACTERIZATION OF THE FLOW CYTOMETRY MUTATION ASSAY AND ITS USE IN NOVEL GENOTOXICITY STUDIES* BE ACCEPTED AS FULFILLING IN PART REQUIREMENTS FOR THE DEGREE OF DOCTOR OF PHILOSOPHY.

Committee on Graduate work



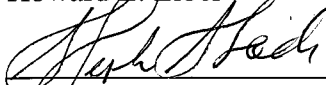
Joel S. Bedford



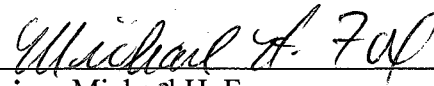
William H. Hanneman



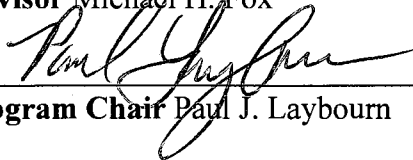
Howard B. Liber



Stephen Stack



Advisor Michael H. Fox



Program Chair Paul J. Laybourn

ABSTRACT OF DISSERTATION

CHARACTERIZATION OF THE FLOW CYTOMETRY MUTATION ASSAY AND ITS USE IN NOVEL GENOTOXICITY STUDIES

The flow cytometry mutation assay (FCMA) has been previously demonstrated to be a rapid and sensitive assay for measuring mutations induced by a wide variety of genotoxic agents. However, details of the assay have not been fully evaluated. The purpose of this research was to first investigate in depth the kinetics of expression of *CD59* mutants in the flow cytometry mutation assay. After characterization I have used the assay to measure mutagenesis induced by a hypoxic environment and examined the effects of DNA repair proteins on survival, cell cycle and mutagenesis.

After treatment with a mutagen, the mutant fraction measured by the FCMA increased to a peak over time and subsequently decreased to a stable plateau. Using ethyl methanesulfonate (EMS), ionizing radiation (IR) and asbestos, I determined that the return to normal cell proliferation and, more importantly, cell survival are indicators of peak mutant expression. Decreased survival and slowed growth of *CD59*⁻ cells contribute to the decline in the mutant fraction and confirms that mutations that are not clonogenically viable are measured by the FCMA on the peak day of expression.

To complement previously published results using ionizing radiation, I analyzed clones isolated from several *CD59*⁻ regions and generated mutant spectra for the point mutagen EMS using flow cytometry. Cells sorted from intermediate regions of *CD59*

expression remained stable over time. Also, mutations induced by EMS were predominantly small intragenic mutations, unlike radiation that produced mainly large deletions.

I then determined that a severely hypoxic environment induced a significant mutant yield. It has been previously shown that hypoxic stress can generate DNA damage and mutations which are likely caused by reactive oxygen species (ROS) released from mitochondria during hypoxia or generated upon reoxygenation. Here I demonstrate that the oxygen radical scavenger dimethyl sulfoxide (DMSO) significantly decreased cell killing and mutagenesis after hypoxia treatment, supporting the concept that ROS are responsible for hypoxia induced mutations.

I also investigated the effects of silencing of DNA repair proteins on cell survival, cell cycle and mutagenesis. The knockdown of homologous recombination repair protein Rad51C slightly increased sensitivity to IR and drastically increased killing by EMS treatment. Rad51C knockdown also caused a significant G2 phase buildup of cells by 18 hours after EMS treatment, but it had no effect on mutagenesis. Silencing of the non-homologous end joining (NHEJ) protein Ku80 slightly increased cell killing by IR and slowed the uptake of BrdU in S phase. Finally, Ku80 knockdown decreased the mutant yield after EMS treatment, implying that this point mutagen generates significant double strand breaks (DSBs) during S phase that are often repaired by NHEJ.

In summary, I have demonstrated that the FCMA is a fast and reliable method to measure mutagenesis induced by an agent and to quantify the degree of damage by obtaining a mutant spectrum. I have used this assay to investigate mechanisms of

mutagenesis by EMS, IR, asbestos and hypoxia and evaluated the effects of DNA repair pathways on cell cycle, cell killing and mutant induction.

Stephen Berkeley Keysar
Graduate Degree Program in Cell & Molecular Biology
Colorado State University
Fort Collins, CO 80523
Summer 2009

Acknowledgements

For the countless hours he has spent discussing and reviewing my research I would like to thank my advisor Dr. Michael Fox. And for the lessons he has taught outside the field of biology have truly made this a great experience. I would also like to thank my committee members Dr. Joel Bedford, Dr. Howard Liber, Dr. William Hanneman and Dr. Steve Stack for their help during my time at Colorado State University.

I would also like to acknowledge all of the support I have received from Phuong Le while working this dissertation and in the lab from Dr. Carley Ross, Tenley French, Leslie Armstrong-Lea and Francois Dengah.

Finally, to my parents and brother who have been essential to my education, thank you.

TABLE OF CONTENTS

CHAPTER 1: Introduction.....	1
Mutagenesis	2
Mutation Assays.....	3
Mouse lymphoma assay	3
TK6 mutation assay	4
CHO A _L complement mediated cytotoxicity assay	5
Flow cytometry mutation assay (FCMA)	8
Flow cytometry generated mutant spectra	13
Glycosyl Phosphatidylinositol (GPI) Anchors.....	15
Genotoxic Agents.....	21
Ethyl methanesulfonate (EMS).....	21
Ionizing radiation (IR)	22
Asbestos	24
Hypoxia.....	25
DNA Damage Response	26
DNA Double-Strand Break (DSB) Repair.....	29
Non-homologous end joining repair (NHEJ).....	29
Homologous recombination repair (HRR).....	30
Repair of Damaged and Mismatched DNA Bases.....	33
Base excision repair (BER).....	34
Nucleotide excision repair (NER).....	34
Mismatch repair (MMR).....	36
Conclusion	36
Reference List.....	37
CHAPTER 2: Kinetics of CHO A_L mutant expression after treatment with γ radiation, EMS and asbestos.....	51
Abstract.....	51
Introduction.....	52
Materials and Methods.....	54
Cell culture.....	54
Cell treatment.....	54
Antibody labeling.....	55
Analysis of T_{pot} and G2 phase.....	55
Daily clonogenic survival	57
Cell sorting.....	57
Mixing experiments	58
Multicolor analysis.....	59
Results.....	59
Temporal variation in mutant expression, T_{pot} and G2 delay	59
Clonogenic survival	60
Mutant region survival	61
Mixing experiments and clonal growth	61
Multicolor analysis.....	62

Discussion.....	71
Reference List.....	76
CHAPTER 3: EMS mutant spectra generated by multi-parameter flow cytometry	79
.....	79
Abstract.....	79
Introduction.....	80
Materials and Methods.....	82
Cell culture.....	82
Treatment with EMS.....	82
Antibody labeling.....	83
Flow cytometry.....	84
Cell sorting.....	84
Results.....	85
Mutant populations.....	85
Mutant region sorting.....	86
EMS mutant spectrum.....	86
Discussion.....	95
Reference List.....	100
CHAPTER 4: Hypoxia induced mutations in mammalian cells detected by the flow cytometry mutation assay and characterized by mutant spectra.....	103
Abstract.....	103
Introduction.....	104
Methods.....	105
Cell culture.....	105
Hypoxia treatment.....	106
CHO A _L complement mediated cytotoxicity assay.....	107
Antibody staining for FCMA.....	107
Multicolor staining for mutant spectrum.....	107
Flow cytometry.....	108
Mutant region sorting.....	108
Clonogenic survival.....	108
Results.....	109
Hypoxia mutant yield in the complement cytotoxicity CHO A _L assay.....	109
FCMA hypoxia mutant yield.....	109
Effects of DMSO on survival and mutagenesis.....	110
Mutant region survival.....	110
Daily clonogenic survival.....	110
Mutant spectra.....	110
Discussion.....	111
Reference List.....	123
CHAPTER 5: Variations in cell cycle and mutant induction in CHO A_L cells after suppression of DNA repair proteins.....	126
Abstract.....	126
Introduction.....	127
Methods.....	129
Cell culture.....	129

siRNA transfection.....	129
Irradiation and EMS treatment.....	130
Antibody staining.....	130
Cell survival.....	131
Cell cycle analysis.....	131
Flow cytometry.....	132
Results.....	133
siRNA transfection and gene silencing.....	133
Cell proliferation and survival.....	133
DNA repair and cell cycle.....	134
DNA repair and mutagenesis.....	143
Discussion.....	143
Reference List.....	148
CHAPTER 6: Conclusions.....	152
Research Overview.....	152
Strengths and Limitations of the FCMA.....	158
Future Directions.....	161
Reference List.....	162

CHAPTER 1

INTRODUCTION

Cancer arises from the accumulation of mutations of cellular genes that regulate proliferation, DNA repair and apoptosis. Mutations are generated when DNA is damaged during exposure to endogenous and exogenous sources and errors during DNA replication. The general public is regularly exposed to carcinogens. The known genotoxicity of many carcinogens places great importance on the ability to accurately assess the mutagenic potential of these compounds. Mutation assays were developed decades ago to determine the mutagenic potential of compounds. The speed and sensitivity to accurately detect mutations generated by a wide range of mutagens have increased over time.

The research described in this dissertation was completed to characterize the kinetics of mutants in the flow cytometry mutation assay (FCMA) and to conduct novel studies using mutagenesis as an endpoint. A variety of techniques were used to measure the survival and proliferation of mammalian cells following treatment with genotoxic agents. These techniques often used flow cytometry as a rapid method to analyze millions of cells in a relatively short amount of time. The types of mutations generated

by known and novel mutagens were investigated and compared in an attempt to determine the mechanism by which they induce DNA damage.

Mutagenesis

Many physical and chemical agents interact with DNA and frequently cause alterations in the chemical and structural properties of the molecule. Agents that cause DNA damage have a wide range of mechanisms from simple DNA base adducts caused by alkylating agents to double-strand breaks generated by ionizing radiation. The manner in which certain agents such as ionizing radiation (1), N-methyl-N'-nitro-N-nitrosoguanidine (MNNG) (2) and ethyl methanesulfonate (EMS) (3) modify DNA have long been characterized and are often used as genotoxic references when developing assays (4,5). The mechanisms behind DNA damage generated by other agents such as asbestos (6), hypoxia (7) and other novel compounds are only now being examined.

Depending on the severity, damage produces several different outcomes both *in vitro* and *in vivo*. If the immediate damage is severe, the affected cell may not recover. This will result in cell death, including necrosis and apoptosis (8,9). However, if the damage is not immediately lethal, cells may attempt to repair the DNA with a mechanism specific for the type of lesion (10,11); this will be discussed in more detail shortly. Finally, damage that is overlooked by the cell or that is not completely repaired may be replicated and become a permanent mutation in the genetic code (12). The array of mutations that can be generated in cells is vast and ranges from simple point mutations and deletions to chromosomal rearrangements, including translocations (13,14).

Depending on zygosity, mutations in genes that are essential to cell survival are often lethal, while most mutations are non-lethal and can be passed on by replication to

future generations of cells. Multiple mutations in genes whose products regulate cellular processes such as proliferation, DNA repair and apoptosis may result in genomic instability and cellular transformation (15). The uncontrolled growth of cells containing mutations in genes that regulate DNA repair and cell death would likely lead to more mutations and possibly malignant cancer (16).

Mutation Assays

Since it was determined that many mutagens are also carcinogens, there has been a need to develop assays that will rapidly and sensitively measure DNA damage and the mutagenic potential of known and unknown agents. There have been many assays developed over the past four decades that measure DNA damage and mutations in a wide range of systems. One of the earliest is the Ames assay, a bacterial reverse mutation assay measuring an agent's ability to generate gain of function mutations in specific biosynthetic genes (17,18). This assay is still used today, stressing its importance. However, genotoxicity in mammalian systems was an up and coming area of research.

Early studies in mammalian systems used the mutations in genes of RNA degradation purine salvage pathways to study mutation induction. Chinese hamster ovary (CHO) cells with single mutations in the X-linked hypoxanthine phosphoribosyltransferase (*hprt*) gene (19) and the heterozygous adenine phosphoribosyltransferase (*aprt*) (20) gene were selected for using the toxic purine analogs 6-thioguanine and 8-azaadenine respectively. Many physical and chemical agents were tested with these systems resulting in modest mutant yields (21,22); these were later enhanced with more modern assays.

L5178Y/Tk⁺ mouse lymphoma assay

The mouse lymphoma mutation assay (MLA), using the L5178Y $tk^{+/-}$ cell line, has been in use for over 30 years to test the genotoxicity of a large variety of agents. This assay is capable of detecting mutations at both the heterozygous thymidine kinase (tk) and the hemizygous $hprt$ genes (23,24). In comparison to the $hprt$ locus, the tk locus is capable of measuring a broader spectrum of mutations from point mutations and intragenic deletions to chromosomal mutations. This is because mutations that encompass adjacent genes could be compensated for by the homologous chromosome (25,26). Tk mutants are selected with the toxic thymidine analog trifluorothymidine (TFT^R).

By measuring colony size at a set time after selection, mutants can be classified as either fast or slow growing. However, there is little concrete evidence demonstrating that colony size is directly related to the type or size of the mutation (25). Although a wide range of mutagens have been evaluated with the MLA (24), the months needed for the selection, colony formation and counting of mutants limit this assay. This is an area where mutation assays in the future can make improvements.

TK6 mutation assay

Like the MLA, the TK6 mutation assay was developed to detect mutations in the tk gene. The $tk^{+/-}$ TK6 cells were developed from the WI-L2 human lymphoblast cell line (4). Similar to the MLA, TFT^R is used to select for $tk^{-/-}$ mutants after treatment with a mutagen. This can be completed within 3 days, and subsequent colony formation of mutants is completed within a few weeks. A broad range of chemical and physical agents have also been tested with the TK6 assay (4,27-29).

Interestingly, it is possible to observe and compare the difference in mutations generated by the same mutagen in the heterozygous *tk* gene as well as the X-linked *hprt* locus. This has been completed by generating mutant spectra for both loci with the same agent (30,31). More recent studies have been conducted using the p53 mutated WTK1 and the p53 null NH32 cell lines, both of which are nearly identical to the TK6 cell line. This allows for the comparison of mutation rates and mutant spectra generated in the p53^{-/-} cell lines and p53^{+/+} TK6 cell lines (32,33).

The TK6 mutation assay has also been used for novel studies attempting to elucidate and characterize the roles of DNA repair proteins in mutagenesis (34-36). The bystander response has also been examined using mutagenesis in TK6 cells as an endpoint (33). The TK6 remains a versatile human cell line mutation assay but is also limited by the necessity of clonogenic survival in order to quantify mutants.

CHO A_L complement mediated mutation assay

Early studies into genetic linkage were completed by fusing Chinese hamster ovary (CHO) cell lines auxotrophic for specific nutrients and with cells. The resulting hybrids contained human chromosomes with genes complementing the CHO auxotrophies and were able to grow in minimal media. Human CD surface antigens were also expressed by genes located on the incorporated human chromosomes (37). Human chromosomes were rapidly lost from the fused cells, and as corresponding CD antigens were lost from the cell surface, investigators were able to determine the auxotrophies that returned; this in turn demonstrated genetic linkage. The CHO A_L cell line was the result of one of these experiments and was later used by Waldren *et al.* to develop a novel mutation assay (5).

The antigen lethal (A_L) cell line is a stable human-hamster hybrid generated by the fusion of a CHO-K1 cell and a human amniotic fluid fibroblast. The cells contain a complete set of hamster chromosomes and one copy of human chromosome 11. Genes along chromosome 11 express several human cell surface antigens. The original linkage studies determined CHO A_L cells are sensitive to killing in the presence of specific monoclonal antibodies and antisera (37). This assay selects for mutants of the *S1/cd59* locus found at 11p13.5 on human chromosome 11, which expresses the cell surface antigen $a_1/CD59$ (38). CD59 mutants are selected by using CD59 specific antibodies and antisera (Fig. 1). The surviving CD59⁻ cells form colonies and the mutant fraction (MF) was calculated by $MF = \# \text{ colonies} / (\# \text{ cells plated} \times \text{plating efficiency})$ (5,39). Later, the A_LN cell line was developed by incorporating a neomycin resistance gene adjacent to *cd59* on chromosome 11, and by treating cells with neomycin, background mutants were reduced (40).

Unlike many traditional assays, the CHO A_L assay has the ability to detect point mutations, intragenic deletions and large deletions (>150 Mb) of nearly the entire length of chromosome 11 (41,42). Loss of the entire chromosome results in death due to essential gene(s) found at 11p15.5 (38). Recently, the cell line A_LC was developed containing two copies of chromosome 11 heterozygous for CD59. This allows for deletions of the entire chromosome to be measured (43,44).

The CHO A_L system has been used to measure mutants generated by a broad spectrum of chemical and physical agents including gamma (γ)-radiation, alpha (α)-particles, asbestos, ultra violet (UV) light, EMS, MNNG, and benzo[a]pyrene (5,6,45,46). The CHO A_L assay has also been used as an endpoint in bystander studies (47-49). This

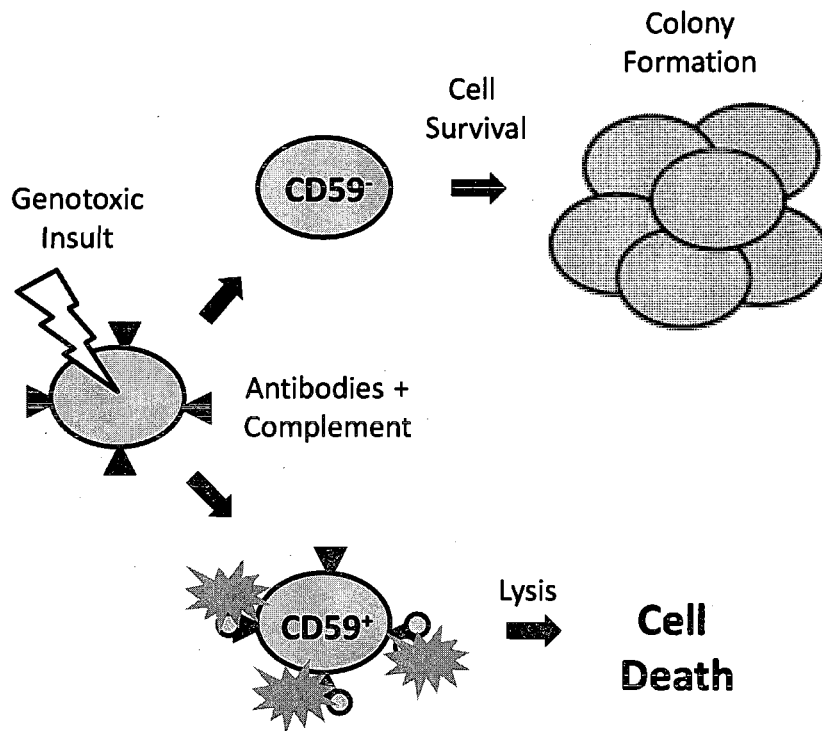


Figure 1. Basic steps involved in the CHO A_L mutation assay. Cells are first treated with a mutagen, cultured for roughly 1 week to allow for mutant expression and finally treated with CD59 specific antibodies and complement. Surviving colonies are used to calculate the mutant fraction.

assay has demonstrated the ability to detect mutations caused by agents that have no activity in bacterial assays (50). Furthermore, multiplex PCR with primers specific for exons 1-4 of CD59 and 5 other markers on chromosome 11 (RAS, LDHA, WT, CAT, APO-A1) have been used to generate mutant spectra for various genotoxic agents (44,50-53). Although this assay proves sensitive to a wide range of mutagens, like other clonogenic assays it is time consuming and takes up to 5 weeks to test an agent.

Flow cytometry mutation assay (FCMA)

As was previously discussed, the abilities of the MLA, TK6 and CHO A_L assays to sensitively detect mutations generated by known and novel mutagenic agents in mammalian cells have been reported for decades. The capability to quickly determine if a novel compound will have deleterious effects on humans has been used for years by research groups and pharmaceutical companies alike. Although these assays are the industry's standard, there are several areas that need improvement. By decreasing the amount of time to analyze an agent and increasing the sensitivity of the assay, a significant amount of money could be saved by companies testing the genotoxicity of novel compounds. These areas for improvement were first proposed when developing the FCMA (2).

The FCMA utilizes the same CHO A_LN cell line as the standard CHO A_L assay but does not rely on the clonogenic survival of CD59⁺ cells as the endpoint. As an alternative to using antibodies and antisera, fluorochrome conjugated monoclonal antibodies against CD59 are used to assay for the presence of the cell surface protein (2,54). Mutations of the *cd59* gene are scored by the decrease in antibody binding to the CD59 antigen when analyzed using flow cytometry. Using this assay we have found

consistent ~400 fold separations in fluorescence intensities between CD59⁻ and CD59⁺ populations (55). Mutants were originally scored by falling within a gate set at 97% of the negative peak (2) and were later counted as cells with <1% of the fluorescence of the control positive peak (55) (Fig. 2). By carefully examining cells sorted from the mutant regions, we have previously proposed that the 1% gating scheme remains a conservative estimate of the true mutant region (56) and this will be examined in more detail in chapters 2 and 3.

French *et al.* 2006 (55) examined the ability of the FCMA to measure the mutagenic potential of 17 physical and chemical agents. First, cell survival curves were generated for all agents to be tested in order to determine the doses required for 20%, 40%, 60% and 80% cell survival after treatment. Cells were then treated with the appropriate doses calculated for each agent and remained in culture until day 6 when they were stained with phycoerythrin (PE)-conjugated monoclonal antibodies against CD59 and run on the flow cytometer. Samples were then obtained and analyzed every 1 to 2 days until day 12 to determine the optimum day of mutant expression. The published mutant fraction results for all doses for the 17 agents are displayed in Table 1*.

Following treatment, the mutant fraction (MF) in clonogenic assays, like the TK6, increases with time and then remains constant. This was determined by MFs at many times (days 0-17) after treatment with mutagens (4). The FCMA differs slightly in that following treatment, the CD59 MF increases to a maximum and then decreases to a stable plateau (Fig. 3). It should be noted that there is a variation in MF over time when results include slow growing mutants (31)

* Of the 17 agents I personally assayed chrysotile "A" rhodesian asbestos, chlorpheniramine maleate and ethyl methanesulfonate. Also tested but not shown were benzene and dioxane.

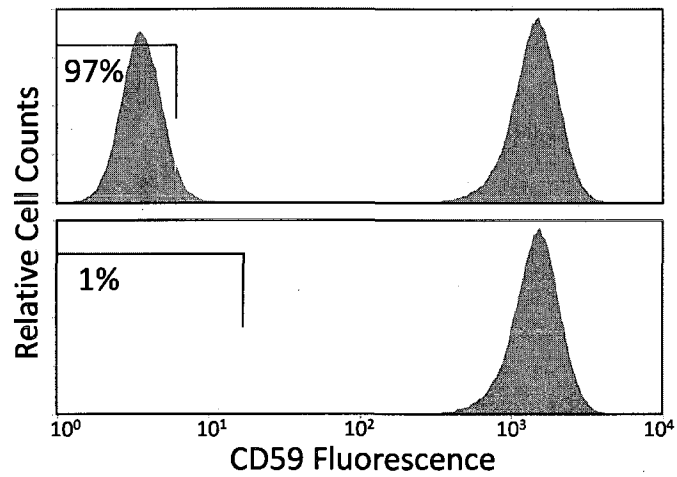


Figure 2. (Top) Original gating region for the FCMA set as 97% of unstained control cells. (Bottom) Mutant region used by French *et al.* 2006 (55) set as 1% of the fluorescence of the mean of the CD59 positive peak.

Agent Tested	CAS number	Control	80% Survival	60% Survival	40% Survival	20% Survival	Fold Increase	Maximum day
Chrysotile "A" Rhodesian Asbestos	12001-29-5	65 ± 9	NT	70 ± 4	412 ± 151*	565 ± 155*	8.7	9
Benzo(a)Pyrene (BaP)	50-32-8	74 ± 38	NT	108 ± 40	197 ± 38†	212 ± 55†	2.9	9
Chlorpheniramine maleate (CM)	113-92-8	79 ± 49	91 ± 52	91 ± 55	NT	82 ± 54	1.0	12
Colchicine	64-86-8	75 ± 6	88 ± 11	93 ± 23	130 ± 11*	NT	1.7	9
Ethidium bromide (EtBr)	1239-45-8	26 ± 7	NT	65 ± 5	141 ± 34*	190 ± 31*	7.3	9
Ethyl methanesulfonate (EMS)	62-50-0	97 ± 19	217 ± 30*	430 ± 78*	581 ± 67*	765 ± 94*	7.9	9
n-Nitroso n-ethylurea (ENU)	759-73-9	68 ± 19	NT	NT	363 ± 69*	721 ± 94*	10.6	14
γ radiation		70 ± 10	650 ± 70*	955 ± 145*	1245 ± 245*	1618 ± 202*	23.1	6
Hydrogen peroxide (H ₂ O ₂)	7722-84-1	77 ± 16	NT	70	80 ± 20	210 ± 34*	2.7	12
Lead acetate (LA)	6080-56-4	68 ± 30	142 ± 58	148 ± 39	557 ± 95*	NT	8.2	6
Methyl cholanthrene	56-49-5	183 ± 9	220 ± 6*	243 ± 19*	227 ± 12*	NT	1.2	9
Methyl nitro nitrosoguanidine (MNNG)	70-25-7	62 ± 42	334 ± 108†	521 ± 116*	785 ± 95*	900 ± 60*	14.5	12
Mitomycin C (MMC)	50-07-7	78 ± 18	148 ± 17*	135 ± 21	297 ± 24*	532 ± 40*	6.8	10
Sodium arsenite (SA)	7784-46-5	59 ± 15	69 ± 26	91 ± 32	192 ± 28*	320 ± 59*	5.4	12
Tetrachloroethane (TTCE)	630-20-6	94 ± 8	127 ± 16	146 ± 35*	162 ± 7†	168 ± 12*	1.8	13
Thalidomide	50-35-1	133 ± 6	163 ± 13	NT	NT	NT	1.2 (NS)	12
UV radiation		108	NT	177 ± 21	281 ± 15	394 ± 16	3.6	10

Table 1. Treatment concentration resulting in approximately 80%, 60%, 40% and 20% survival for the 17 agents tested, revised from French *et al* 2006 (55). Fold increase is the ratio of the maximum induced mutant frequency to the control mutant frequency. Numerical values represent the average mutant frequency ± SEM in 1×10^5 cells from at least three independent experiments with triplicate samples in each experiment, except BaP and cholchicine (2 experiments) and methylcholanthrene (1 experiment). The CD59⁻ mutant region was defined as those cells exhibiting a fluorescence signal of less than 1% of the mean fluorescence value from the CD59⁺ population of control cells. *indicates significance difference relative to control ($p < 0.05$). †indicates significant difference ($p < 0.1$). NT: not tested. NS: not significantly different.

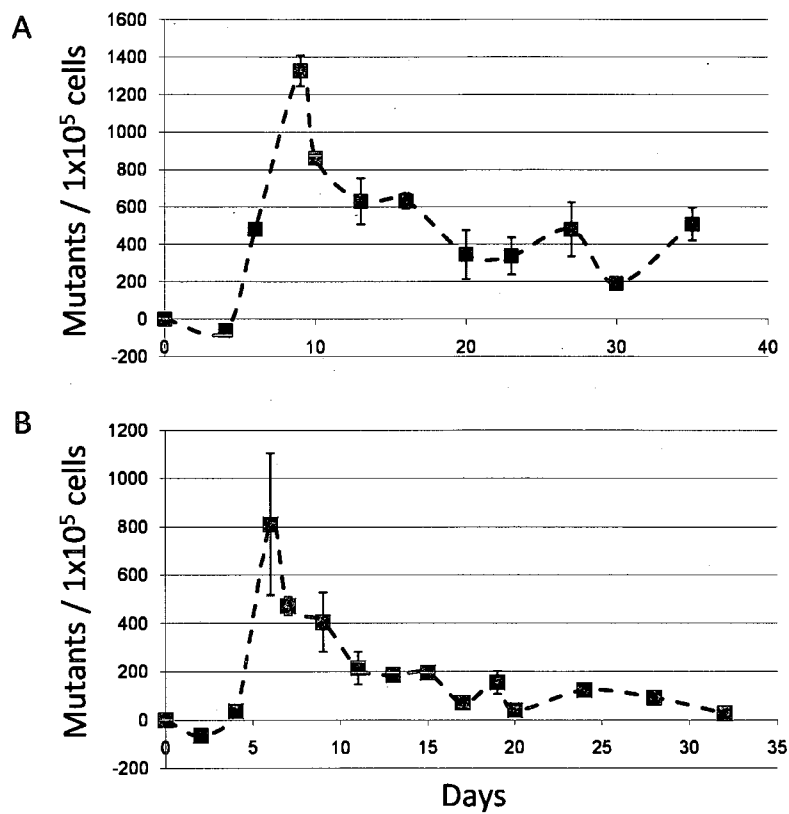


Figure 3. Mutant fraction over time results for (A) 8 mM EMS and (B) 4 Gy γ -rays from day 0 to day 35 and day 34 respectively. The peak days of mutant expression are days 9 and 6 for EMS and radiation respectively.

The question that arises is: what is the FCMA actually measuring on the peak day of expression? This question will be explored in detail in Chapter 2.

The speed in which the FCMA can detect CD59⁺ cells after treatment is apparent in that samples are analyzed within 6 to 12 days after treatment and do not require several weeks for colony formation and counting as the MLA, TK6 and CHO A_L assays require (4,5,57). The FCMA has also correctly classified agents that are false negatives in other assays such as chlorpheniramine maleate (58) and false positives such as thalidomide (59). Also, low responders such as tetrachloroethane (TTCE) (60) and asbestos (6) were determined to be moderately mutagenic with the FCMA. With the speed and the sensitivity to detect mutations generated by a wide range of agents it is important to fully characterize the assay, allowing its use in the study of novel agents and experiments with mutagenesis as an endpoint.

Flow cytometry generated mutant spectra

The sensitivity of the FCMA to rapidly assess the genotoxicity of chemical and physical agents has previously been reported to be equal to or greater than traditional mammalian assays (55,61). After determining the mutagenic potential of agents, a mutant spectrum can be generated which gives the size and number of the mutations generated by an agent, from point mutations to large deletions. Other assays have relied on PCR, DNA sequencing and Southern Blot analysis of isolated mutant clonal populations to generate mutant spectra (32,44,50), but these processes are time consuming and are not completed when most agents are assayed. Other assays have also been limited by the size of mutations they can measure since essential genes were adjacent to the genes of interest (62). Importantly with the A_L cell line only a small

region on the p-arm of chromosome 11 is needed for viability allowing deletions of >150 Mb to be measured with the FCMA (44).

Using the CHO A_L assay, mutant spectra have been generated for many agents using PCR on the DNA isolated from the resulting CD59⁻ colonies (6,63). Primers specific for the 4 exons of *cd59* (64) (Fig. 4) as well as 5 additional genes (RAS, LDHA, WT, CAT and APO-A1) located along the length of chromosome 11 have been used in multiplex PCR reactions to determine the presence or absence of the genes. Although these results are accurate and useful in understanding the mode of action for various genotoxic agents, it remains a laborious task taking several months from the time of cell treatment.

We have previously reported a method in which a mutant spectrum can be generated by multi-parameter flow cytometry on the peak day of mutant expression or by analyzing mutant clonal populations isolated by cell sorting (65). Like the *CD59* gene located on chromosome 11 that expresses the CD59 cell surface protein, there are 4 other genes located along the length of the chromosome that also express surface antigens (CD151, CD44, CD90, CD98). Cells can be stained for the presence of Glycosyl phosphatidylinositol (GPI) anchors using FLAER, a fluorochrome conjugated bacterial toxin, aerolysin, that specifically binds GPI proteins (66). It was previously proposed that some CD59⁻ cells are mutated in a GPI biosynthesis gene that prevents the GPI linked CD59 and CD90 proteins to be bound to the cell surface, so mutations of a GPI synthesis gene instead of the *CD59* gene itself can lead to the CD59⁻ phenotype (67). GPI linkage and its relationship to the FCMA will be discussed in more detail in a following section.

In order to generate a mutant spectrum using flow cytometry, individual CD59⁺ cells were sorted from the FCMA mutant region 6 days after exposure to 4 Gy using γ -irradiation. The resulting clonal populations were then analyzed for the presence of the five surface antigens and GPI linkage. PCR analysis was completed on DNA isolated from the same clonal populations to validate the results obtained by flow cytometry. The locations of the genes (RAS, LDHA, WT, CAT, APO-A1) as well as the genes for the 5 surface antigens on chromosome 11 are displayed in Figure 5. Importantly, the results of both the flow cytometry and PCR were compiled and found to be in total agreement (Fig. 6). With the ability to generate mutant spectra rapidly using flow cytometry and with the accuracy of PCR, we are now able to generate spectra for a variety of agents.

Glycosyl phosphatidylinositol (GPI) anchors

Cell surface proteins have many important roles, including acting as cell-cell recognition sites, cell adhesion sites, receptors and nutrient/ion transporters. Traditionally, all cell surface proteins were thought to contain transmembrane domains holding them in the lipid bilayer (68). Early studies using phosphatidylinositol (PI) specific phospholipase C (PI-PLC) to cleave PI sites demonstrated that the enzyme alkaline phosphatase was bound to the cell surface by GPI linkage and not a transmembrane domain (69,70).

In order to generate GPI linked proteins, several distinct processes must occur. Biosynthesis of GPI takes place on the cytoplasmic side of the endoplasmic reticulum (ER) (71,72). This then translocates to the ER lumen where the phosphatidyl group associates with the inner leaflet of the lipid bilayer (73). All GPI linked proteins have a hydrophilic NH₂-terminal signal peptide to direct them into the ER lumen and a

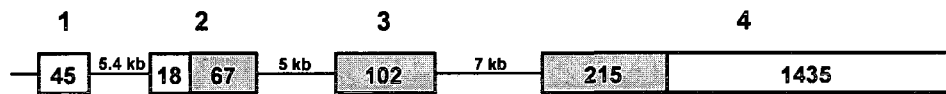


Figure 4. The 4 exons of human cd59 adapted from Petranka *et al.* 1992 (64). The translated sequence is shaded.

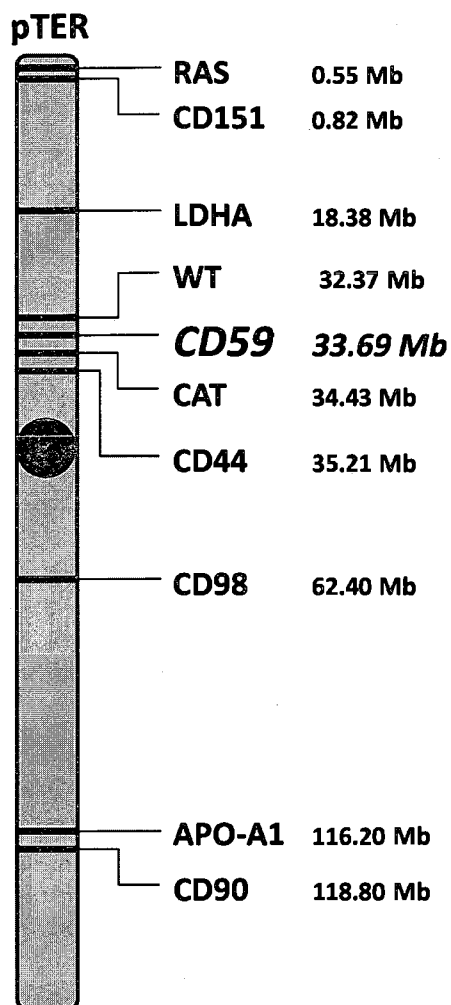


Figure 5. Diagram with the location on human chromosome 11 of 5 genes expressing CD antigens that are analyzed by flow cytometry and 5 genes analyzed by PCR. Measurements are in mega base pairs from the pTer of chromosome 11. Measurements retrieved from www.ncbi.nlm.nih.gov.

	Con	A	B	C	D	E	F	G	H	I	J	K	L	M	N	O	P	Q	R	S
RAS	+	+	+	+	+	+	+	+	+	+	+	+	+	+	+	+	+	+	+	+
Cd151	+	+	+	+	+	+	+	+	+	+	+	+	+	+	+	+	+	+	+	+
LDHA	+	+	+	+	+	+	+	+	+	+	+	+	+	+	+	+	+	+	+	+
WT	+	+	+	+	+	+	+	+	+	+	+	+	+	+	+	+	+	+	+	+
CD59	+	+	+	+	+	+	+	+	+	+	+	+	+	+	+	+	+	+	+	+
Exon 1	+	+	+	+	+	+	+	+	+	+	+	+	+	+	+	+	+	+	+	+
Exon 2	+	+	+	+	+	+	+	+	+	+	+	+	+	+	+	+	+	+	+	+
Exon 3	+	+	+	+	+	+	+	+	+	+	+	+	+	+	+	+	+	+	+	+
Exon 4	+	+	+	+	+	+	+	+	+	+	+	+	+	+	+	+	+	+	+	+
CAT	+	+	+	+	+	+	+	+	+	+	+	+	+	+	+	+	+	+	+	+
CD44	+	+	+	+	+	+	+	+	+	+	+	+	+	+	+	+	+	+	+	+
CD98	+	+	+	+	+	+	+	+	+	+	+	+	+	+	+	+	+	+	+	+
APO-A1	+	+	+	+	+	+	+	+	+	+	+	+	+	+	+	+	+	+	+	+
CD90	+	+	+	+	+	+	+	+	+	+	+	+	+	+	+	+	+	+	+	+
FLAER	+	+	+	+	+	+	+	+	+	+	+	+	+	+	+	+	+	+	+	+

Figure 6. Adapted from C.D. Ross *et. al.* 2007 (65). Mutant spectra of 19 different CHO A_L clones that had been irradiated and then cloned by cell sorting. The individual clones were analyzed both by PCR (indicated by white labels) and flow cytometry (indicated by grey labels). Clones were also analyzed for the four exons of CD59 and the presence of a GPI-anchor using FLAER. The presence or absence of markers is indicated by + and -.

hydrophobic COOH-terminal sequence that serve as a recognition site for a transamidase, which transfers the protein to the GPI anchor (68). The final structure consists of the protein linked to a phosphoethanolamine that serves as a bridge to the core glycan and a phospholipid tail that attaches the glycan to the cell membrane (74) (Fig. 7). GPI anchored proteins are then transported to the cell surface, and in the case of CD59, this occurs via the Golgi complex (75).

GPI anchored proteins are known to associate with lipid rafts in order to organize cellular processes such as signal transduction (74). The importance of GPI linkage is apparent given that certain genetic defects in GPI linkage are embryonic lethal in mammals (76), and in hematopoietic progenitor cells mutations of the X-linked GPI gene phosphatidylinositol glycan-class A (*PigA*) lead to paroxysmal nocturnal hemoglobinuria (PNH) (77). *PigA* is a protein necessary for the biosynthesis of a GPI intermediate (67). Mutations of *PigA* causes the clonal expansion of GPI⁻ blood cells leading to PNH, a disease characterized by intravascular hemolysis and bone marrow failure (78-80).

The possible role of GPI mutations in the CHO A_L assay has been discussed previously; CD59 is a GPI linked cell surface protein and loss of GPI may falsely imply mutation of *cd59* (81). Since the *PigA* gene is X-linked, single mutations could easily lead to the CD59⁻ phenotype (67). We have previously determined that some cells quantified by the FCMA as CD59⁻ are actually lacking GPI anchors by using a fluorescently labeled inactive variant of the pore forming toxin aerolysin (FLAER) (56,65). The non-toxic form of aerolysin binds specifically to GPI anchors and is commonly used in diagnosis of PNH (66). In the following chapters, I will discuss how

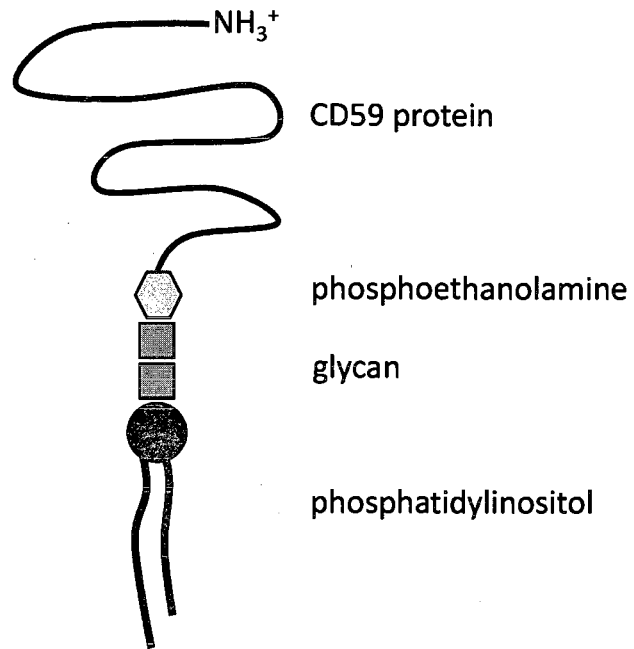


Figure 7. Adapted from Lodish 2008 (82), the basic structure of a GPI linked cell surface protein (CD59). The protein is linked through a phosphoethanolamine bridge to the core glycan/s and the phospholipid tail attaches the entire complex to the cell membrane.

GPI anchors play a role in the overall composition of the CD59⁺ population when using the FCMA.

Genotoxic Agents

A wide range of genotoxic agents were used when initially testing the FCMA. In the following chapters I have used several fully characterized mutagens as well as agents that are only now being studied. Here I briefly discuss the diverse mechanisms by which these agents generate DNA damage and in turn mutations.

Ethyl methanesulfonate (EMS)

Initial studies characterizing the FMCA used ionizing radiation, a known clastogen, that consistently generates large deletions in many assays (65,83). In order to more fully characterize the FCMA, I used EMS in the studies reported here. EMS is a point mutagen and interaction with DNA is understood in depth (3,22).

EMS is an ethylating agent, a known mutagen and carcinogen, and it has been used for decades in mutagenesis studies (84). Alkylating agents introduce adducts into the bases of DNA, and the type of adducts depend on the nucleophilic selectivity of the reaction intermediates. EMS reacts predominantly with nitrogen atoms since they are stronger nucleophiles but may also react with oxygen atoms (85). Early work quantifying the formation of adducts was completed using the enzyme linked immunosorbent assay (ELISA) (12). Alkylation of oxygen can result in direct point mutations, where as nitrogen alkylation has been correlated with structural chromosomal aberrations (13).

EMS exposure generates the commonly mutagenic adduct O6-ethylguanine (O6EG) that is commonly matched with thymine during replication. This leads directly to GC to AT transitions (11,86) and single strand-breaks (87) that can lead to the

formation of double-strand breaks during replication (88). The frequency of O6EG formation has been directly correlated to induced mutations across species, supporting its role as the mutagenic adduct (3). GC to AT transitions were the dominant lesions generated by EMS at the *hprt* locus of CHO cells, but there was also a threshold for mutations generated by EMS that was not seen with other alkylating agents. This is likely due to the low levels of O6EG generated by EMS allowing O6-alkylguanine DNA alkyltransferase to remove the ethyl groups from the O⁶ position of guanine, an irreversible reaction for the protein, until the protein's threshold is reached (89).

Ionizing radiation

For over a century the effects of ionizing radiation on human tissues have been observed (90), and for the past 60 years, the ability of radiation to generate DNA damage and chromosomal aberrations has been well documented (91-94). In the following chapters, investigations using radiation in the form of γ -rays were conducted using a ¹³⁷Cs source irradiator (J.L. Shepherd and Associates, Glendale, CA). Electromagnetic radiations, including γ -rays, have both direct and indirect effects on DNA. Directly damaging effects are caused by secondary fast electrons generated by the absorption of a photon, while indirect damage is generated by radicals formed by the interaction of fast electrons and water (90).

Much of the energy deposition of γ -radiation occurs within regions with dimensions similar to the width of DNA (95) in the form of "spurs" (96). Ionizing radiation may generate spurs that result in up to 5 possible ion pairs and 5 electrons ejected in an area encompassing up to 20 DNA base pairs (97,98). This amount of energy deposition in a small area results in significant damage in a relatively short length

Type	Yield
Single-strand breaks	1000
8-hydroxyadenine	700
Thymine damage	250
DNA-protein crosslinks	150
Double-strand breaks	40

Table 2. Adapted from Ward 1988 (1), the relative amount of different types of DNA damage produced in one cell per 1 Gy x-rays.

of DNA. For every Gy of ionizing radiation, there are thousands of damaged sites ranging from base damage to double-strand breaks (1) (Table 2). Double-strand breaks are considered the most deleterious radiation induced damage and are the most difficult for cells to repair (95). If the dose a cell receives is not lethal, much of the damage will be repaired by specific mechanisms (99), but some damage may result in mutations ranging from point mutations to large deletions (100,101). The mutations that radiation generates in cells are known precursors to carcinogenesis (16,102).

Asbestos

The term “asbestos” refers to the fibrous form of a set of silicates from serpentine and amphibole mineral groups including crocidolite and chrysotile. Chrysotile asbestos makes up 95% of the total asbestos mined and used in manufacturing in the United States (103). Cohort studies of mine workers in Canada exposed to chrysotile asbestos (104), mine workers in Australia exposed to crocidolite asbestos (105) and workers exposed to a wide variety of particulates in manufacturing plants (103) have associated exposure to many diseases including pulmonary fibrosis, lung cancers and mesotheliomas (106). Cell and animal assays have also been used to determine the genotoxicity of particulates and it has been reported that asbestos fibers are mutagens (6,107).

The manner in which silicate fibers can induce mutations in cells, animals and humans has also been investigated. The basic structure of the fibers alone can generate reactive oxygen species (ROS) and reactive nitrogen species (RNS) (108). Mitochondrial membranes have also been proposed to be damaged by the fibers triggering a cascading ROS production by lipid peroxidation (109). This damage has been predicted as a possible mechanism for how asbestos can inflict DNA damage without entering the

nucleus (110). The role of ROS in asbestos induced DNA damage has been solidified by studies demonstrating increases in ROS in treated cells using radical probes (110). Also, researchers found decreased mutagenesis in cells simultaneously treated with asbestos and radical scavengers (111).

The types of DNA damage and mutations induced by asbestos exposure have also been investigated. Cells exposed to fibers for >24 hr have increased DNA double strand breaks (112). Mutant spectra generated from cells exposed to asbestos are comprised mostly of large deletions, ranging from a few thousand to several million base pairs (6). Other groups have reported increased G to T transversions induced by the pre-mutagenic adduct 8-hydroxydeoxyguanosine (8-OHdG), an adduct commonly generated by ROS (107).

People in the United States, and now more significantly in the developing world (110), are exposed to asbestos on a daily basis. The mechanisms by which these fibers induce mutations and consequently cancer are currently being clarified. This genotoxic agent exemplifies the importance of correct classification when developing a new mutation assay.

Hypoxia

The negative effects of the hypoxic tumor environment on cancer treatment and prognosis, specifically in the area of radiotherapy, have been discussed for nearly 80 years (113,114). Decreased oxygen in the environment significantly reduces the mutagenic potential of ionizing radiation, leading to an increased dose required to successfully treat the tumor (115). Recently it has been reported that the stress of being

under hypoxic conditions in itself may increase mutagenesis and genetic instability in cell lines, human tissues and tumors (116).

Several pathways of hypoxia induced mutagenesis have been proposed; DNA damage generated by reactive oxygen species (ROS) produced upon reoxygenation (117), ROS leakage from the mitochondria (118) and decreased DNA repair activity in homologous recombination repair (HRR) (119,120) and mismatch repair (MMR) pathways (121). To date hypoxia induced mutagenesis has not been quantified using traditional mammalian mutation assays.

DNA damage response

Genotoxic agents generate a wide range of damage, but of these DNA double-strand breaks are considered the most deleterious to cells and most likely to induce carcinogenesis (1,102). Cells have developed specialized mechanisms to deal with damage and prevent cellular transformation. Multiple checkpoints throughout the cell cycle recognize damage, including double-strand breaks. Cell cycle progression is halted at G1 and G2 checkpoints after irradiation (122). If the DNA damage is too extensive, prior to or after repair, some cell types also have the ability to enter a programmed cell death or apoptosis. Apoptosis is the “last straw” in preventing DNA damage from being passed on to subsequent generations (123). Figure 8 contains a basic flow chart diagramming a cell’s response to DNA damage from signaling to repair, cell cycle progression or apoptosis.

Induced G1 checkpoints are due to the presence of DNA breaks that are detected predominantly by the ataxia telangiectasia mutated kinase (ATM) and to a lesser extent ataxia telangiectasia related kinase (ATR); these elicit both a fast and slow response

(122). The fast response is generated when ATM or ATR activate Chk1, and in turn Chk1 can phosphorylate Cdc25A, targeting it for ubiquitination (124). The degradation of Cdc25A means the Cdk2-cyclin E complex remains inactive since dephosphorylation of specific residues is required for activation (125). This complex hyperphosphorylates pRB and is therefore required for entrance into S phase (126). The slow G1 response to DNA damage involves the stabilization of p53 and transcriptional activation of its target genes. The stabilization of p53 occurs when it is phosphorylated at specific serines directly by ATM and ATR or indirectly by Chk1 and Chk2. Stable p53 increases transcription of p21, and this inhibits Cdk2-cyclin E (126,127).

Like the G1/S transition, the G2 phase to M phase transition has a check point but it is p53 independent and only occurs when the Cdk1-cyclinB complex, also known as the mitosis-promoting factor (MPF), is fully activated by the phosphorylation of the correct residues (128). When associated with cyclin-B, Cdk1 is inhibited by phosphorylation of Y15 by Wee1 (129,130). The T160 residue is then phosphorylated by Cdk activating kinase (CAK) (131), allowing Cdc25C phosphatase to remove the phosphate from Y15 and consequently activating the MPF complex (132). A G2/M block occurs when damage is recognized by ATM and/or ATR. These activate Chk2 and Chk1 respectively, which in turn phosphorylate and inactivate Cdc25C (122). Without the removal of the phosphate group from Y15 by Cdc25C, the MPF complex remains inactive and cells will not move into mitosis (132), allowing time for DNA repair.

*Conceptual Organization of
DNA Damage Checkpoint Response*

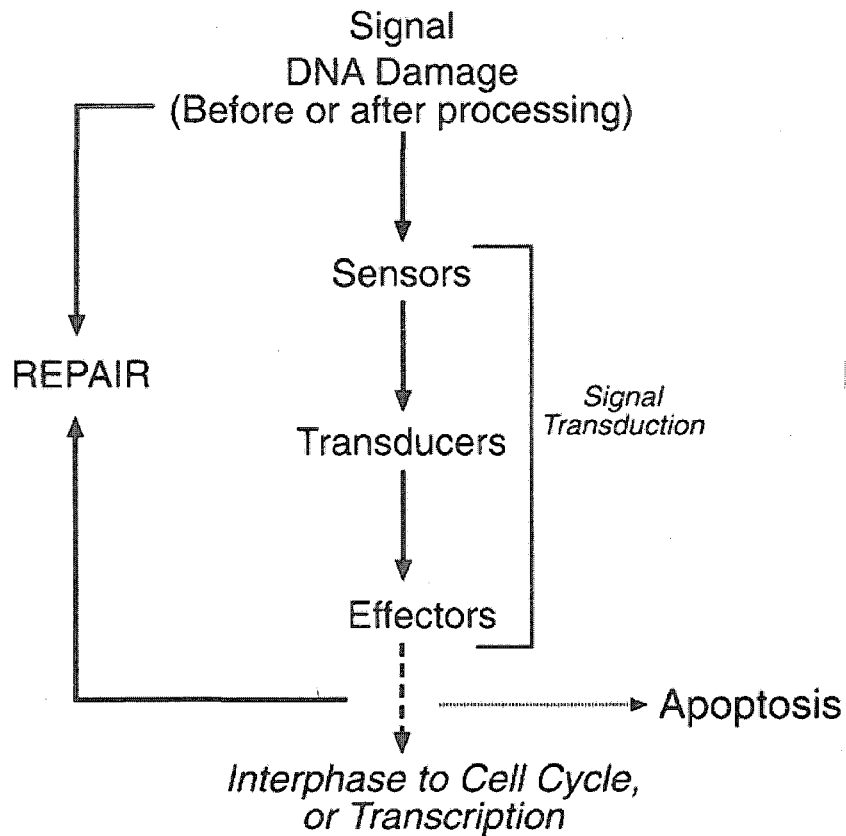


Figure 8. Adapted from Iliakis *et al.* 2003 (122). DNA damage sensing and signal transduction pathway induced by ionizing radiation.

DNA Double-Strand Break Repair

Non-homologous end-joining repair

An important role of the DNA damage response is in the repairing of double-strand breaks. *Saccharomyces cerevisiae* predominantly uses homologous recombination repair (HRR) to fix double-strand breaks, and since homologous chromosomes are used as a template for copying information there is minimal loss of genetic information (88). However, most mammalian cells rely on non-homologous end-joining (NHEJ) to join broken chromosomes. Unlike HRR, NHEJ does not use a homologous chromosome as a template for repair and may result in deletions. NHEJ may be the predominant repair mechanism in vertebrate cells; because much of the mammalian genome is comprised of repetitive DNA sequences, a homology search to conduct HRR may occasionally be insurmountable (133).

The Ku70/80 heterodimer is proposed to be one of the first protein complexes to recognize the broken ends of chromosomes (134); it binds DNA with the broken ends fitting into a specific opening of the dimer (135). Ku70 and Ku80 are constitutively expressed proteins and make-up an abundant protein complex with an estimated 4×10^5 molecules per mammalian cell (135). The importance of this complex is readily apparent, because Ku80 heterozygosity leads to genomic instability (136). Ku80 also has a role in telomere maintenance and its deficiency leads to early senescence in cells (137).

The binding of Ku70/80 attracts the catalytic subunit of DNA-dependent protein kinase (DNA-PK_{cs}) (138). NHEJ is regulated by the autophosphorylation of DNA-PK_{cs} (139) and the juxtaposition of the two broken ends only occurs when DNA-PK_{cs} is efficiently phosphorylated (140). The complex comprised of MRE11, RAD50 and NBS1

(MRN) has been proposed to have a role in holding the broken ends in close proximity to each other (141) and will only form in the presence of ATM phosphorylated histone variant H2AX (γ H2AX) (142). γ H2AX may be necessary in order to provide the proper chromatin environment for MRN foci formation (143).

Often the ends of the chromosomes are not broken “cleanly”, such is seen when the strand breaks are generated by ionizing radiation. Since damage induced by ionizing radiation occurs within spurs or blobs, the bases and the DNA backbone near the break are often damaged and require processing prior to ligation (144). The protein Artemis has been found to mediate end processing often resulting in a small deletion (145,146). When the broken ends are brought together they can be immediately joined by the Ligase IV/XRCC4 complex, which is stimulated by XRCC4-like factor (XLF or Cernunnos) (147,148) (Fig. 9).

Homologous recombination repair

HRR is also used to repair double-strand breaks caused by genotoxic agents. Unlike NHEJ, HRR of double-strand breaks is relatively error free as long as the template DNA used during repair is identical to the original DNA sequence (149). There are three major steps involved in the processing of the DNA damage and copying of the correct DNA sequence. First, the 5' ended DNA strand is resected at the break points leaving a 3' single strand. Second, the 3' end invades the homologous DNA duplex to initiate strand exchange. Finally, after strand exchange the 3' end of the invading strand primes replication and repair (150) (Fig. 10).

Resecting of the 5' end occurs only after the DNA double-strand break ends are recognized and bound by the MRN complex (151,152). Bases and backbone residues

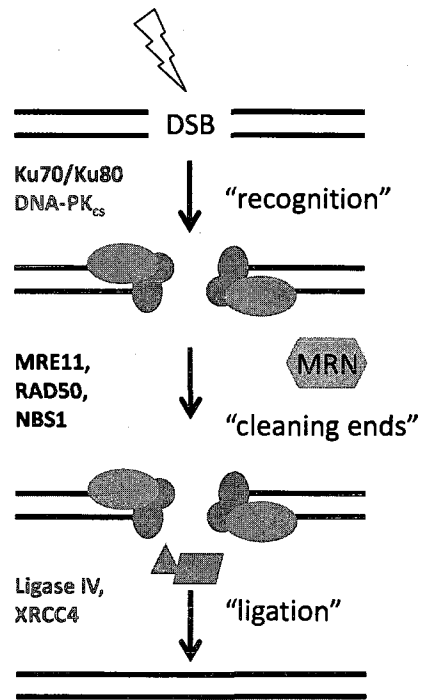


Figure 9. Basic mechanism of the repair of DNA double-stranded breaks by non-homologous endjoining.

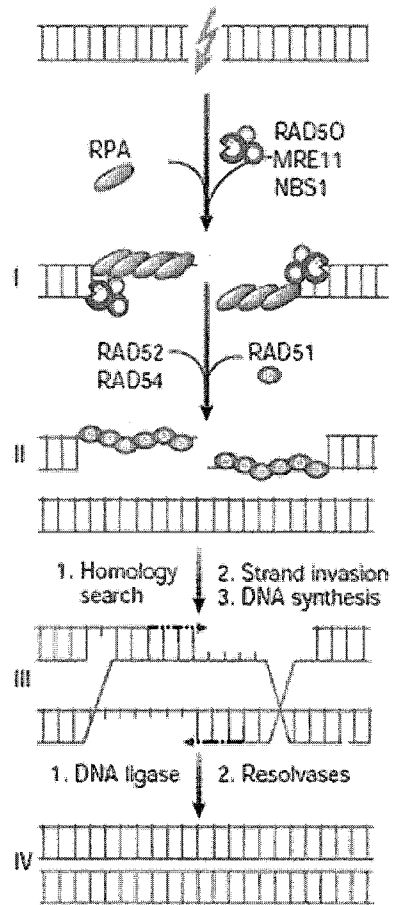


Figure 10. Adapted from Hoeijmakers 2001 (16). Basic schematic of homologous recombination repair of a DNA double-strand break.

adjacent to breaks generated by ionizing radiation are often damaged (144) and may need to be “cleaned” by the nuclease activity of MRE11 (153). Resecting of the 5' end is likely completed by the EXO1 5'-3' nuclease (154). This leaves single stranded 3' ends that are able to perform a homology search and consequently initiate invasion of the homologous region.

Prior to strand invasion, multiple Rad51 recombinase proteins bind the single strand, “coating” it and forming the nucleoprotein filament. Rad51 binding is facilitated by replication protein-A (RPA) (155), which functions to remove secondary structures of DNA and allow for proper Rad51 binding (156). Rad52 also interacts with RPA and is necessary for proper recombination (157), and the Rad54 protein plays an important role in the homology search. Once the nucleoprotein filament has formed, it displaces one strand of the homologous region by forming a displacement-loop (D-loop) (158).

As previously stated, replication is primed by the 3' end of the invading strand. The resulting elongation displaces the homologous template strands, consequently increasing the size of the D-loop. By DNA annealing, the loop can then capture the second broken end and is also elongated by DNA synthesis (149). Following DNA synthesis, gap-filling and ligation results in formation of two Holliday junctions, four branched DNA structures. Different sites of cleavage in these junctions, by proteins yet to be identified, result in either genetic crossover or non-crossover events (150).

Repair of Damaged and Mismatched DNA Bases

Organisms ranging from bacteria to mammals have developed mechanisms to repair damaged DNA bases and to prevent the propagation of errors during DNA replication. Exposure to alkylating agents can generate base adducts including O6EG.

These are commonly matched with thymine during replication, resulting in, GC to AT transitions (11,86). Proteins like O⁶-methylguanine methyltransferase can directly reverse simple alkylations prior to it becoming a permanent mutation (159). Other types of base damage, including mismatches, are too complex for this simple repair and require specific mechanisms (Fig. 10).

Base excision repair (BER)

Many of the common DNA modifications, generated by endogenous sources like ROS, are repaired by BER. Excision of bases altered by oxidative damage is completed by DNA glycosylases. When the damaged nucleotide is removed, the APE1 endonuclease replaces the glycosylase. Preparation for the new nucleotide includes APE1, cleavage at the 5' side of the abasic site. The presence of APE1 recruits Pol β , which inserts the correct base, and the final nick is sealed by the LIG3-XRCC1 complex (16,159,160).

Nucleotide excision repair (NER)

Helix-distorting damage like pyrimidine dimers generated by UV radiation and bulky adducts caused by benzo[a]pyrene are repaired by NER. The XPC protein recognizes the damaged site, and the helicase activities of several subunits of TFIIH, XPA and RPA form an open bubble DNA structure. The 3' side of the damage is cleaved by the XPG nuclease, while the 5' side is nicked by the nuclease activity of the ERCC1-XPF complex. A 24-32 residue piece is released, filled by PCNA dependent Pol ϵ or Pol δ and sealed by LIG1 (16,159,160).

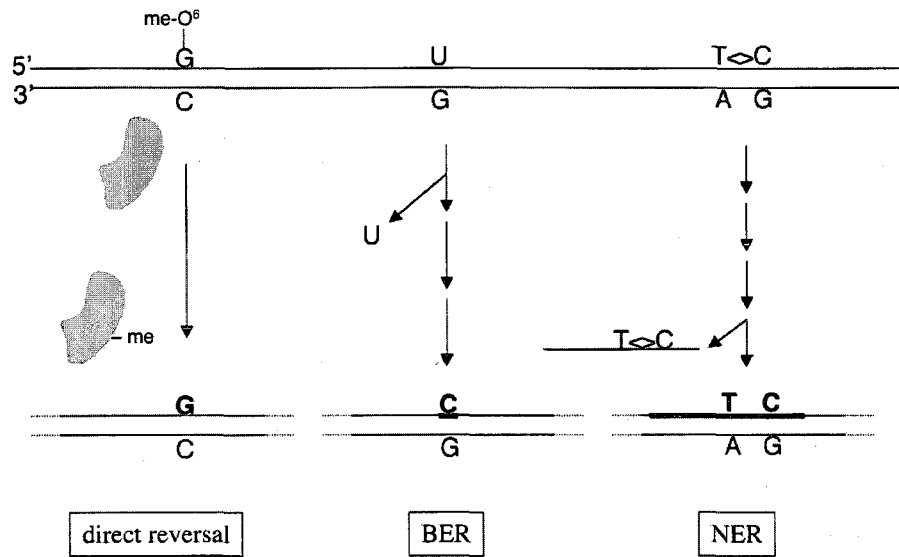


Figure 11. Adapted from Lindahl and Wood 1999 (160); a basic diagram of how different types of DNA base damage are repaired by alkyl-transferases, base excision repair and nucleotide excision repair.

Mismatch repair (MMR)

Unpaired and mis-paired bases in DNA can arise from spontaneous or induced base modifications and replication errors (161). Mismatch repair is able to reverse base-base mismatches and insertion/deletion loops caused by DNA polymerase slippage; these occur during DNA synthesis (162). The MSH2-MSH6 complex recognizes base-base mismatches while MSH2-MSH3 recognizes larger insertion/deletion damage. These complexes can both recognize and bind single base insertions and deletions (163). Nicking of the damaged strand by the endonuclease function of PMS2 is followed by EXO1 excision of the sequence. RPA proteins then bind and coat the single stranded DNA gap. DNA synthesis is then completed by Pol δ , and the resulting nick is sealed by DNA ligase (164).

Conclusion

In this introduction, I have briefly touched on the historical development of mammalian mutation assays and the search for more sensitive and less time consuming systems. The ability of the FCMA to detect significant mutation fractions generated by a broad spectrum of physical and chemical agents has previously been reported. The processes by which these agents act on DNA and the response of mammalian cells to these insults have also been discussed in this chapter. In the following chapters I characterize the mutant kinetics of the FMCA after treatment with a range of genotoxic agents. I have also used the FCMA to assess the mutagenic potential and types of mutations generated by agents like asbestos, and hypoxia that have not been studied in depth using mammalian mutation assays; I will discuss these experiments and results in detail in the following chapters.

Reference List

1. Ward JF. DNA damage produced by ionizing radiation in mammalian cells: identities, mechanisms of formation, and reparability. *Prog Nucleic Acid Res Mol Biol* 1988;35:95-125.
2. Ross CD, Lim CU, Fox MH. Assay to measure CD59 mutations in CHO A(L) cells using flow cytometry. *Cytometry A* 2005;66:85-90.
3. van Zeeland AA, Mohn GR, Neuhauser-Klaus A, Ehling UH. Quantitative comparison of genetic effects of ethylating agents on the basis of DNA adduct formation. Use of O6-ethylguanine as molecular dosimeter for extrapolation from cells in culture to the mouse. *Environ Health Perspect* 1985;62:163-169.
4. Liber HL, Thilly WG. Mutation assay at the thymidine kinase locus in diploid human lymphoblasts. *Mutat Res* 1982;94:467-485.
5. Waldren C, Jones C, Puck TT. Measurement of mutagenesis in mammalian cells. *Proc Natl Acad Sci U S A* 1979;76:1358-1362.
6. Hei TK, Piao CQ, He ZY, Vannais D, Waldren CA. Chrysotile fiber is a strong mutagen in mammalian cells. *Cancer Res* 1992;52:6305-6309.
7. Reynolds TY, Rockwell S, Glazer PM. Genetic instability induced by the tumor microenvironment. *Cancer Res* 1996;56:5754-5757.
8. Cory S, Huang DC, Adams JM. The Bcl-2 family: roles in cell survival and oncogenesis. *Oncogene* 2003;22:8590-8607.
9. Vakifahmetoglu H, Olsson M, Tamm C, Heidari N, Orrenius S, Zhivotovsky B. DNA damage induces two distinct modes of cell death in ovarian carcinomas. *Cell Death Differ* 2008;15:555-566.
10. Hall EJ: Repair of Radiation Damage and the Dose-Rate Effect. In: *Radiobiology or the Radiologist*, 5th. ed. Edition, John J, Sutton P, and Marino D (eds). Lippincott, Williams & Wilkins, Philadelphia, 2000, pp. 67-90.
11. Ellison KS, Dogliotti E, Connors TD, Basu AK, Essigmann JM. Site-specific mutagenesis by O6-alkylguanines located in the chromosomes of mammalian cells: influence of the mammalian O6-alkylguanine-DNA alkyltransferase. *Proc Natl Acad Sci U S A* 1989;86:8620-8624.
12. Mohn GR, Kerklaan PR, van Zeeland AA, Ellenberger J, Baan RA, Lohman PH, Pons FW. Methodologies for the determination of various genetic effects in permeable strains of *E. coli* K-12 differing in DNA repair capacity. Quantification of DNA adduct formation, experiments with organ

homogenates and hepatocytes, and animal-mediated assays. *Mutat Res* 1984;125:153-184.

13. Vogel E, Natarajan AT. The relation between reaction kinetics and mutagenic action of mono-functional alkylating agents in higher eukaryotic systems. I. Recessive lethal mutations and translocations in *Drosophila*. *Mutat Res* 1979;62:51-100.
14. Hei TK, Wu L, Liu S, Vannais DB, Waldren CA, Randers-Pehrson G. Mutagenic effects of a single and an exact number of alpha particles in mammalian cells. *Proc Natl Acad Sci* 1997;94:3765-3770.
15. Mendonca MS, Temples TM, Farrington DL, Bloch C. Evidence for a role of delayed death and genomic instability in radiation-induced neoplastic transformation of human hybrid cells. *Int J Radiat Biol* 1998;74:755-764.
16. Hoeijmakers JH. Genome maintenance mechanisms for preventing cancer. *Nature* 2001;411:366-374.
17. Ames BN, Durston WE, Yamasaki E, Lee FD. Carcinogens are Mutagens: A Simple Test System Combining Liver Homogenates for Activation and Bacteria for Detection. *Proc Natl Acad Sci* 1973;70:2281-2285.
18. McCann J, Ames BN. Detection of carcinogens as mutagens in the *Salmonella*/microsome test: assay of 300 chemicals. *Proc Natl Acad Sci* 1976;73:950-954.
19. O'Neill JP, Brimer PA, Machanoff R, Hirsch GP, Hsie AW. A quantitative assay of mutation induction at the hypoxanthine-guanine phosphoribosyl transferase locus in Chinese hamster ovary cells (CHO/HGPRT system): development and definition of the system. *Mutat Res* 1977;45:91-101.
20. Thompson LH, Fong S, Brookman K. Validation of conditions for efficient detection of HPRT and APRT mutations in suspension-cultured Chinese hamster ovary cells. *Mutat Res* 1980;74:21-36.
21. O'Neill JP, Couch DB, Machanoff R, San Sebastian JR, Brimer PA, Hsie AW. A quantitative assay of mutation induction at the hypoxanthine-guanine phosphoribosyl transferase locus in Chinese hamster ovary cells (CHO/HGPRT system): utilization with a variety of mutagenic agents. *Mutat Res* 1977;45:103-109.
22. Hsie AW, Machanoff R, Couch DB, Holland JM. Mutagenicity of dimethylnitrosamine and ethyl methanesulfonate as determined by the host-mediated CHO/HGPRT assay. *Mutat Res* 1978;51:77-84.

23. Clive D, Spector JFS. Laboratory procedure for assessing specific locus mutations at the TK locus in cultured L5178Y mouse lymphoma cells. *Mutation Research* 1975;31:17-29.
24. Combes RD, Stopper H, Caspary WJ. The use of L5178Y mouse lymphoma cells to assess the mutagenic, clastogenic and aneugenic properties of chemicals. *Mutagenesis* 1995;10:403-408.
25. Clive D, Johnson KO, Spector JF, Batson AG, Brown MM. Validation and characterization of the L5178Y/TK+/- mouse lymphoma mutagen assay system. *Mutat Res* 1979;59:61-108.
26. Chen T, Harrington-Brock K, Moore MM. Mutant frequency and mutational spectra in the Tk and Hprt genes of N-ethyl-N-nitrosourea-treated mouse lymphoma cells. *Environmental and Molecular Mutagenesis* 2002;39:296-305.
27. Liber HL, Call KM, Little JB. Molecular and biochemical analyses of spontaneous and X-ray-induced mutants in human lymphoblastoid cells. *Mutation Research* 1987;178:143-153.
28. Liber HL, Denault CM. Mutagenicity of 2-amino-N6-hydroxyadenine to TK6 human lymphoblast cells. *Mutat Res* 1991;253:91-95.
29. Metting NF, Palayoor ST, Macklis RM, Atcher RW, Liber HL, Little JB. Induction of mutations by bismuth-212 alpha particles at two genetic loci in human B-lymphoblasts. *Radiat Res* 1992;132:339-345.
30. Liber HL, Call KM, Little JB. Molecular and biochemical analyses of spontaneous and X-ray-induced mutants in human lymphoblastoid cells. *Mutation Research* 1987;178:143-153.
31. Liber HL, Yandell DW, Little JB. A comparison of mutation induction at the tk and hprt loci in human lymphoblastoid cells; quantitative differences are due to an additional class of mutations at the autosomal tk locus. *Mutation Research* 1989;216:9-17.
32. Phillips EN, Xia F, Kelsey KT, Liber HL. Spectra of spontaneous and X-ray-induced mutations at the hprt locus in related human lymphoblast cell lines that express wild-type or mutant p53. *Radiation Research* 1995;143:255-262.
33. Zhang Y, Zhou J, Held KD, Redmond RW, Prise KM, Liber HL. Deficiencies of double-strand break repair factors and effects on mutagenesis in directly gamma-irradiated and medium-mediated bystander human lymphoblastoid cells. *Radiat Res* 2008;169:197-206.

34. Zhang Y, Lim CU, Williams ES, Zhou J, Zhang Q, Fox MH, Bailey SM, Liber HL. NBS1 knockdown by small interfering RNA increases ionizing radiation mutagenesis and telomere association in human cells. *Cancer Res* 2005;65:5544-5553.
35. Schwartz JL, Jordan R, Slovic J, Moruzzi AM, Kimmel RR, Liber HL. Induction and loss of a TP53-dependent radioadaptive response in the human lymphoblastoid cell model TK6 and its abrogation by BCL2 over-expression. *Int J Radiat Biol* 2007;83:153-159.
36. Zhang Q, Williams ES, Askin KF, Peng Y, Bedford JS, Liber HL, Bailey SM. Suppression of DNA-PK by RNAi has different quantitative effects on telomere dysfunction and mutagenesis in human lymphoblasts treated with gamma rays or HZE particles. *Radiat Res* 2005;164:497-504.
37. Puck TT, Wuthier P, Jones C, Kao F. Genetics of Somatic Mammalian Cells: Lethal Antigens as Genetic Markers for Study of Human Linkage Groups. *Proc Natl Acad Sci* 1971;68:3102-3106.
38. Jones C, Bill J, Larizza L, Pym B, Goodfellow P, Tunnacliffe A. Relationships Between Genes on Human Chromosome 11 Encoding Cell-Surface Antigens. *Somatic Cell and Molecular Genetics* 1984;4:423-428.
39. Waldren C, Correll L, Sognier MA, Puck TT. Measurement of low levels of x-ray mutagenesis in relation to human disease. *Proc Natl Acad Sci* 1986;83:4839-4843.
40. Waldren C, Braaton M, Vannais D, Fouladi B, Parker RD. The use of human repetitive DNA to target selectable markers into only the human chromosome of a human-hamster hybrid cell line (AL). *Somat Cell Mol Genet* 1992;18:417-422.
41. Hei TK, Liu SX, Waldren C. Mutagenicity of arsenic in mammalian cells: role of reactive oxygen species. *Proc Natl Acad Sci* 1998;95:8103-8107.
42. Kraemer SM, Vannais DB, Kronenberg A, Ueno A, Waldren CA. Gamma-ray mutagenesis studies in a new human-hamster hybrid, A(L)CD59(+/-), which has two human chromosomes 11 but is hemizygous for the CD59 gene. *Radiat Res* 2001;156:10-19.
43. Kraemer SM, Waldren CA. Chromosomal mutations and chromosome loss measured in a new human-hamster hybrid cell line, ALC: studies with colcemid, ultraviolet irradiation, and ¹³⁷Cs gamma-rays. *Mutat Res* 1997;379:151-166.
44. Kraemer SM, Kronenberg A, Ueno A, Waldren CA. Measuring the spectrum of mutation induced by nitrogen ions and protons in the human-hamster hybrid cell line A(L)C. *Radiat Res* 2000;153:743-751.

45. Waldren C, Correll L, Sognier MA, Puck TT. Measurement of low levels of x-ray mutagenesis in relation to human disease. *Proc Natl Acad Sci* 1986;83:4839-4843.
46. Hei TK, Wu L, Liu S, Vannais DB, Waldren CA, Randers-Pehrson G. Mutagenic effects of a single and an exact number of alpha particles in mammalian cells. *Proc Natl Acad Sci* 1997;94:3765-3770.
47. Zhou H, Randers-Pehrson G, Waldren CA, Vannais DB, Hall EJ, Hei TK. Induction of a bystander mutagenic effect of alpha particles in mammalian cells. *Proc Natl Acad Sci* 2000;97:2099-2104.
48. Zhou H, Randers-Pehrson G, Geard CR, Brenner DJ, Hall EJ, Hei TK. Interaction between radiation-induced adaptive response and bystander mutagenesis in mammalian cells. *Radiation Research* 2003;160:512-516.
49. Suzuki M, Zhou H, Geard CR, Hei TK. Effect of medium on chromatin damage in bystander mammalian cells. *Radiation Research* 2004;162:264-269.
50. Waldren CA, Ueno AM, Schaeffer BK, Wood SG, Sinclair PR, Doolittle DJ, Smith CJ, Harvey WF, Shibuya ML, Gustafson DL, Vannais DB, Puck TT, Sinclair JF. Mutant yields and mutational spectra of the heterocyclic amines MeIQ and PhIP at the S1 locus of human-hamster AL cells with activation by chick embryo liver (CELC) co-cultures. *Mutat Res* 1999;425:29-46.
51. Hei TK, Wu L, Liu S, Vannais DB, Waldren CA, Randers-Pehrson G. Mutagenic effects of a single and an exact number of alpha particles in mammalian cells. *Proc Natl Acad Sci* 1997;94:3765-3770.
52. Hei TK, Liu SX, Waldren C. Mutagenicity of arsenic in mammalian cells: role of reactive oxygen species. *Proc Natl Acad Sci* 1998;95:8103-8107.
53. Waldren CA, Vannais DB, Ueno AM. A role for long-lived radicals (LLR) in radiation-induced mutation and persistent chromosomal instability: counteraction by ascorbate and RibCys but not DMSO. *Mutation Research* 2005;551:255-265.
54. Wedemeyer N, Greve B, Uthe D, Potter T, Denklau D, Severin E, Hacker-Klom U, Kohnlein W, Gohde W. Frequency of CD59 mutations induced in human-hamster hybrid A(L) cells by low-dose X-irradiation. *Mutat Res* 2001;473:73-84.
55. French CT, Ross CD, Keysar SB, Joshi DD, Lim CU, Fox MH. Comparison of the mutagenic potential of 17 physical and chemical agents analyzed by the flow cytometry mutation assay. *Mutat Res* 2006;602:14-25.

56. Ross CD, Fox MH. Multiparameter Analysis of CHO A(L) Mutant Populations Sorted on CD59 Expression after Gamma Irradiation. *Radiat Res* 2008;170:628-637.
 57. Hozier J, Sawyer J, Moore M, Howard B, Clive D. Cytogenetic analysis of the L5178Y/TK+/- leads to TK-/- mouse lymphoma mutagenesis assay system. *Mutation Research* 1981;84:169-181.
 58. McGregor DB, Brown AG, Howgate S, McBride D, Riach C, Caspary WJ. Responses of the L5178Y mouse Lymphoma cell forward mutation assay. V: 27 coded chemicals. *Environ Mol Mutagen* 1991;17:196-219.
 59. Ashby J, Tinwell H, Callander RD, Kimber I, Clay P, Galloway SM, Hill RB, Greenwood SK, Gaulden ME, Ferguson MJ, Vogel E, Nivard M, Parry JM, Williamson J. Thalidomide: lack of mutagenic activity across phyla and genetic endpoints. *Mutat Res* 1997;396:45-64.
 60. Kirkland D, Aardema M, Henderson L, Muller L. Evaluation of the ability of a battery of three in vitro genotoxicity tests to discriminate rodent carcinogens and non-carcinogens I. Sensitivity, specificity and relative predictivity. *Mutation Research* 2005;584:1-256.
 61. Ross, C. D. Development of a mammalian cell mutation assay based on flow cytometry and its use in analyzing mutations induced by ionizing radiation and chemicals. 2006. Colorado State University.
- Ref Type: Thesis/Dissertation
62. Davies MJ, Phillips BJ, Rumsby PC. Molecular analysis of mutations at the tk locus of L5178Y mouse-lymphoma cells induced by ethyl methanesulphonate and mitomycin C. *Mutation Research* 1993;290:145-153.
 63. Hei TK, Wu L, Liu S, Vannais DB, Waldren CA, Randers-Pehrson G. Mutagenic effects of a single and an exact number of alpha particles in mammalian cells. *Proc Natl Acad Sci* 1997;94:3765-3770.
 64. Petranka JG, Fleenor DE, Sykes K, Kaufman RE, Rosse WF. Structure of the CD59-encoding gene: further evidence of a relationship to murine lymphocyte antigen Ly-6 protein. *Proc Natl Acad Sci U S A* 1992;89:7876-7879.
 65. Ross CD, French CT, Keysar SB, Fox MH. Mutant spectra of irradiated CHO A(L) cells determined with multiple markers analyzed by flow cytometry. *Mutat Res* 2007;624:61-70.
 66. Brodsky RA, Mukhina GL, Li S, Nelson KL, Chiurazzi PL, Buckley JT, Borowitz MJ. Improved detection and characterization of paroxysmal nocturnal

hemoglobinuria using fluorescent aerolysin. *Am J Clin Pathol* 2000;114:459-466.

67. Miyata T, Takeda J, Iida Y, Yamada N, Inoue N, Takahashi M, Maeda K, Kitani T, Kinoshita T. The cloning of PIG-A, a component in the early step of GPI-anchor biosynthesis. *Science* 1993;259:1318-1320.
68. Udenfriend S, Kodukula K. How glycosylphosphatidylinositol-anchored membrane proteins are made. *Annu Rev Biochem* 1995;64:563-591.
69. Ikezawa H, Yamanegi M, Taguchi R, Miyashita T, Ohyabu T. Studies on phosphatidylinositol phosphodiesterase (phospholipase C type) of *Bacillus cereus*. I. purification, properties and phosphatase-releasing activity. *Biochim Biophys Acta* 1976;450:154-164.
70. Low MG, Finean JB. Release of alkaline phosphatase from membranes by a phosphatidylinositol-specific phospholipase C. *Biochem J* 1977;167:281-284.
71. Mayor S, Menon AK, Cross GA. Transfer of glycosyl-phosphatidylinositol membrane anchors to polypeptide acceptors in a cell-free system. *J Cell Biol* 1991;114:61-71.
72. Vidugiriene J, Menon AK. Early lipid intermediates in glycosyl-phosphatidylinositol anchor assembly are synthesized in the ER and located in the cytoplasmic leaflet of the ER membrane bilayer. *J Cell Biol* 1993;121:987-996.
73. Vidugiriene J, Menon AK. The GPI anchor of cell-surface proteins is synthesized on the cytoplasmic face of the endoplasmic reticulum. *J Cell Biol* 1994;127:333-341.
74. Paulick MG, Bertozzi CR. The glycosylphosphatidylinositol anchor: a complex membrane-anchoring structure for proteins. *Biochemistry* 2008;47:6991-7000.
75. Nichols BJ, Kenworthy AK, Polishchuk RS, Lodge R, Roberts TH, Hirschberg K, Phair RD, Lippincott-Schwartz J. Rapid cycling of lipid raft markers between the cell surface and Golgi complex. *J Cell Biol* 2001;153:529-541.
76. Kawagoe K, Kitamura D, Okabe M, Taniuchi I, Ikawa M, Watanabe T, Kinoshita T, Takeda J. Glycosylphosphatidylinositol-anchor-deficient mice: implications for clonal dominance of mutant cells in paroxysmal nocturnal hemoglobinuria. *Blood* 1996;87:3600-3606.
77. Takeda J, Miyata T, Kawagoe K, Iida Y, Endo Y, Fujita T, Takahashi M, Kitani T, Kinoshita T. Deficiency of the GPI anchor caused by a somatic mutation

of the PIG-A gene in paroxysmal nocturnal hemoglobinuria. *Cell* 1993;73:703-711.

78. Barcellini W, Fermo E, Guia IF, Zaninoni A, Bianchi P, Boschetti C, Zanella A. Increased resistance of PIG-A- bone marrow progenitors to tumor necrosis factor α and interferon γ : possible implications for the in vivo dominance of paroxysmal nocturnal hemoglobinuria clones. *Haematologica* 2004;89:651-656.
79. Szpurka H, Schade AE, Jankowska AM, Maciejewski JP. Altered lipid raft composition and defective cell death signal transduction in glycosylphosphatidylinositol anchor-deficient PIG-A mutant cells. *Br J Haematol* 2008;
80. Kulkarni S, Bessler M. The effect of GPI-anchor deficiency on apoptosis in mice carrying a Piga gene mutation in hematopoietic cells. *J Leukoc Biol* 2002;72:1228-1233.
81. Wilson AB, Seilly D, Willers C, Vannais DB, McGraw M, Waldren CA, Hei TK, Davies A. Antigen S1, encoded by the MIC1 gene, is characterized as an epitope of human CD59, enabling measurement of mutagen-induced intragenic deletions in the AL cell system. *Somat Cell Mol Genet* 1999;25:147-157.
82. Lodish H, Berk A, Kaiser CA, Krieger M, Scott MP, Bretscher A, Ploegh H: *Molecular Cell Biology*. sixth edition Edition. W.H. Freeman and Company, New York, 2008.
83. Waldren C, Correll L, Sognier MA, Puck TT. Measurement of low levels of x-ray mutagenesis in relation to human disease. *Proc Natl Acad Sci* 1986;83:4839-4843.
84. Sega GA. A review of the genetic effects of ethyl methanesulfonate. *Mutat Res* 1984;134:113-142.
85. Beranek DT. Distribution of methyl and ethyl adducts following alkylation with monofunctional alkylating agents. *Mutat Res* 1990;231:11-30.
86. Loechler EL, Green CL, Essigmann JM. In vivo mutagenesis by O6-methylguanine built into a unique site in a viral genome. *Proc Natl Acad Sci U S A* 1984;81:6271-6275.
87. Abbondandolo A, Dogliotti E, Lohman PH, Berends F. Molecular dosimetry of DNA damage caused by alkylation. I. Single-strand breaks induced by ethylating agents in cultured mammalian cells in relation to survival. *Mutat Res* 1982;92:361-377.

88. Lieber MR, Ma Y, Pannicke U, Schwarz K. Mechanism and regulation of human non-homologous DNA end-joining. *Nat Rev Mol Cell Biol* 2003;4:712-720.
89. Jansen JG, Vrieling H, van Teijlingen CM, Mohn GR, Bates AD, van Zeeland AA. Marked differences in the role of O6-alkylguanine in hprt mutagenesis in T-lymphocytes of rats exposed in vivo to ethylmethanesulfonate, N-(2-hydroxyethyl)-N-nitrosourea, or N-ethyl-N-nitrosourea. *Cancer Res* 1995;55:1875-1882.
90. Hall EJ: The Physics and Chemistry of Radiation Absorption. In: *Radiobiology for the Radiologist*, 5th ed. Edition, John J, Sutton P, and Marino D (eds). Lippincott Williams & Wilkins, Philadelphia, 2000, pp. 1-16.
91. NEARY GJ, EVANS HJ. Chromatid breakage by irradiation and the oxygen effect. *Nature* 1958;182:890-891.
92. BARENSEN GW, BEUSKER TL, VERGROESEN AJ, BUDKE L. Effects of different radiations on human cells in tissue culture. II. Biological experiments. *Radiat Res* 1960;13:841-849.
93. Cornforth MN, Bedford JS. X-ray--induced breakage and rejoining of human interphase chromosomes. *Science* 1983;222:1141-1143.
94. Bedford JS, Cornforth MN. Relationship between the recovery from sublethal X-ray damage and the rejoining of chromosome breaks in normal human fibroblasts. *Radiat Res* 1987;111:406-423.
95. Hall EJ: DNA Strand Breaks and Chromosomal Aberrations. In: *Radiobiology for the Radiologist*, 5th ed. Edition, John J, Sutton P, and Marino D (eds). Lippincott Williams & Wilkins, Philadelphia, 2000, pp. 17-31.
96. Mozumder A, Magee JL. Model of tracks of ionizing radiations for radical reaction mechanisms. *Radiat Res* 1966;28:203-214.
97. Magee JL, FUNABASHI K. The clustering of ions in irradiated gases. *Radiat Res* 1959;10:622-635.
98. DEWHURST HA, SAMUEL AH, Magee JL. A theoretical survey of the radiation chemistry of water and aqueous solutions. *Radiat Res* 1954;1:62-84.
99. Wood RD, Mitchell M, Lindahl T. Human DNA repair genes, 2005. *Mutation Research* 2005;577:275-283.
100. Sankaranarayanan K. Ionizing radiation and genetic risks. III. Nature of spontaneous and radiation-induced mutations in mammalian in vitro systems and mechanisms of induction of mutations by radiation. *Mutat Res* 1991;258:75-97.

101. Carrano AV. Chromosome aberrations and radiation-induced cell death. I. Transmission and survival parameters of aberrations. *Mutat Res* 1973;17:341-353.
102. Hall EJ: Radiation Carcinogenesis. In: *Radiobiology for the Radiologist*, 5th ed. Edition, John J, Sutton P, and Marino D (eds). Lippincott, Williams & Wilkins, Philadelphia, 2000, pp. 144-165.
103. Berman DW, Crump KS. Update of potency factors for asbestos-related lung cancer and mesothelioma. *Crit Rev Toxicol* 2008;38 Suppl 1:1-47.
104. Liddell FD, McDonald AD, McDonald JC. The 1891-1920 birth cohort of Quebec chrysotile miners and millers: development from 1904 and mortality to 1992. *Ann Occup Hyg* 1997;41:13-36.
105. Lee YC, de Klerk NH, Musk AW. Asbestos-related pleural disease in Western Australian gold-miners. *Med J Aust* 1999;170:263-265.
106. Merchant JA. Human epidemiology: a review of fiber type and characteristics in the development of malignant and nonmalignant disease. *Environ Health Perspect* 1990;88:287-293.
107. Unfried K, Schurkes C, Abel J. Distinct spectrum of mutations induced by crocidolite asbestos: clue for 8-hydroxydeoxyguanosine-dependent mutagenesis in vivo. *Cancer Res* 2002;62:99-104.
108. Zalma R, Guignard J, Copin E, Pezerat H. Studies on surface properties of asbestos. IV. Catalytic role of asbestos in fluorene oxidation. *Environ Res* 1986;41:296-301.
109. Howden PJ, Faux SP. Fibre-induced lipid peroxidation leads to DNA adduct formation in *Salmonella typhimurium* TA104 and rat lung fibroblasts. *Carcinogenesis* 1996;17:413-419.
110. Xu A, Zhou H, Yu DZ, Hei TK. Mechanisms of the genotoxicity of crocidolite asbestos in mammalian cells: implication from mutation patterns induced by reactive oxygen species. *Environ Health Perspect* 2002;110:1003-1008.
111. Hei TK, He ZY, Suzuki K. Effects of antioxidants on fiber mutagenesis. *Carcinogenesis* 1995;16:1573-1578.
112. Okayasu R, Takahashi S, Yamada S, Hei TK, Ullrich RL. Asbestos and DNA double strand breaks. *Cancer Res* 1999;59:298-300.
113. Moulder JE, Rockwell S. Tumor hypoxia: its impact on cancer therapy. *Cancer Metastasis Rev* 1987;5:313-341.

114. Brizel DM, Scully SP, Harrelson JM, Layfield LJ, Bean JM, Prosnitz LR, Dewhirst MW. Tumor oxygenation predicts for the likelihood of distant metastases in human soft tissue sarcoma. *Cancer Res* 1996;56:941-943.
115. Hall EJ: The Oxygen Effect and Reoxygenation. In: *Radiobiology for the Radiologist*, 5th ed. Edition, John J, Sutton P, and Marino D (eds). Lippincott Williams & Wilkins, Philadelphia, 2000, pp. 91-111.
116. Bristow RG, Hill RP. Hypoxia and metabolism. Hypoxia, DNA repair and genetic instability. *Nat Rev Cancer* 2008;8:180-192.
117. Risom L, Lundby C, Thomsen JJ, Mikkelsen L, Loft S, Friis G, Moller P. Acute hypoxia and reoxygenation-induced DNA oxidation in human mononuclear blood cells. *Mutat Res* 2007;625:125-133.
118. Moller P, Loft S, Lundby C, Olsen NV. Acute hypoxia and hypoxic exercise induce DNA strand breaks and oxidative DNA damage in humans. *FASEB J* 2001;15:1181-1186.
119. Bindra RS, Schaffer PJ, Meng A, Woo J, Maseide K, Roth ME, Lizardi P, Hedley DW, Bristow RG, Glazer PM. Down-regulation of Rad51 and decreased homologous recombination in hypoxic cancer cells. *Molecular and Cellular Biology* 2004;24:8504-8518.
120. Meng AX, Jalali F, Cuddihy A, Chan N, Bindra RS, Glazer PM, Bristow RG. Hypoxia down-regulates DNA double strand break repair gene expression in prostate cancer cells. *Radiother Oncol* 2005;76:168-176.
121. Rodriguez-Jimenez FJ, Moreno-Manzano V, Lucas-Dominguez R, Sanchez-Puelles JM. Hypoxia causes downregulation of mismatch repair system and genomic instability in stem cells. *Stem Cells* 2008;26:2052-2062.
122. Iliakis G, Wang Y, Guan J, Wang H. DNA damage checkpoint control in cells exposed to ionizing radiation. *Oncogene* 2003;22:5834-5847.
123. Roos WP, Kaina B. DNA damage-induced cell death by apoptosis. *Trends Mol Med* 2006;12:440-450.
124. Niida H, Nakanishi M. DNA damage checkpoints in mammals. *Mutagenesis* 2006;21:3-9.
125. Sherr CJ. Mammalian G1 cyclins and cell cycle progression. *Proc Assoc Am Physicians* 1995;107:181-186.
126. Sherr CJ. Cancer cell cycles. *Science* 1996;274:1672-1677.
127. Sherr CJ, Roberts JM. Inhibitors of mammalian G1 cyclin-dependent kinases. *Genes Dev* 1995;9:1149-1163.

128. Norbury C, Nurse P. Animal cell cycles and their control. *Annu Rev Biochem* 1992;61:441-470.
129. Booher RN, Holman PS, Fattaey A. Human Myt1 is a cell cycle-regulated kinase that inhibits Cdc2 but not Cdk2 activity. *J Biol Chem* 1997;272:22300-22306.
130. Parker LL, Piwnica-Worms H. Inactivation of the p34cdc2-cyclin B complex by the human WEE1 tyrosine kinase. *Science* 1992;257:1955-1957.
131. Poon RY, Yamashita K, Howell M, Ershler MA, Belyavsky A, Hunt T. Cell cycle regulation of the p34cdc2/p33cdk2-activating kinase p40MO15. *J Cell Sci* 1994;107 (Pt 10):2789-2799.
132. Draetta G, Eckstein J. Cdc25 protein phosphatases in cell proliferation. *Biochim Biophys Acta* 1997;1332:M53-M63.
133. van Gent DC, van der BM. Non-homologous end-joining, a sticky affair. *Oncogene* 2007;26:7731-7740.
134. Weterings E, van Gent DC. The mechanism of non-homologous end-joining: a synopsis of synapsis. *DNA Repair (Amst)* 2004;3:1425-1435.
135. Walker JR, Corpina RA, Goldberg J. Structure of the Ku heterodimer bound to DNA and its implications for double-strand break repair. *Nature* 2001;412:607-614.
136. Karanjawala ZE, Grawunder U, Hsieh CL, Lieber MR. The nonhomologous DNA end joining pathway is important for chromosome stability in primary fibroblasts. *Curr Biol* 1999;9:1501-1504.
137. Nussenzweig A, Chen C, da CS, V, Sanchez M, Sokol K, Nussenzweig MC, Li GC. Requirement for Ku80 in growth and immunoglobulin V(D)J recombination. *Nature* 1996;382:551-555.
138. Smith GC, Jackson SP. The DNA-dependent protein kinase. *Genes Dev* 1999;13:916-934.
139. Chan DW, Chen BP, Prithivirajsingh S, Kurimasa A, Story MD, Qin J, Chen DJ. Autophosphorylation of the DNA-dependent protein kinase catalytic subunit is required for rejoining of DNA double-strand breaks. *Genes Dev* 2002;16:2333-2338.
140. Meek K, Douglas P, Cui X, Ding Q, Lees-Miller SP. trans Autophosphorylation at DNA-dependent protein kinase's two major autophosphorylation site clusters facilitates end processing but not end joining. *Mol Cell Biol* 2007;27:3881-3890.

141. de Jager M, van Noort J, van Gent DC, Dekker C, Kanaar R, Wyman C. Human Rad50/Mre11 is a flexible complex that can tether DNA ends. *Mol Cell* 2001;8:1129-1135.
142. Celeste A, Fernandez-Capetillo O, Kruhlak MJ, Pilch DR, Staudt DW, Lee A, Bonner RF, Bonner WM, Nussenzweig A. Histone H2AX phosphorylation is dispensable for the initial recognition of DNA breaks. *Nat Cell Biol* 2003;5:675-679.
143. Ward IM, Minn K, Jorda KG, Chen J. Accumulation of checkpoint protein 53BP1 at DNA breaks involves its binding to phosphorylated histone H2AX. *J Biol Chem* 2003;278:19579-19582.
144. Nikjoo H, Uehara S, Wilson WE, Hoshi M, Goodhead DT. Track structure in radiation biology: theory and applications. *Int J Radiat Biol* 1998;73:355-364.
145. Riballo E, Kuhne M, Rief N, Doherty A, Smith GC, Recio MJ, Reis C, Dahm K, Fricke A, Krempler A, Parker AR, Jackson SP, Gennery A, Jeggo PA, Lobrich M. A pathway of double-strand break rejoining dependent upon ATM, Artemis, and proteins locating to gamma-H2AX foci. *Mol Cell* 2004;16:715-724.
146. Wang H, Boecker W, Wang H, Wang X, Guan J, Thompson LH, Nickoloff JA, Iliakis G. Caffeine inhibits homology-directed repair of I-SceI-induced DNA double-strand breaks. *Oncogene* 2004;23:824-834.
147. Ahnesorg P, Smith P, Jackson SP. XLF interacts with the XRCC4-DNA ligase IV complex to promote DNA nonhomologous end-joining. *Cell* 2006;124:301-313.
148. Buck D, Malivert L, de Chasseval R, Barraud A, Fondaneche MC, Sanal O, Plebani A, Stephan JL, Hufnagel M, le Deist F, Fischer A, Durandy A, de Villartay JP, Revy P. Cernunnos, a novel nonhomologous end-joining factor, is mutated in human immunodeficiency with microcephaly. *Cell* 2006;124:287-299.
149. Pardo B, Gomez-Gonzalez B, Aguilera A. DNA double-strand break repair: how to fix a broken relationship. *Cell Mol Life Sci* 2009;
150. Szostak JW, Orr-Weaver TL, Rothstein RJ, Stahl FW. The double-strand-break repair model for recombination. *Cell* 1983;33:25-35.
151. Bressan DA, Baxter BK, Petrini JH. The Mre11-Rad50-Xrs2 protein complex facilitates homologous recombination-based double-strand break repair in *Saccharomyces cerevisiae*. *Mol Cell Biol* 1999;19:7681-7687.

152. Johzuka K, Ogawa H. Interaction of Mre11 and Rad50: two proteins required for DNA repair and meiosis-specific double-strand break formation in *Saccharomyces cerevisiae*. *Genetics* 1995;139:1521-1532.
153. Llorente B, Symington LS. The Mre11 nuclease is not required for 5' to 3' resection at multiple HO-induced double-strand breaks. *Mol Cell Biol* 2004;24:9682-9694.
154. Tsubouchi H, Ogawa H. Exo1 roles for repair of DNA double-strand breaks and meiotic crossing over in *Saccharomyces cerevisiae*. *Mol Biol Cell* 2000;11:2221-2233.
155. Song B, Sung P. Functional interactions among yeast Rad51 recombinase, Rad52 mediator, and replication protein A in DNA strand exchange. *J Biol Chem* 2000;275:15895-15904.
156. Alani E, Thresher R, Griffith JD, Kolodner RD. Characterization of DNA-binding and strand-exchange stimulation properties of γ -RPA, a yeast single-strand-DNA-binding protein. *J Mol Biol* 1992;227:54-71.
157. Hays SL, Firmenich AA, Massey P, Banerjee R, Berg P. Studies of the interaction between Rad52 protein and the yeast single-stranded DNA binding protein RPA. *Mol Cell Biol* 1998;18:4400-4406.
158. Chu G. Double strand break repair. *The Journal of Biological Chemistry* 1997;272:24097-24100.
159. Wood RD. DNA repair in eukaryotes. *Annu Rev Biochem* 1996;65:135-167.
160. Lindahl T, Wood RD. Quality control by DNA repair. *Science* 1999;286:1897-1905.
161. Marti TM, Kunz C, Fleck O. DNA mismatch repair and mutation avoidance pathways. *J Cell Physiol* 2002;191:28-41.
162. Peltomaki P. DNA mismatch repair and cancer. *Mutat Res* 2001;488:77-85.
163. Kolodner RD, Marsischky GT. Eukaryotic DNA mismatch repair. *Curr Opin Genet Dev* 1999;9:89-96.
164. Hsieh P, Yamane K. DNA mismatch repair: molecular mechanism, cancer, and ageing. *Mech Ageing Dev* 2008;129:391-407.

CHAPTER 2

Kinetics of CHO A_L mutant expression after treatment with γ radiation, EMS and asbestos.

Cytometry A. 2009

Abstract

The flow cytometry mutation assay (FCMA) uses hybrid CHO A_L cells to measure mutations of the *CD59* gene located on human chromosome 11 by the absence of fluorochrome-conjugated antibody binding to the CD59 surface antigen. Mutant expression peaks between 6-12 days, then decreases to a stable plateau, instead of a constant mutant fraction obtained by clonogenic assays. To evaluate this variable mutant expression time, cells were treated with radiation, EMS or asbestos and cell proliferation and survival were measured at times leading up to peak mutant expression. Potential doubling time (T_{pot}) values increased by at least 75% for each agent by 3 hr after treatment but returned to control levels after only three days. Survival returned to 90% of control within a week, close to the peak expression day for all 3 agents. The survival of CD59⁻ cells sorted on the peak day of expression was roughly half that of CD59⁺ cells. Cloned EMS-treated CD59⁻ cells had a doubling time of 16.7 hr vs. 14.1 hr for CD59⁺

cells. Triple mutants (CD59⁻/CD44⁻/CD90⁻) were preferentially lost from the population over time, while the proportion of CD59⁻/CD90⁻ increased. In conclusion, the peak day of mutant expression occurs only when cells recover from the toxic effects of the mutagen. A fraction of cells originally quantified as mutants are lost over time due to lethal deletions and slower growth.

Keywords: mutation, CD59, CHO, flow cytometry, EMS, radiation, asbestos

Introduction

People may be exposed to a wide range of potentially genotoxic substances in the environment. Furthermore, regulatory agencies require many commercial compounds to be tested for mutagenicity prior to production (1). Since it was discovered that many mutagens are also carcinogens, there have been efforts to develop more sensitive methods to detect mutations caused by various agents, including mammalian cell assays such as the mouse lymphoma assay and Chinese hamster ovary–human hybrid (CHO A_L) assay (2-4). We and others have developed a flow cytometry mutation assay (FCMA) using the hybrid CHO A_L cell line that measures mutant yield in less than two weeks (5-7). Mutations in the *CD59* gene located on human chromosome 11 are measured by the absence of fluorochrome-conjugated antibody binding to the CD59 antigen on the cell surface, instead of relying on clonogenic survival.

We have previously characterized the sensitivity of the FCMA to detect mutations induced by a wide range of genotoxic agents, including low responders, while discriminating between true mutagens and false positives (8). Due to the significant differences in mutant detection between clonogenic assays and the FCMA, it is important to determine if mutant fractions generated by the two methods are similar. Significantly

larger mutant fractions for the same agents have been measured using the FCMA when compared to clonogenic assays such as the mouse lymphoma assay (MLA) or the HPRT, which is expected since only a small region of the p-arm of human chromosome 11 is essential for survival (9). Also, the FCMA yields much larger mutant fractions than the clonogenic CHO A_L assay when comparing the same agent (10,11), even though both assays rely on the loss of CD59 expression on the cell surface for mutant detection.

The peak day of mutant expression for various agents using the FCMA ranges from days 6 to 12 after treatment (8), whereas clonogenic assays measure a stable mutant population 3 to 6 days after treatment that does not vary over time (12). Variations in mutant expression and mutant fraction over time suggest a change in growth and/or survival characteristics of cells with mutations of the *CD59* gene. Since *CD59* is not an essential gene for the hybrid cells, deletions of the entire gene would not be expected to change cell growth characteristics. Large deletions of chromosome 11 caused by radiation are not lethal and are a significant part of the mutant fraction (13).

To elucidate why the peak day of mutant expression and the mutant fraction vary over time, we investigated growth and survival characteristics of cells treated with a wide range of mutagenic agents, including a clastogen (γ -radiation) (14), an alkylating agent (EMS) (15,16), and asbestos that indirectly acts on DNA by generating reactive oxygen species (17,18). To investigate the variation in the day of peak mutant expression, daily survival and potential doubling time (T_{pot}) (19,20) were calculated for cells after treatment to determine if mutants are maximally expressed only after cells recover from genotoxic and cellular damage. The variation in mutant fraction over time may be due to loss of cells from the population which are originally scored as CD59 negative. Thus we

measured the survival of CD59 negative cells sorted from the mutant region on the peak day of expression, as well as growth characteristics for CD59 negative clones, and compared them to CD59 positive cells.

Methods

Cell culture

The CHO A_L cells were originally obtained from C.A Waldren (Colorado State University). These cells consist of a standard set of Chinese hamster ovary K1 chromosomes as well as a single copy of human chromosome 11. Cells designated as CHO A_L(N), which we used in these experiments, contain a neomycin resistance gene on chromosome 11 which confers resistance to the antibiotic G418. By treating cells periodically with 800 µg/ml G418 antibiotic (Sigma-Aldrich, St. Louis, MO), spontaneous background mutants were reduced. Cells were cultured in Ham's F-12 nutrient mix supplemented with 10% fetal bovine serum (Gemini Bio-Products, Woodland, CA), penicillin/streptomycin (0.14 and 0.2 g/L, respectively) and 7.5% (w/v) sodium bicarbonate, pH 7.3. Cells were maintained in T75 tissue culture flasks at 37°C in a humidified 5% CO₂ incubator. The cells were passed every 3 to 4 days to avoid confluence. After 3 to 4 months of continual use, the flasks of stock cells were discarded and new cells were thawed and maintained as above.

Cell treatment

Twenty four hr prior to treatment, 4×10^5 cells were seeded in T-75 flasks so that there would be approximately 1×10^6 cells at treatment time. Cells were then treated with the following: ¹³⁷Cs γ radiation (4 Gy at 0.93 Gy/min at room temperature), ethyl methane sulfonate (EMS) (6.5 or 8 mM for 3 hr) or chrysotile "A" Rhodesian asbestos

(20 µg/ml for 24 hr). Mock treatments were used as controls. Following treatment, cells were washed twice with warm phosphate buffered saline (PBS) and given fresh medium.

Antibody labeling

Labeling for the presence of CD59 was done using phycoerythrin (PE) – conjugated mouse anti-human CD59 monoclonal antibodies (Caltag Laboratories, Burlingame, CA). The cells were first trypsinized, counted and 1×10^6 cells were transferred to 15 ml conical tubes for processing. With exception of the incubation period, the cells and buffers were kept on ice at all times prior to analysis on the flow cytometer. The tubes were then centrifuged for 3 min at 1500 rpm to pellet the cells. After aspirating the supernatant, the cells were suspended in 1 ml cold staining buffer (1% BSA, 0.1% sodium azide in PBS) and transferred to 1.2 ml microcentrifuge tubes. Following another centrifugation, the supernatant was aspirated and the cells were carefully resuspended in 50 µl staining buffer containing a 1:40 dilution of the anti-CD59 antibody. The tubes were incubated at 37° C for 30 min and subsequently washed once more in 1 ml cold staining buffer. After pelleting the cells, they were resuspended in 0.5 ml staining buffer and passed through a 40 µm nylon mesh filter into flow cytometry analysis tubes.

Analysis of T_{pot} and G2 phase

At time points ranging from 3 hr to 8 days after treatment with EMS, asbestos or radiation, non-confluent dividing cells were pulse labeled with 10 µM bromodeoxyuridine (BrdU) for 20 minutes by adding BrdU directly to the culture medium. Cells were then washed twice with warm PBS and returned to the incubator for 3 hr to allow for uptake of BrdU during DNA synthesis. After 3 hr, cells were

trypsinized, counted and 5×10^5 cells were transferred to 15 ml conical tubes for processing. Samples were centrifuged for 3 min at 1500 rpm to pellet cells. The supernatant was aspirated and the cells were resuspended in 2 ml cold PBS. The samples were then fixed by adding 5 ml cold 100% ethanol (70% final concentration) drop wise while vortexing gently. Samples were kept on ice for at least 30 min prior to denaturation and staining.

After 30 min samples were centrifuged, the supernatant was removed and cells were resuspended in 0.1 ml PBS. 2 ml of pepsin/HCl (0.2 mg/ml in 2 N HCl) was slowly added to the samples while gently vortexing and samples were incubated at 37° C for 20 min. After incubating, 3 ml of 1 M Tris was added to samples to terminate pepsin hydrolysis and the samples were centrifuged. The supernatant was aspirated and the cells were resuspended in 2 ml PBS and centrifuged again. The PBS was then aspirated and the pellet was resuspended in 100 μ l of a 1:30 dilution of the primary mouse anti-BrdU antibody (Dako, Denmark) in TBFP buffer (0.5% Tween 20, 1% BSA, 1% FBS in PBS). Samples were incubated for 25 min at room temperature and then rinsed with 5 ml PBS and centrifuged. The supernatant was decanted and the pellet was resuspended in 200 μ l of a 1:200 dilution of the secondary antibody goat anti-mouse IgG conjugated to Alexa Fluor® 488 (Molecular Probes, Eugene, OR) in deionized water and the samples were incubated for 25 min at room temperature in the dark. The samples were again rinsed with 5 ml PBS and resuspended in 1 ml of propidium iodide (PI) (10 μ l/ml in PBS) containing RNase (40 KU/ml). Samples were incubated at room temperature for 20 min prior to flow cytometry analysis.

An EPICS V (Beckman Coulter, Miami, FL) and a MoFlo™ (Beckman Coulter, Fort Collins, CO) flow cytometers were used for cell cycle experiments utilizing BrdU and PI. For the EPICS V a 488 nm laser was used for excitation along with 515 nm longpass, 590 nm dichroic, 590 nm longpass (red photomultiplier tube) and 530 nm shortpass (green photomultiplier tube) filters. Gating of forward scatter and integral red fluorescence versus peak integral red fluorescence was used to select for whole cells with incorporated PI. Histograms of PI and PI versus log integral green fluorescence (LIGFL) for 30,000 events were collected for each sample. Histograms were analyzed using MultiCycle and Multi2D software (Phoenix Flow Systems, San Diego, CA. A method to calculate Relative Movement of green fluorescent cells (S phase cells) was previously described, as well as determining time in S phase (T_s) and T_{pot} values (19,21). The percentage of cells in G2 phase was determined by analyzing the PI cell cycle distributions with MultiCycle.

Daily clonogenic survival

Cells were trypsinized, counted and plated for survival in 6-well plates from 2 to 12 days after treatment with EMS, asbestos or radiation. Three wells containing 4 ml medium were plated with 300 to 500 treated cells depending on the time after treatment and three wells were plated with 300 control cells. Cells were grown for 7 to 8 days before they were stained with crystal violet for colony counting. Control wells were used to calculate plating efficiency (PE) and surviving fraction of treated cells was calculated by (colonies / (PE x cells plated)).

Cell sorting

CD59 negative cells from the mutant region of the FCMA were isolated using a MoFlo™ Cell Sorter (Beckman Coulter, Fort Collins, CO), using the same filter set-up and gating scheme as previously published (8). Single cells were sorted into individual wells of 96-well culture plates containing 200 µl of medium. Sorted cells were grown for 18 to 21 days, replacing medium twice, until they formed visible colonies. Cloned cells were transferred by pipette to T25 tissue culture flasks, allowed to expand and passed when nearly confluent.

On the day of peak mutant expression after treatment with EMS (9 days) and γ -radiation (6 days), 300 cells were sorted from four regions of the mutant peak into 35 mm culture dishes containing 4 ml of medium using a MoFlo™ cell sorter. Cells were allowed to grow for 7 to 8 days before colonies were stained with crystal violet and counted for surviving fraction.

Mixing experiments

Single cells sorted from mutant regions 1-3 (Fig. 4A) nine days after treatment with 8 mM EMS were expanded to 11 stable CD59 negative clonal populations. Four clones were isolated from region 1, 5 clones from region 2, and 2 clones from region 3. One million cells were seeded in T75 flasks at a 1:1 ratio of isolated mutant clone cells and sorted CHO A_L control cells (CD59 positive). Cells were trypsinized, counted and passed (2×10^5) on days 3, 6 and 10 after mixing. Isolated cells were stained with CD59 specific antibodies and the number of CD59 positive and CD59 negative cells was determined by gating within flow cytometry histograms.

A CyAn™ flow cytometer (Beckman Coulter, Ft. Collins, CO) was used with a 488 nm solid-state laser for excitation and a 545 nm dichroic longpass and 575/25

bandpass filter for PE detection. A total of 1×10^5 cells were analyzed for each sample. A gating region was set on forward scatter versus side scatter to eliminate cellular debris. The photomultiplier tube voltage was set so that control CD59⁺ cells were approximately in channel 1200.

Multicolor analysis

Multicolor staining for CD59/CD90/CD44 was done as previously described (22). For CD59/CD90/CD44, cells were isolated and washed once, then suspended in 50 μ l staining solution (1.3 μ l anti-CD59-PE, 10 μ l anti-CD44-biotin (Serotec, Raleigh, NC), 10 μ l anti-CD90-Alexa647 (Serotec, Raleigh, NC) and 28.7 μ l staining buffer). Samples were incubated on ice for 30 min, then 1 ml staining buffer was added to each sample and samples were centrifuged. Samples were resuspended in 100 μ l Streptavidin-Alexa488 (1:100 dilution in staining buffer) (Molecular Probes, Eugene, OR) and were incubated on ice for 30 min. The pellet was resuspended in 0.5 ml staining buffer and passed through a 40 μ m mesh filter into flow cytometry analysis tubes. The fraction of CD59 mutants was determined by gating on 10% of the CD59⁺ peak, as discussed by Ross and Fox (22).

Results

Temporal variation in mutant expression, T_{pot} and G2 delay

The variation in the fraction of mutant cells measured by the FCMA after treatment with EMS, radiation or asbestos shows a peak in mutant expression (6-9 days) followed by a decrease over time (Fig. 1). As previously reported, the peak day of mutant expression varies for different treatments (8).

We first determined whether this variation in peak day of mutant expression was the result of alterations in cell growth or the cell cycle. By using bivariate histograms of DNA content versus BrdU incorporation, the relative movement of cells through S phase and in turn the potential doubling time of treated cells was calculated by standard methods. T_{pot} values for control cells before treatment with EMS, radiation and asbestos was determined to be 14.1 ± 1.2 hr, which corresponds well to the CHO A_L doubling time of 14.5 hr established by our lab using growth curves. T_{pot} values for cell populations more than doubled 3 hr after treatment with 8 mM EMS, increased 75 % by 6 hr after treatment with asbestos, and the percentage of cells in G2 phase more than tripled after treatment with 4 Gy γ -rays (Fig. 2). Because of the large G2 delay caused by radiation, it was not possible to get an accurate measure of T_{pot} . By day 3 after treatment normal cycling had resumed, giving T_{pot} values similar to controls, which is well before the peak day of mutant expression for all three agents. Thus, the peak day of mutant expression cannot be explained simply by alterations in cell growth.

Clonogenic survival

We next evaluated whether the variation in peak mutant expression was due to the difference in the time for the recovery of clonogenic survival. Cells were treated with 6.5 or 8.0 mM EMS, 20 μ g/ml asbestos or 4 Gy γ -radiations. At various times up to 12 days after treatment, cells were isolated and plated for clonogenic survival along with controls for each sample. After growing for 7-8 days, colonies were counted and surviving fractions were determined (Fig. 3). The survival on the peak day of mutant expression was ~96% for both 6.5 and 8.0 mM EMS, ~97% for asbestos and ~70% for cells treated

with radiation. The survival of cells treated with all agents recovered significantly from times right after treatment to the peak day of mutant expression.

Mutant region survival

The fraction of CD59 negative cells was reduced substantially after the peak day of mutant expression (Fig. 1), as previously reported (8). Cells were sorted from six regions of the mutant peak of radiation and EMS treated cells and were plated for clonogenic survival (Fig. 4A). These 6 regions were selected because we have previously shown that, while the majority of CD59 mutants are in regions 1 and 2, some mutants are also present in regions 3-6 also (22). Cells treated with 4 Gy γ -rays and isolated from region 1 had a survival of ~20% while regions 2-6 were ~50% of control cells (Fig. 4B). Cells sorted from the 6 mutant regions 9 days after treatment with 8 mM EMS had a survival of less than 40% compared to untreated control cells and only 50% of cells sorted from the positive peak, while the treated cells in the CD59⁺ peak had a survival of 80% compared to the control (Fig. 4B). However the survival of cells sorted from the 6 mutant regions 35 days after treatment with 8 mM EMS was indistinguishable from controls (Fig. 5). This suggests that a large fraction of CD59⁻ cells that are counted on the peak day of mutant expression are not viable, are lost from the population and will not be detected when samples are stained several days later.

Mixing experiment and clonal growth

To determine if CD59 mutants grew at a slower rate than CD59 positive cells, single cells sorted from mutant regions 1-3 (Fig. 4A) 9 days after treatment with 8 mM EMS were expanded to 11 stable CD59⁻ clonal populations. On days 3, 6 and 10 after mixing with CD59 positive control clones, the percentage of CD59⁻ cells in the total

population was determined by flow cytometry. By compiling the results for all 11 clones (Fig. 6) we find CD59⁻ cells are lost from the mixed population at an exponential rate. The average doubling time (T_d) of the 11 clonal populations was determined by growth curves at least 30 days after treatment with EMS to be 16.7 ± 0.9 h while the T_d for stock CHO A_L cells has been measure by our lab to be 14.5 hr. Again, it is important to note that these clones were in culture for over 30 days prior to mixing and were selected as the fastest growing clones from the 96 well plates.

Multicolor Analysis

In order to ascertain if complex mutations are lost at a disproportionate rate from the population, we measured the expression of 3 different mutations simultaneously (Fig 7). From days 6 to 24 after treatment with 8 mM EMS, CD59⁻ cells were analyzed for the presence or absence of CD90 and/or CD44 (Fig. 8). Spontaneous background mutant fractions were stable over months as follows: CD59⁻ ($13.0 \pm 5.4\%$), CD59⁻/CD44⁻ ($27.7 \pm 3.5\%$), CD59⁻/CD90⁻ ($8.0 \pm 2.6\%$) and triple mutants ($51.3 \pm 8.3 \%$). These percentages are of a total background CD59 mutant fraction of $\sim 0.3\%$ of the total population. Six days after treatment the fractions of CD59 mutants that were also negative for another marker changed dramatically. CD59 only mutants increased to about 30% of the total CD59⁻ population on day 6 but stabilized at about 10% by day 9. Triple mutants slowly decreased from 35% on day 6 to slightly more than 20% on day 24. The fraction of CD59⁻/CD44⁻ cells decreased from 28% to 12% over the same time. Finally, only 10% of CD59⁻ cells were also CD90⁻ on day 6 after treatment but rapidly increased to nearly 60% of CD59 mutants by day 24.

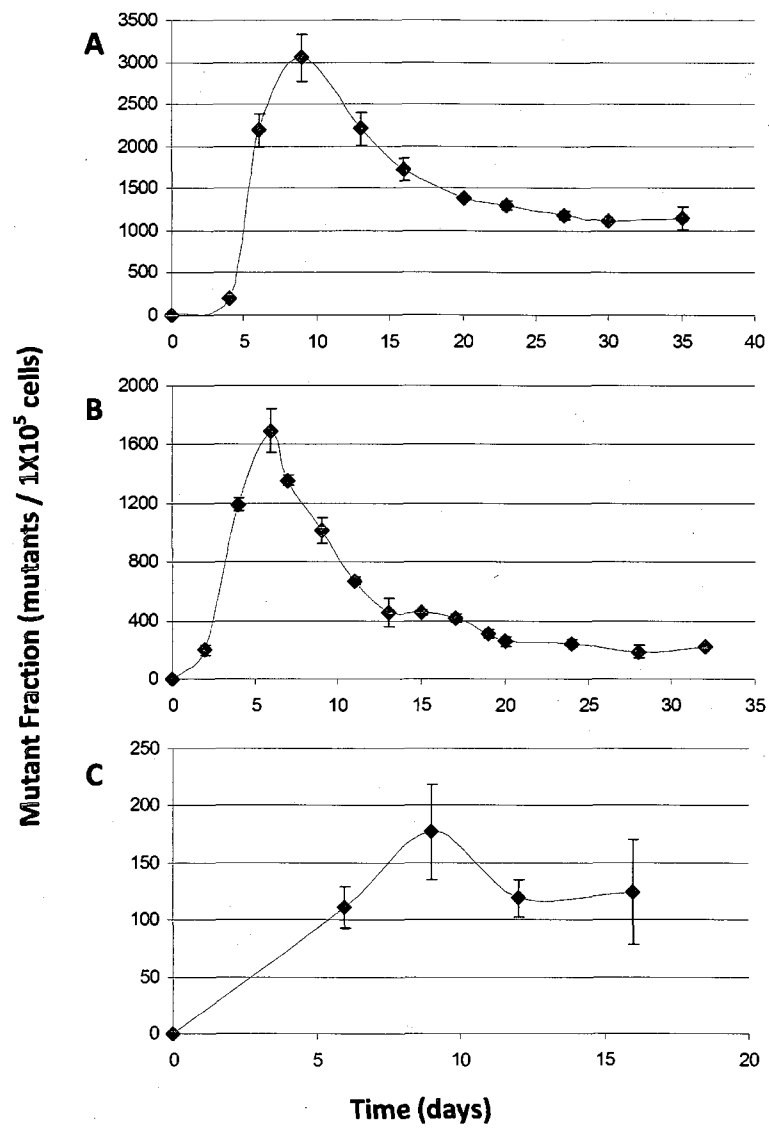


Figure 1. Mutant fraction (mutants/ 1×10^5 cells) over time for cells treated with (A) 8 mM EMS (1 experiment run in triplicate) (B) 4 Gy γ -rays (2 experiments run in triplicate) and (C) 20 μ g/ml asbestos (2 experiments run in triplicate). Error bars represent the SEM. All results are corrected for background mutants which were ~0.3-0.5%

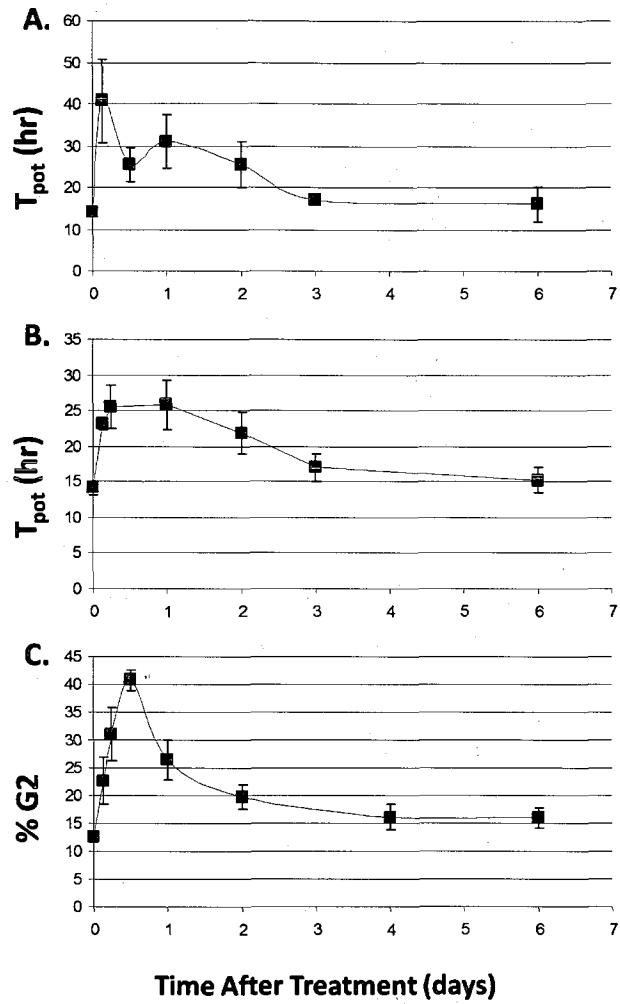


Figure 2. Potential doubling time of CHO A_L cells calculated by incorporation of BrdU after treatment with (A) 8 mM EMS (2 experiments), (B) 20 μ g/ml asbestos (2 experiments), and (C) percentage of cells in G2 phase after treatment with 4 Gy γ -rays (3 experiments). Error bars represent the SEM.

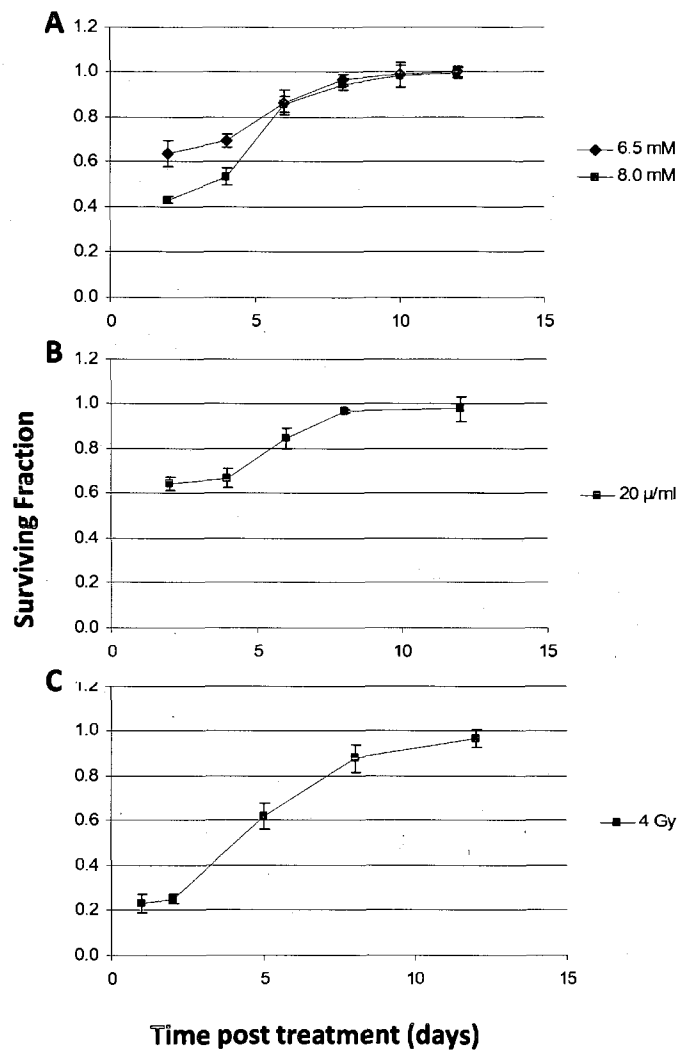


Figure 3. Clonogenic survival of CHO A_L cells at time points following treatment with (A) 6.5 and 8.0 mM EMS (1 experiment run in triplicate) (B) 20 $\mu\text{g/ml}$ asbestos (1 experiment run in triplicate) and (C) 4 Gy γ -rays (2 experiments run in triplicate). All error bars represent the standard deviation.

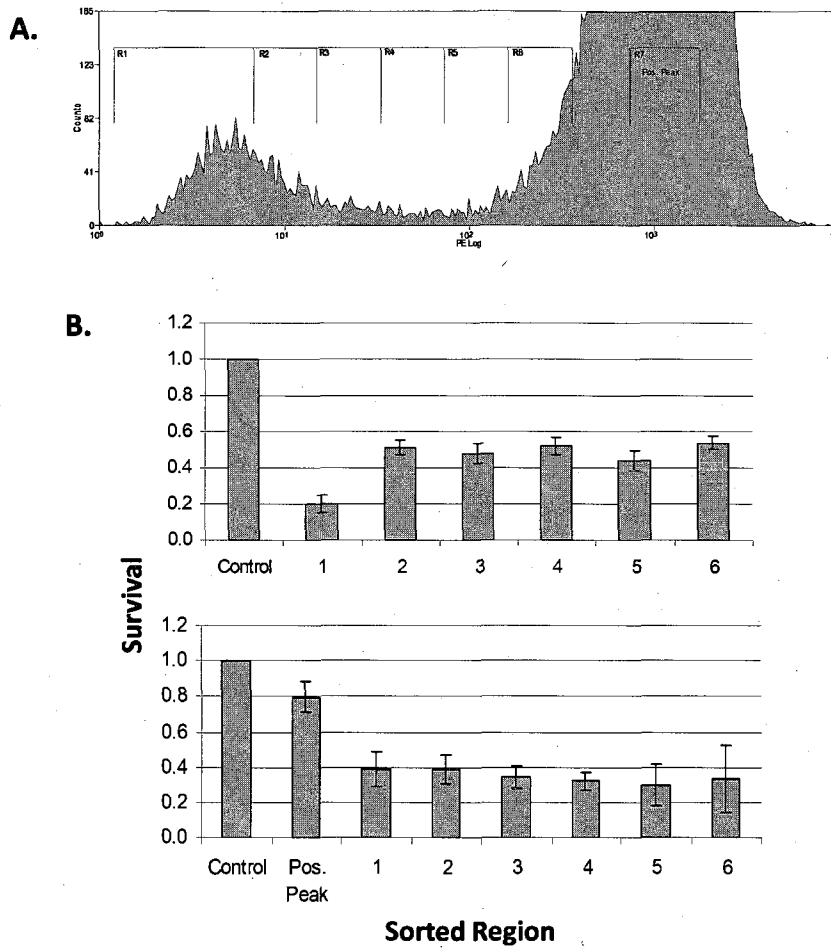


Figure 4. Clonogenic survival of cells based on CD59 expression. **(A)** Six regions of a CD59 histogram on the peak day of mutant expression after γ radiation; **(B)** surviving fraction of cells from various regions **(top)** 6 days after γ radiation (4 experiments run in triplicate, error bars represent the SEM), **(bottom)** 9 days after treatment with 8 mM EMS (3 experiments run in triplicate with error bars representing the SEM).

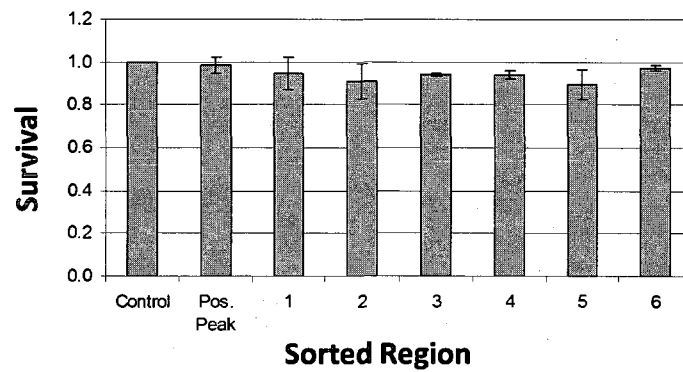


Figure 5. Clonogenic survival of cells sorted from six CD59 negative regions of the mutant peak (**Figure 4A**) on day 35 after treatment with 8 mM EMS, 26 days after the peak day of mutant expression (1 experiment run in triplicate with error bars representing the standard deviation).

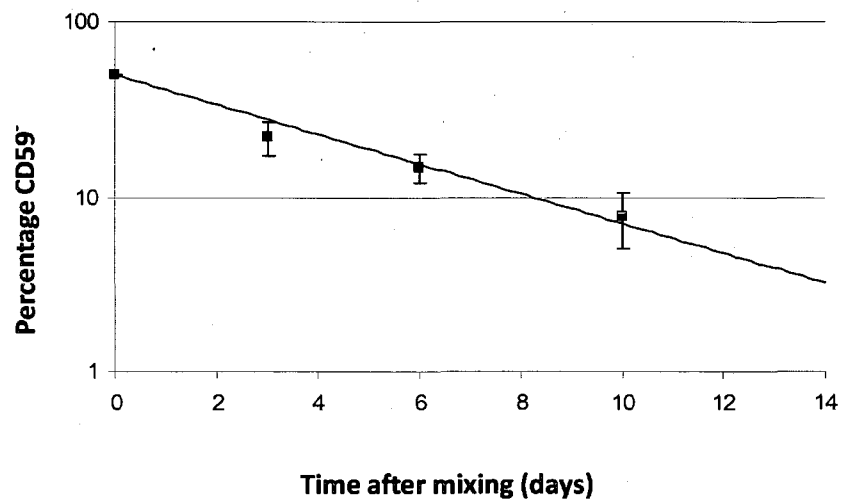


Figure 6. Rate at which 11 CD59⁻ mutant clonal populations were lost after being mixed at 1:1 ratios with CD59⁺ clonal populations. The line is the best-fit exponential ($y=50e^{-0.1955t}$) for the loss of cells from the mixed population.

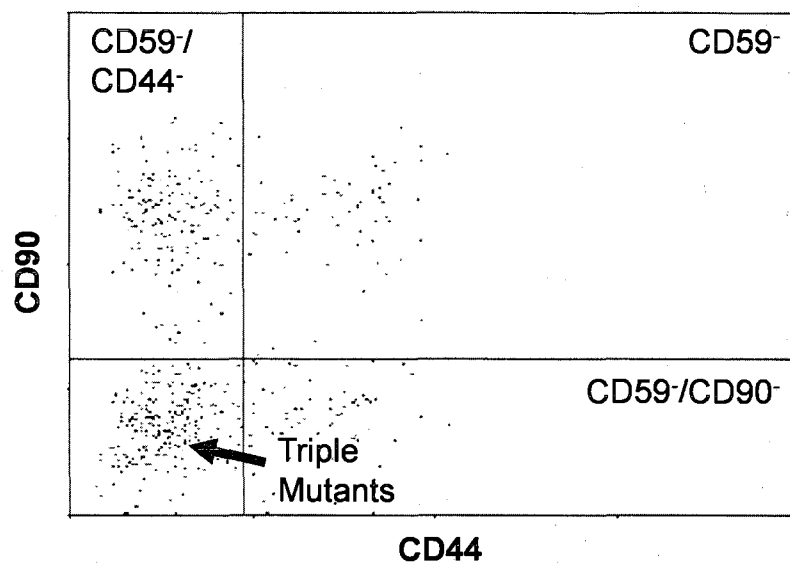


Figure 7. Bivariate histogram gated on CD59⁻ cells (Regions 1-2 in Fig 4) then analyzed for CD44 and CD90 expression 9 days after treatment with EMS.

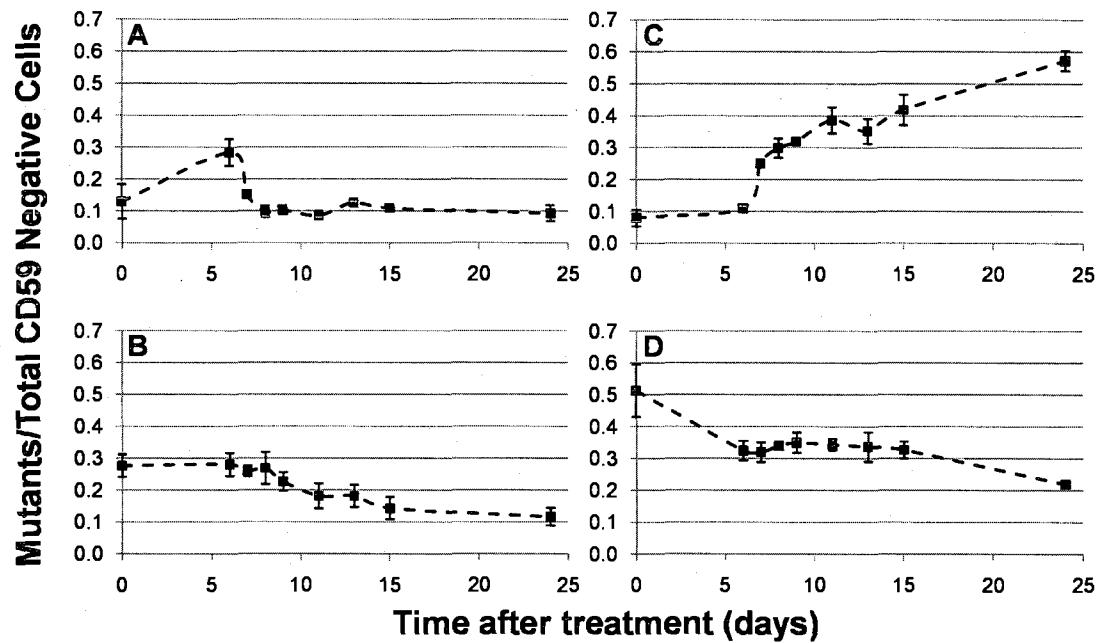


Figure 8. Fraction of CD59 negative cells scored as (A) only CD59⁻, (B) CD59⁻ and CD44⁻, (C) CD59⁻ and CD90⁻ and (D) CD59⁻, CD44⁻ and CD90⁻. Data were obtained from histograms similar to that shown in Figure 7. Two independent experiments run in triplicate with error bars representing the SEM.

Discussion

The purpose of our study was to characterize the kinetics of mutant expression measured by the FCMA by determining the causes of the variation in the peak day of mutant expression for different agents as well as the subsequent decrease in the mutant fraction over time. Logistically, differences in the peak day of expression can be overcome by sampling and measuring mutants on a range of days following treatment with a novel agent on days 6, 9 and 12 for example, which would include the peak day for mutant expression for every mutagen tested with the FCMA to date. Though this would increase the amount of time required in testing a new compound, the FCMA is already more rapid than standard assays (MLA, CHO A_L) by a matter of weeks (8).

To better understand the variation in peak mutant expression between different genotoxic agents we analyzed the clonogenic survival of cells over time after treatment, in conjunction with measuring T_{pot} and fraction of G₂ cells, to determine if peak mutant expression corresponded to a return of treated cells to untreated cell growth and survival characteristics. T_{pot} analysis for EMS and asbestos treated cells showed that normal cell proliferation resumed within 3 days after treatment. The percentage of cells in G₂ phase was calculated for irradiated cells since the well characterized G₂ block induced by radiation in mammalian cells (23) made it impossible to calculate T_{pot} . The percentage of G₂ phase cells in the irradiated population returned to control levels within three days, indicating normal cell cycling had resumed. Three days is well before the earliest peak mutant expression of day 6 for radiation, and normal cell cycling has resumed nearly a week before the peak day for cells treated with asbestos and EMS. Thus these changes in

cell growth parameters cannot fully explain the delay and variation in peak mutant expression.

Unlike cell proliferation, survival of treated cells did not return to control levels until the peak day of mutant expression (EMS and asbestos) or just after (radiation). Therefore, the time at which survival of the treated population returns to control levels can be considered a rough indicator for the maximal day of mutant expression and is supported by results for other DNA damaging agents like N-methyl-N'-nitro-N-nitrosoguanidine (MNNG) with survival at ~95% on the peak day of expression (day 12) (8). This is most likely due to the loss of cells that are destined to die from the population so the remaining cells are nearly all viable.

After the peak day of mutant expression, the mutant fraction decreased to a stable plateau. The FCMA differs from traditional mammalian mutation assays in that mutants are measured by the lack of CD59 staining instead of selective clonogenic survival, allowing for the possibility of counting dying cells, cells blocked in the cell cycle, or slower growing cells, which would not be scored in the clonogenic assays. To determine if the peak mutant fraction is artificially high due to the inclusion of cells that will ultimately die, we examined the survival of CD59⁻ and CD59⁺ cells. The survival of CD59⁻ cells on the peak day of expression after irradiation was roughly half that of CD59⁺ cells, suggesting that CD59⁻ cells would be disproportionately lost from the population as we have previously proposed. This would indicate that the plateau level is likely the fraction of mutants that are able to survive and would be similar to the mutant yield that would be measured by a clonogenic assay.

It is worth noting that the level of the plateau relative to the peak is not constant for the three different mutagens analyzed here. The plateau is about 40% of the peak for EMS, less than 20% for gamma radiation and not significantly different for asbestos. The peak levels also vary substantially. This is likely a reflection of the type of mutations caused by the three agents. Ionizing radiation is known to be a clastogen (14) which often causes very large deletions (see Ref 13 for example); EMS is an alkylating agent (15,16) that causes small mutations, though it can also cause some large deletions (manuscript in preparation); and asbestos induces ROS (reactive oxygen species) (17,18) and hence causes point mutations. It is consistent with the mechanisms that radiation would cause greater cell killing than EMS which would be greater than asbestos. The plateau levels would reflect the varying degrees of cell killing, which would explain the different peak/plateau ratios we observed.

To verify that CD59⁻ cells are disproportionately lost from populations due to growth characteristics, we mixed clonal CD59⁻ and CD59⁺ cell populations and found that mutants were rapidly lost from the population and on average had doubling times over 2 hr longer than control cells. Slowly growing mutants have also been observed in the L5178Y/TK^{+/-} Mouse Lymphoma Assay (24) and TK6 assay (25). Since the *cd59* gene is located on a nonessential copy of human chromosome 11, mutations of *cd59* and even large deletions of adjacent genes should have no effect on growth, unlike thymidine kinase assays like the MLA where deletions of adjacent genes lead to slowly growing mutants or cell death (26). It is interesting to note that our previous results with γ -radiation did not show a decreased growth rate in the mutant population (22). The difference between EMS-induced mutants and radiation-induced mutants may be that

EMS causes smaller mutations that may not kill cells but slows their growth whereas radiation causes large deletions that kill cells if mutations occur in other chromosomes besides chromosome 11.

Another factor leading to the loss of CD59⁻ cells over time may be large deletions or the loss of entire chromosome 11, including the essential region on the short arm at 11p15.5 (27). The loss of this essential region may not be immediately lethal, resulting in cells with this deletion to be lost over several weeks. The FCMA allows for the possibility of measuring multiple mutations on chromosome 11 simultaneously to better understand the mutagenic lesions caused by various genotoxic agents (22). The fraction of cells with mutations only in CD59 slightly increases on day 6 but were stable at ~10% at later times. However, complex mutants and larger deletions such as CD59⁻/CD44⁻ and triple mutants become a smaller proportion of all CD59⁻ cells over the 24 day period. On the other hand the fraction of CD59⁻/CD90⁻ mutants increased over time. Most of these mutants are not complex deletions but instead single mutations in glycosylphosphatidylinositol (GPI) anchor X-linked gene *Piga* (28). CD59 and CD90 are anchored to the extracellular membrane by GPI so cells with mutated *Piga* will be negative when stained with anti-CD59/CD90 antibodies. Of 32 EMS generated mutants that lack surface staining for both CD59 and CD90, over 90% lack GPI anchors when stained with FLAER, a bacterial toxin aerolysin conjugated to Alexa-488 (13).

The variation in the peak day of mutant expression is likely due to the difference in the amount of time needed for cells to recover from genetic insult and express the mutated phenotype. We conclude that the decrease in the mutant fraction after the peak day of expression is caused by the loss of cells destined to die that may have lost

chromosome 11 entirely and to slowly growing mutants. We have previously shown that A_L cells with triple mutants after ionizing radiation are preferentially lost from the cell population over time (22). Some cells scored as mutants with the FCMA may not be viable and would not be detected using the clonogenic assay. While these $CD59^-$ cells may not be considered true mutants since they are inviable, they do give a more accurate measure of DNA damage caused by genotoxic agents since they clearly do show that there is a higher fraction of induced mutations than would be indicated by a clonogenic assay.

Reference List

1. Thybaud V, Aardema M, Clements J, Dearfield K, Galloway S, Hayashi M, Jacobson-Kram D, Kirkland D, MacGregor JT, Marzin D, Ohyama W, Schuler M, Suzuki H, Zeiger E. Strategy for genotoxicity testing: hazard identification and risk assessment in relation to in vitro testing. *Mutat Res* 2007;627:41-58.
2. Clive D, Johnson KO, Spector JF, Batson AG, Brown MM. Validation and characterization of the L5178Y/TK \pm mouse lymphoma mutagen assay system. *Mutat Res* 1979;59:61-108.
3. Waldren C, Jones C, Puck TT. Measurement of mutagenesis in mammalian cells. *Proc Natl Acad Sci U S A* 1979;76:1358-1362.
4. Moore MM, Honma M, Clements J, Harrington-Brock K, Awogi T, Bolcsfoldi G, Cifone M, Collard D, Fellows M, Flanders K, Gollapudi B, Jenkinson P, Kirby P, Kirchner S, Kraycer J, McEnaney S, Muster W, Myhr B, O'Donovan M, Oliver J, Ouldelhkim MC, Pant K, Preston R, Riach C, San R, Shimada H, Stankowski LF, Jr.. Mouse lymphoma thymidine kinase gene mutation assay: follow-up International Workshop on Genotoxicity Test Procedures, New Orleans, Louisiana, April 2000. *Environ Mol Mutagen* 2002;40:292-299.
5. Wedemeyer N, Greve B, Uthe D, Potter T, Denklau D, Severin E, Hacker-Klom U, Kohnlein W, Gohde W. Frequency of CD59 mutations induced in human-hamster hybrid A(L) cells by low-dose X-irradiation. *Mutat Res* 2001;473:73-84.
6. Ross CD, Lim CU, Fox MH. Assay to measure CD59 mutations in CHO A(L) cells using flow cytometry. *Cytometry A* 2005;66:85-90.
7. Zhou H, Xu A, Gillispie JA, Waldren CA, Hei TK. Quantification of CD59-mutants in human-hamster hybrid (AL) cells by flow cytometry. *Mutat Res* 2006;594:113-119.
8. French CT, Ross CD, Keysar SB, Joshi DD, Lim CU, Fox MH. Comparison of the mutagenic potential of 17 physical and chemical agents analyzed by the flow cytometry mutation assay. *Mutat Res* 2006;602:14-25.
9. Kraemer SM, Waldren CA. Chromosomal mutations and chromosome loss measured in a new human-hamster hybrid cell line, ALC: studies with colcemid, ultraviolet irradiation, and ^{137}Cs gamma-rays. *Mutat Res* 1997;379:151-166.
10. Zhou H, Xu A, Gillispie JA, Waldren CA, Hei TK. Quantification of CD59-mutants in human-hamster hybrid (AL) cells by flow cytometry. *Mutat Res* 2006;594:113-119.

11. Ross, C. D. Development of a mammalian cell mutation assay based on flow cytometry and its use in analyzing mutations induced by ionizing radiation and chemicals. 2006. Colorado State University, Fort Collins, CO.
12. Liber HL, Thilly WG. Mutation assay at the thymidine kinase locus in diploid human lymphoblasts. *Mutat Res* 1982;94:467-485.
13. Ross CD, French CT, Keysar SB, Fox MH. Mutant spectra of irradiated CHO A(L) cells determined with multiple markers analyzed by flow cytometry. *Mutat Res* 2007;624:61-70.
14. Kraemer SM, Vannais DB, Kronenberg A, Ueno A, Waldren CA. Gamma-ray mutagenesis studies in a new human-hamster hybrid, A(L)CD59(+/-), which has two human chromosomes 11 but is hemizygous for the CD59 gene. *Radiat Res* 2001;156:10-19.
15. Hsie AW, Machanoff R, Couch DB, Holland JM. Mutagenicity of dimethylnitrosamine and ethyl methanesulfonate as determined by the host-mediated CHO/HGPRT assay. *Mutat Res* 1978;51:77-84.
16. Perez ML, Stamato TD. Time versus replication dependence of EMS-induced delayed mutation in Chinese hamster cells. *Mutat Res* 1999;423:55-63.
17. Unfried K, Schurkes C, Abel J. Distinct spectrum of mutations induced by crocidolite asbestos: clue for 8-hydroxydeoxyguanosine-dependent mutagenesis in vivo. *Cancer Res* 2002;62:99-104.
18. Xu A, Zhou H, Yu DZ, Hei TK. Mechanisms of the genotoxicity of crocidolite asbestos in mammalian cells: implication from mutation patterns induced by reactive oxygen species. *Environ Health Perspect* 2002;110:1003-1008.
19. White RA, Terry NHA, Meistrich ML. New methods for calculating kinetic properties of cells in vitro using pulse labelling with bromodeoxyuridine. *Cell Tissue Kinet* 1990;23:561-573.
20. Higashikubo R, Ragouzis M, Roti Roti JL. Flow cytometric BrdUrd-pulse-chase study of X-ray-induced alterations in cell cycle progression. *Cell Prolif* 1996;29:43-57.
21. Begg AC, McNally NJ, Shrieve DC, Karcher H. A method to measure the duration of DNA synthesis and the potential doubling time from a single sample. *Cytometry* 1985;6:620-626.
22. Ross CD, Fox MH. Multiparameter Analysis of CHO A(L) Mutant Populations Sorted on CD59 Expression after Gamma Irradiation. *Radiat Res* 2008;170:628-637.

23. Iliakis G, Wang Y, Guan J, Wang H. DNA damage checkpoint control in cells exposed to ionizing radiation. *Oncogene* 2003;22:5834-5847.
24. Moore MM, Clive D, Hozier JC, Howard BE, Batson AG, Turner NT, Sawyer J. Analysis of trifluorothymidine-resistant (TFTr) mutants of L5178Y/TK+/- mouse lymphoma cells. *Mutat Res* 1985;151:161-174.
25. Amundson SA, Liber HL. A comparison of induced mutation at homologous alleles of the tk locus in human cells. *Mutat Res* 1991;247:19-27.
26. Moore MM, Doerr CL. Comparison of chromosome aberration frequency and small-colony TK-deficient mutant frequency in L5178Y/TK(+/-)-3.7.2C mouse lymphoma cells. *Mutagenesis* 1990;5:609-614.
27. Kraemer SM, Kronenberg A, Ueno A, Waldren CA. Measuring the spectrum of mutation induced by nitrogen ions and protons in the human-hamster hybrid cell line A(L)C. *Radiat Res* 2000;153:743-751.
28. Miyata T, Takeda J, Iida Y, Yamada N, Inoue N, Takahashi M, Maeda K, Kitani T, Kinoshita T. The cloning of PIG-A, a component in the early step of GPI-anchor biosynthesis. *Science* 1993;259:1318-1320.

CHAPTER 3

EMS mutant spectra generated by multi-parameter flow cytometry

Abstract

The CHO A_L cell line contains a single copy of human chromosome 11 that encodes several cell surface proteins including glycosyl phosphatidylinositol (GPI) linked CD59 and CD90, as well as CD98, CD44 and CD151 which are not GPI-linked. The flow cytometry mutation assay (FCMA) measures mutations of the *CD59* gene by the absence of fluorescence when stained with antibodies against the CD59 cell surface protein. We have measured simultaneous mutations in CD59, CD44, CD90, CD98 and CD151 to generate a mutant spectrum for ionizing radiation. After treatment with ethyl methanesulfonate (EMS) many cells have an intermediate level of CD59 staining. Single cells were sorted from CD59⁻ regions with varying levels of fluorescence and the resulting clonal populations had a stable phenotype for CD59 expression. Mutant spectra were generated by flow cytometry using the isolated clones and nearly all clones were mutated in *CD59* only. Interestingly, about 60% of the CD59 negative clones were actually GPI mutants determined by staining with the GPI specific fluorescently labeled bacterial toxin aerolysin (FLAER). The GPI negative cells are most likely caused by mutations in the X-linked *pigA* gene important in GPI biosynthesis. Small mutations of *pigA* and *CD59* were expected for the alkylating agent EMS and the resulting spectra are

significantly different than the large deletions found when analyzing radiation mutants. After analyzing the CD59⁻ clonal populations we have adjusted the FCMA mutant regions from 1% to 10% of the mean of the CD59 positive peak to include the majority of CD59 mutants.

Introduction

We have previously characterized the flow cytometry mutation assay (FCMA) as a sensitive and rapid method of measuring the genotoxicity of known and unknown chemical and physical agents (1-3). The FCMA uses the CHO A_L cell line that has an incorporated human chromosome 11 as well as the entire hamster genome. This cell line was originally used in the standard complement based CHO A_L clonogenic mutation assay (4,5). Chromosome 11 contains genes encoding cell surface proteins including CD59, mutations of which are scored by the absence of fluorescence when stained with phycoerythrin (PE) - conjugated monoclonal antibodies against CD59. Individual mutants can be sorted and cloned for further analysis. Additional genes on chromosome 11 encode proteins that are expressed on the surface of the cells, including CD44, CD90, CD98 and CD151. These genes are not encoded by the normal hamster genome, only by human chromosome 11. By measuring the presence or absence of these proteins also, it is possible to generate mutant spectra using flow cytometry (6) more rapidly and efficiently than spectra generated by PCR (7,8) and Southern Blot (9). The term "mutant spectra" is used here to indicate the distribution of mutations in genes along chromosome 11 indicated by the loss of surface expression of the gene product. We have previously shown that the loss of the surface protein expression is completely correlated with the loss of the respective gene(s) based on PCR results (6).

We previously defined the mutant region of the FCMA as cells with fluorescence less than 1% of the mean fluorescence of the positive peak (2). This was a conservative measurement and we subsequently showed that many cells mutated in *CD59* by the clastogen gamma radiation (10) were not being scored in that region (11), suggesting that a larger region should be used. In that report we also showed that the mutants that initially have an intermediate level of fluorescence lose *CD59* expression over time to background (unstained) control levels of fluorescence (11). The complete loss of fluorescence can be explained by large deletions within or encompassing the *CD59* gene so no *CD59* protein is expressed on the plasma membrane.

Since ionizing radiation is a clastogen and is well known to cause large deletions, it is important to identify whether other mutagens that primarily cause small mutations would generate similar mutants. In this report we investigate *CD59*⁻ populations and clones generated by exposure to the known alkylating agent ethyl methanesulfonate (EMS) (12,13) that are believed to be mostly point mutations. Point mutations allow for mutated conformations of *CD59* on the cell surface and in turn intermediate staining, suggesting that a larger region should be used for mutant detection. Furthermore, these point mutations should lead to stable phenotypes of *CD59* fluorescence that would not reduce to background levels over time.

Many cell surface proteins including *CD59* are linked to the cell membrane by glycosyl phosphatidylinositol (GPI) anchors (14,15). Interestingly, many *CD59*⁻ clones, including nearly all *CD59*⁻/*CD90*⁻ clones, were found to be negative for GPI anchors when stained with the GPI protein specific fluorochrome conjugated toxin aerolysin

(FLAER) (16). The lack of GPI linkage is most likely due to the mutation of *piga*, an X-linked GPI biosynthesis protein (17).

In this paper we analyze clones with intermediate CD59 fluorescence and subsequently generate mutant spectra. Our results show that the mutant region of the FCMA should be enlarged to encompass more of the CD59⁺ region, making an even more sensitive assay. Also, by having the ability to generate mutant spectra using flow cytometry we are able to rapidly and with accuracy determine the nature of mutations generated by novel agents.

Materials and Methods

Cell Culture

The CHO A_L(N) cell line contains the entire Chinese hamster KI cell line genome with an incorporated copy of human chromosome 11 including a gene conferring resistance to the antibiotic G418 (Sigma-Aldrich, St. Louis, MO). By treating cells periodically with 800 µg/ml G418, spontaneous background mutants were reduced. Cells were cultured in Ham's F12 medium supplemented with 10% fetal bovine serum (Gemini Bio-Products, Woodland, CA), penicillin/streptomycin (0.14 and 0.2 g/L, respectively) and 7.5% (w/v) sodium bicarbonate, pH 7.3. Cells were trypsinized and passed every three to four days to avoid confluence that can increase the background mutant fraction. Cells were maintained in humidified 5% CO₂ incubators at 37° C.

Treatment with EMS

One day prior to treatment, 4x10⁵ cells were seeded in T-75 flasks, giving approximately 1x10⁶ cells at treatment time. Cells were treated with 8 mM ethyl methanesulfonate (EMS) (CAS number 62-50-0) diluted in F12 medium for 3 hr in 37° C

incubators. This dose results in 20% survival of cells (2). After the treatment, cells were washed twice with warm PBS and F12 medium was replaced.

Antibody Labeling

One million cells were stained for CD59 using phycoerythrin (PE)-conjugated mouse anti-human CD59 monoclonal antibodies (Caltag Laboratories, Burlingame, CA) as previously described (1,2).

Multicolor staining for CD59/CD90/CD44 and CD98/CD151 was carried out separately as previously described (6). For CD59/CD90/CD44 analysis, cells were suspended in 50 μ l staining solution (1.3 μ l anti-CD59-PE, 10 μ l anti-CD44-biotin (Serotec, Raleigh, NC), 10 μ l anti-CD90-Alexa-647 (Serotec, Raleigh, NC) and 28.7 μ l staining buffer), incubated on ice for 30 min, then 1 ml staining buffer (1% BSA, 0.1% sodium azide in PBS) was added to each sample and samples were centrifuged. Samples were resuspended in 100 μ l Streptavidin-Alexa-488 (Molecular Probes, Eugene, OR) (1:100 dilution in staining buffer) and were incubated on ice for 30 min. The pellet was resuspended in 0.5 ml staining buffer and passed through a 40 μ m mesh filter into flow cytometry analysis tubes. Separately, cells were stained with 50 μ l staining solution containing 10 μ l anti-CD151-PE (BD Biosciences, San Jose, CA), 10 μ l anti-CD98-FITC (BD Biosciences, San Jose, CA) and 30 μ l staining buffer.

The GPI-anchor was detected using the bacterial toxin aerolysin conjugated to Alexa-488 at a concentration of 10 nM per sample. Cells were resuspended in 250 μ l FLAER (Protox Biotech, Victoria, Canada) (1:10 dilution in staining buffer) and were then incubated for 30 min on ice (6).

Flow Cytometry

Samples were analyzed on a CyAn™ flow cytometer (Beckman Coulter, Fort Collins, CO) with 488 and 635 nm solid-state lasers for excitation. Fluorescence was detected by the following filter configuration: 545 nm dichroic longpass (DLP) and 575/25 nm bandpass (BP), 545 nm DLP and 530/40 nm BP for Alexa-488 and 650 nm DLP and 665/20 nm BP for Alexa-647. The same PMT voltages were used for various experiments and the fluorescence intensities of positive and negative control populations were stable over time. A gating region was set on forward scatter versus side scatter to eliminate debris. When analyzing clonal populations for the presence of CD59, 5×10^4 to 1×10^5 events were collected per sample and all populations were sampled twice at least one week apart, while multicolor analysis was completed only once.

Cell Sorting

Using an Epics V cell sorter, 1000 anti-CD59-PE stained cells were sorted into 35 mm Petri dishes from 6 CD59 negative regions and one region of the CD59 positive peak 9 days after treatment with 8 mM EMS. Sorted populations were expanded in dishes for 7 days and then transferred to T-75 flasks to keep in culture. When the populations were stable they were stained again with anti-CD59-PE and single cells were sorted into 96 well plates from 4 regions using a MoFlow™ Cyclone (Beckman Coulter, Fort Collins, CO). Clones were allowed to grow for 18-21 days with one refeeding of 200 μ l F12. Clones were transferred to T-25 flasks for continuous culturing.

In a separate experiment, a MoFlo™ Cyclone was used to sort single cells into 96 well plates from 4 regions of the CD59 negative population and 1 region of the positive

peak 9 days after treatment with 8 mM EMS. Clones were grown for 18-21 days with one refeeding and then were transferred to T-25 flasks for culturing.

Results

Mutant Populations

One thousand cells were sorted from six CD59⁻ regions (Fig. 1) 9 days after treatment with 8 mM EMS to determine if they remain negative and have fluorescence levels similar to their sorted regions. The sorted cells were expanded into populations and were stained several times over the course of several weeks for CD59 and were indeed found to be comprised of stable populations (Fig. 2). Population A is almost completely negative while the opposite is true for populations E and F. The populations sorted from the middle regions of B, C and D contains the entire spectrum of CD59⁻ to CD59⁺ cells. It is important to note that these populations remained stable and had very similar profiles while remaining in culture for several months.

The populations B, C and D were chosen for sorting because they are heterogeneous in fluorescence when stained for CD59. Single cells were sorted from 4 CD59 negative regions (Fig. 2) into 96 well plates and the expanded populations were stained for CD59 twice over several weeks to determine if clonal populations are stable in fluorescence intensity. All clonal populations remained fluorescently stable over several weeks with intensities well within the same order of magnitude (Fig. 3).

The average CD59 staining fluorescence was calculated for the four regions of populations B, C and D by averaging the intensities of all clones sorted from the regions (Fig. 4). Negative controls were unstained stock cells while positive controls were the same stock cells stained for CD59. The fluorescence of region 4 of populations B, C and

D were all significantly lower than positive controls with values of $p=0.001$, $p<0.001$ and $p=0.03$ respectively. Also, fluorescence of clones sorted from regions 1 through 4 increases in order for all three populations, demonstrating that clones have fluorescence levels relative to the region from which they were sorted. After initial analysis of the clones, they were continuously grown in culture for 1-2 weeks and then re-analyzed to determine that the fluorescence intensity was stable.

Mutant Region Sorting

In a separate set of experiments we sorted single cells directly from four CD59 negative regions and the positive peak (Fig. 5A) 9 days after treatment with 8 mM EMS, and expanded them into stable clonal populations. Region 1 represents 1% of the mean positive peak or the region used to score for CD59 mutants with the FCMA, while regions 2, 3 and 4 are between the mutant region and the positive peak. Clones were stained for CD59 and average fluorescence was calculated for each region (Fig. 5B). The average fluorescence for regions 1-3 were all significantly less than that of the positive peak while region 4 was nearly significant ($p=0.055$).

EMS Mutant Spectrum

Cells were sorted directly from the mutant region (1% of the mean of the positive peak) of stock CHO A_L cells and were expanded into 23 stable clonal populations. The background mutant fraction in this region is approximately 0.1%. Clones were then stained for the presence of CD59, CD44, CD90, CD151 and CD98, generating a mutant spectrum of spontaneous background mutants (Fig. 6). Of the 23 clones over half are negative for both CD59 and CD44 which can most easily be explained as a deletion encompassing both genes that are less than 2 Mbp apart. Five of the background mutants

were found to be positive only for CD151, which could be the result of a large deletion encompassing nearly the entire chromosome. Interestingly, 5 mutants were negative for both CD59 and CD90 only and, as will be discussed, are likely GPI mutants.

Clones isolated from regions 1-4 of populations B, C and D (Fig. 2) were analyzed in the same manner as background mutants to generate a mutant spectrum of EMS generated mutants. Along with the five CD surface proteins, clones were also stained with FLAER, which is a GPI anchor specific toxin conjugated to a fluorochrome that can detect the presence of GPI anchors in the cell membrane.

Of the 16 clones isolated from the 4 regions of population B only 1 was positive for CD59 with fluorescence slightly less than half of control stained cells (Fig. 7). Nine clones were CD59 negative only while 6 clones were negative for both CD59 and CD90 but also FLAER, pointing to mutations in the GPI anchor instead of chromosome 11. Twenty clones were isolated from the 4 CD59⁻ regions of population C. Only one clone was positive for CD59 (in region 4), 5 of the 20 clones were only CD59 negative but 14 of the 20 clones are negative for CD59, CD90 and the GPI anchor (FLAER). Of the 17 clones isolated from the 4 regions of population D, two clones were complex, including a large deletion and one clone with mutations in both CD59 and CD90 independently (Fig. 7). Also, 9 clones from population D were GPI mutants, 3 were CD59 negative while 3 were CD59 positive. It is important to note that nearly all of the CD59⁺ clones came from region 4 which is on the tail of the distribution of positive cells. Thus, these may represent cells that are outliers of the normal distribution and not true mutants.

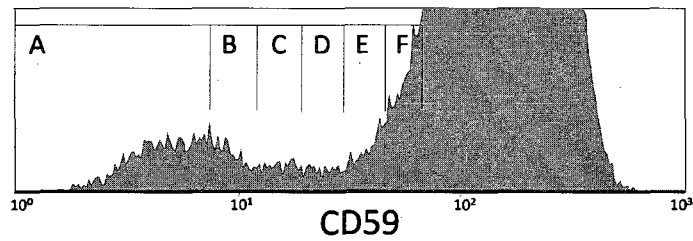


Figure 1. (A) CHO A_L cells stained for CD59 9 days after treatment with 8 mM EMS. Six regions (A-F) were set for sorting cells with varying levels of CD59 fluorescence. Region A is the mutant region, $\leq 1\%$ of the mean of the positive peak.

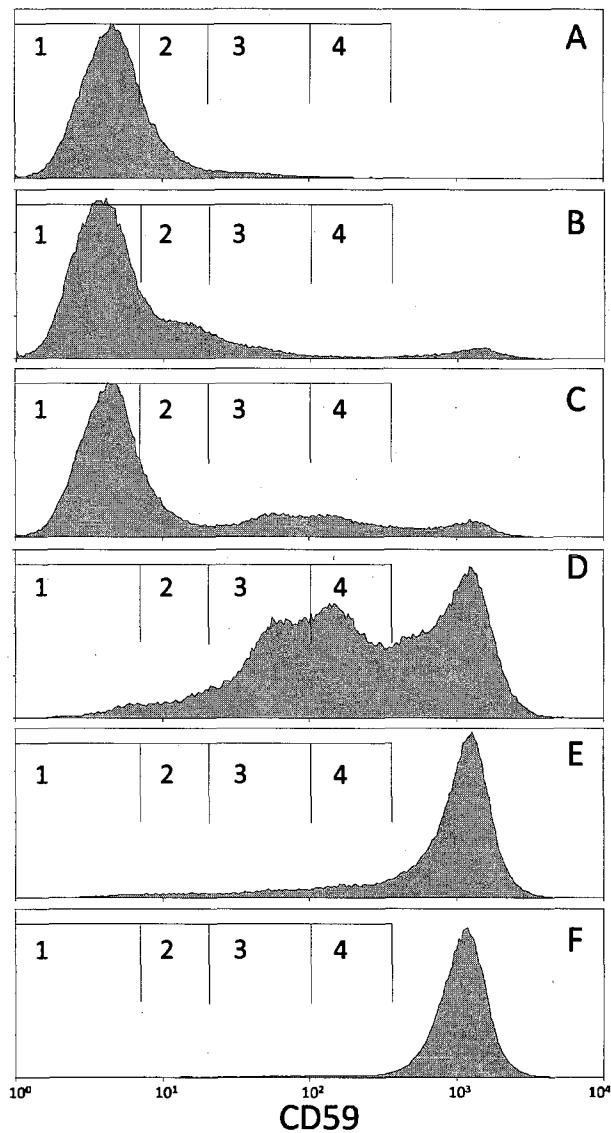


Figure 2. 1000 cells each were sorted from regions A-F and expanded into stable populations. Individual cells were then sorted from regions 1-4 from populations B, C and D and were expanded into stable clonal populations. The X-axis represents the fluorescence intensity of anti-CD59-stained cells and the Y-axis is the relative number of cells.

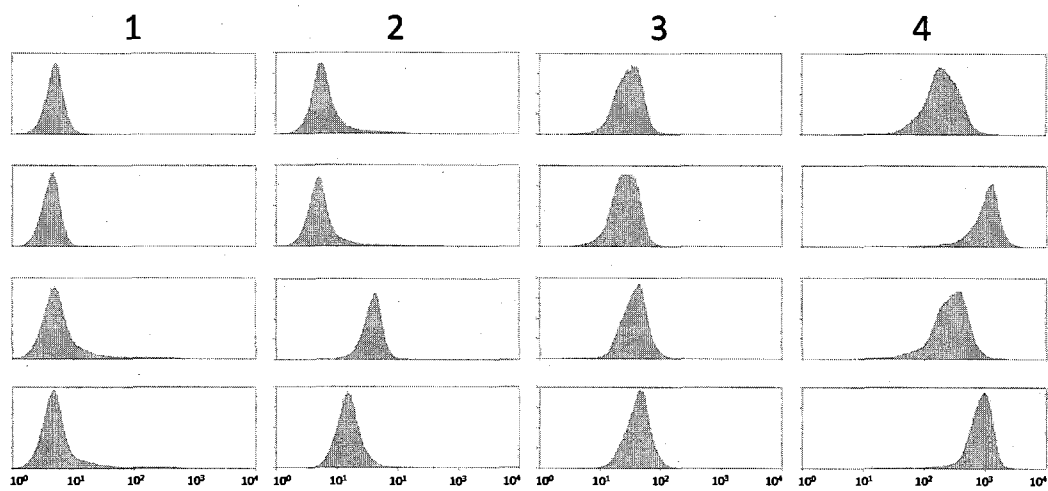


Figure 3. Examples of individual clonal populations grown from single cells sorted from regions C1-4 shown in Figure 1. The X-axis in each histogram is the fluorescence intensity of anti-CD59-stained cells and the Y-axis is the relative number of cells.

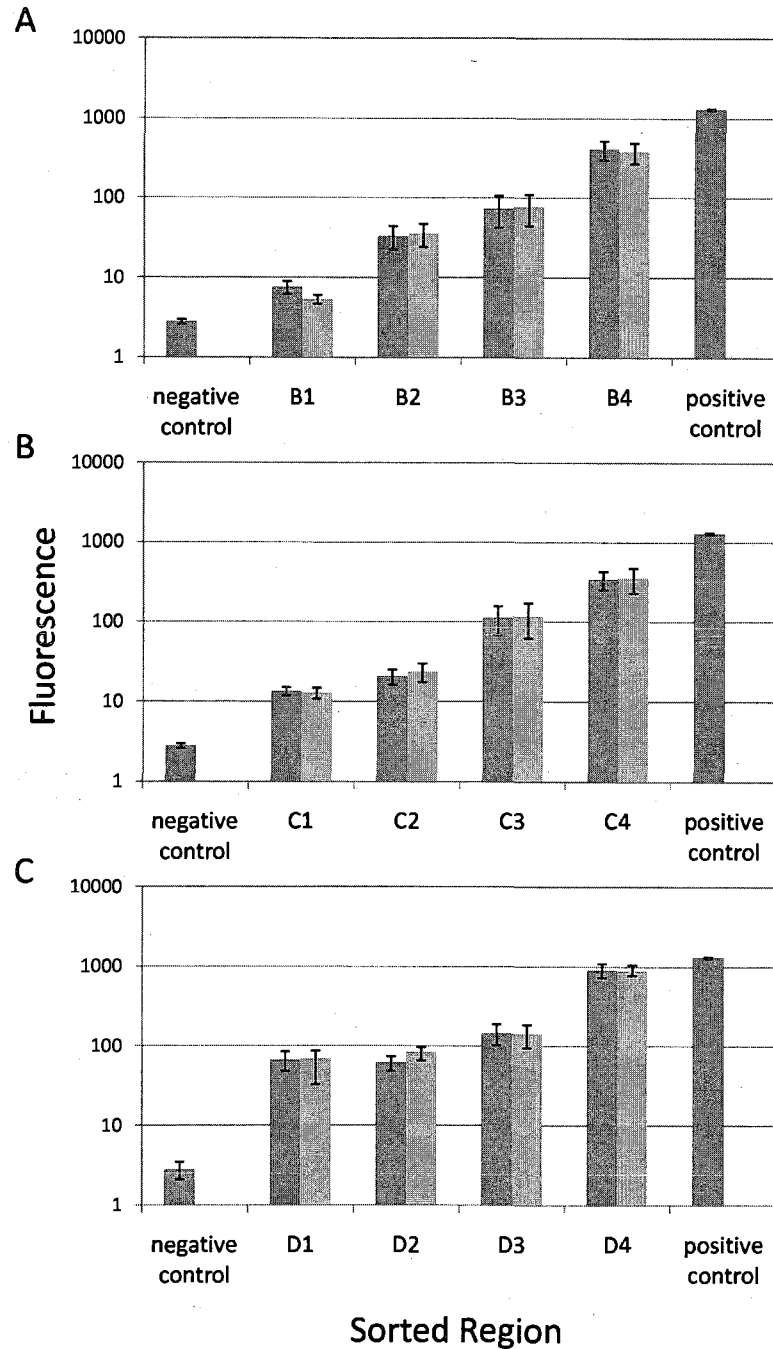


Figure 4. The average fluorescence for clones grown from individual cells sorted from the 4 CD59⁻ regions populations B, C and D in Fig. 1. Each histogram represents from 6-12 separate clones. Positive and negative controls are stained and unstained stock cells respectively. The dark bars are for cells analyzed initially and the light bars are for cells analyzed 1-2 weeks later after continuous culture. A) Clones from Fig. 1.B.B; B) Clones from Fig. 1.B.C.; C) Clones from Fig. 1.B.D. Error bars represent the standard error of the mean (SEM).

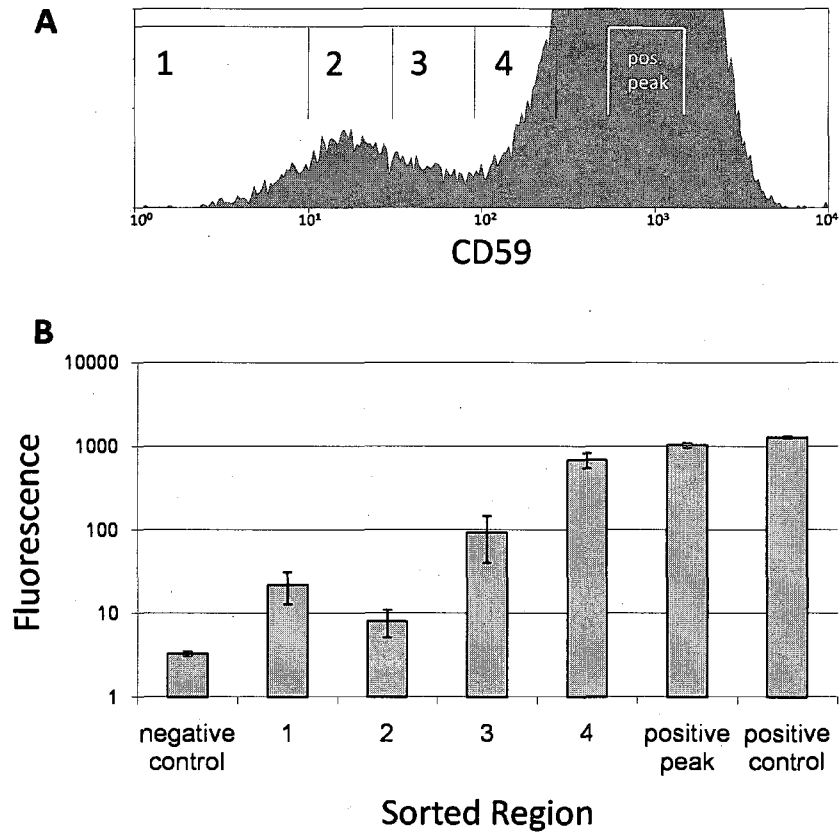


Figure 5. (A) Individual cells were sorted directly from 4 CD59⁻ regions and the positive peak of cells 9 days after treatment with 8 mM EMS. (B) Isolated clonal populations were stained for CD59 and the average fluorescence from 8-14 clones was calculated for each region. Error bars represent the SEM.

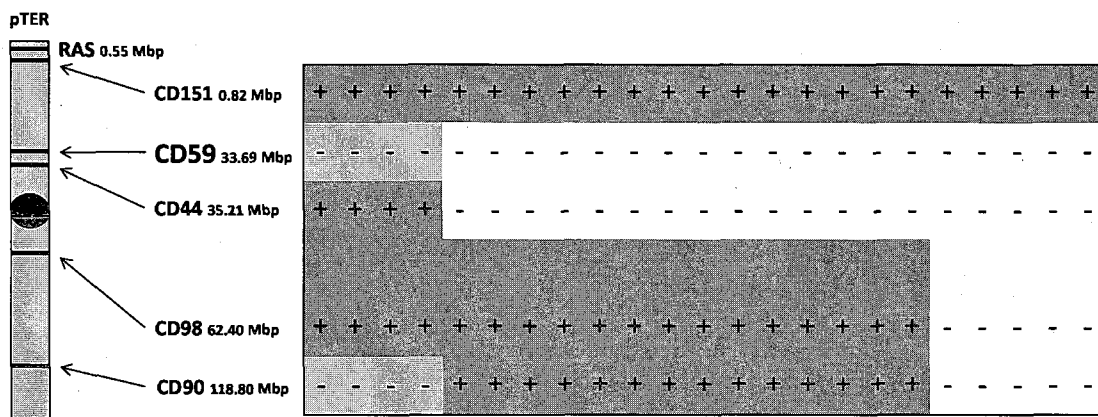


Figure 6. Flow cytometry generated mutant spectrum for clones isolated from the mutant region (1% of the mean of the positive peak) of untreated stock CHO A_L cells. Dark regions stained positive for the CD marker and white regions were negative and are likely mutations. Chromosomal distances are measured from the p-terminus.

Region B

	1			2			3			4			
CD151	+	+	+	+	+	+	+	+	+	+	+	+	+
CD59	-	-	-	-	-	-	-	-	-	-	-	-	+
CD44	+	+	+	+	+	+	+	+	+	+	+	+	+
CD98	+	+	+	+	+	+	+	+	+	+	+	+	+
CD90	-	+	+	-	-	+	-	+	+	+	-	-	+
FLAER	-	+	+	-	-	+	-	+	+	+	-	-	+

Region C

	1			2			3			4			
CD151	+	+	+	+	+	+	+	+	+	+	+	+	+
CD59	-	-	-	-	-	-	-	-	-	-	-	-	+
CD44	+	+	+	+	+	+	+	+	+	+	+	+	+
CD98	+	+	+	+	+	+	+	+	+	+	+	+	+
CD90	-	-	-	-	-	-	-	-	+	-	-	+	+
FLAER	-	-	-	-	-	-	-	-	+	-	-	+	+

Region D

	1			2			3			4			
CD151	+	+	+	+	+	+	+	+	+	+	+	+	+
CD59	-	-	-	-	-	-	-	-	-	-	+	-	+
CD44	-	+	+	+	+	+	+	+	+	+	+	+	+
CD98	-	+	+	+	+	+	+	+	+	+	+	+	+
CD90	-	-	-	+	-	-	-	-	-	-	+	+	+
FLAER	+	-	-	+	-	-	-	-	-	-	+	+	+

Figures 7. Flow cytometry generated mutant spectrum for clones isolated from 4 regions of populations B, C and D from Fig. 1. Cells were stained for five surface antigens as well as for the presence of GPI anchors using FLAER. Dark regions stained positive for the CD marker while white regions were negative and are likely mutations. The medium shade represents GPI mutants, which are also negatively stained for CD59 and CD90 since they are GPI linked proteins.

Discussion

Traditional clonogenic mutations assays are based on the ability of mutated cells to survive and multiply when challenged, which in itself can be very time consuming on the order of several weeks to more than a month (18-20). Generating a mutant spectrum using PCR with DNA isolated from clones after running a traditional mutation assay (7) or the FCMA (6) is possible but it adds significantly more time and can be difficult to get all reactions working simultaneously. In this paper we propose that detecting mutations caused by genotoxic agents is much less time consuming and more sensitive using the FCMA and the newly defined mutant regions. Also, we suggest as we have previously reported (6) that flow cytometry generated mutant spectra are not only faster, but simpler and possibly more accurate for DNA damaging agents. Furthermore, we have previously validated the flow cytometry mutant spectra with PCR (6). Because of the lack of availability of a complete set of labeled antibodies that could be run simultaneously for all 5 markers plus FLAER, we were not able to actually do a complete mutant spectrum in one analysis. However, we have shown that in principle this could be done, given the availability of the proper antibodies. This would make the flow cytometry based assay even more rapid and flexible.

To determine if varying degrees of DNA damage cause different levels of CD59 expression, CD59⁻ cells were isolated. By sorting populations of cells from the mutant region 9 days after treatment with EMS we show that, unlike previously reported results for ionizing radiation where cells were entirely negative or positive for CD59 (11), EMS generates mutants with intermediate levels of CD59 expression that remain stable. This conspicuous difference in CD59⁻ cells generated by radiation and EMS is likely due to

the way each agent acts on DNA. Radiation is known to cause double strand breaks leading to deletions (21,22), leading to the complete loss of CD59 expression on the cell surface while EMS is an alkylating agent often generating base substitutions (12,13), which could lead to changes in protein folding and in turn antibody affinity for CD59 on the protein surface. This in turn would lead to varying levels of expression of fluorescence in this flow cytometry based assay.

To further understand the intermediate expression of EMS generated *CD59* mutants, and to determine if their fluorescence is stable over time, individual cells were isolated from four *CD59⁻* regions. The resulting clonal populations were stained twice for *CD59* with cells grown for 1-2 weeks between staining, resulting in very little variation in their fluorescence. This stability further supports our hypothesis that these cells with intermediate *CD59* expression are mutants that consistently express a mutated phenotype of the *CD59* protein and not wild-type *CD59* with protein levels changing on the cell surface over time, which would cause fluorescence to vary. The average fluorescence of these clones increases from regions 1 to 4 and are significantly less than positive controls, meaning all four regions are negative in some degree for *CD59*. Clones isolated from the *CD59⁻* region of cells 9 days after treatment with EMS support our findings that *CD59* mutants are stable and are not just a result of having been sorted previously into populations.

The background mutant spectrum we obtained from cells sorted from the mutant region of stock CHO *A_L* cells supports our previous hypothesis (11) that most spontaneous mutants are larger deletions. All of the isolated mutants were found to be mutated in more than just *CD59*: 13 were also *CD44* mutants while 5 were large

deletions only positive for *CD151*. It is very unlikely to find many *CD151* mutants since it is relatively close to an essential gene needed for cell survival located on the end of the p-arm of chromosome 11 (8,23). It is important to note that the 4 mutants that were found to be negatively stained for both CD59 and CD90 are likely not mutated independently in both genes but are instead mutations in an X-linked GPI linkage gene, as discussed below.

The mutant spectra we obtained from individual mutant clones treated with EMS were quite different from either background mutants or those induced by ionizing radiation that we have previously reported (6). Almost all of the mutants were mutations only in the *CD59* gene or GPI mutants that are also most likely single small mutations. We have previously used the fluorescently labeled inactive variant of the protein aerolysin (FLAER) (6), which is a bacterial toxin that binds GPI anchor proteins (16,24), to distinguish between clonal populations with *CD59* mutations and ones with mutated GPI linkage genes after ionizing radiation. The most probable cause in the loss of GPI linkage would be a mutation in the X-linked hamster gene *pigA*, which encodes an important protein for the biosynthesis of GPI anchors (17). It can also be assumed that GPI mutants would also be small since *pigA* is X-linked and a large deletion could encompass neighboring genes that are essential for survival. Small mutations in *pigA* would also explain why some cells have an intermediate expression of CD59. There could still be partially functional GPI linkage but less efficient than normal, so there is still some expression of CD59 on the surface of some of the cells that are mutated in *pigA*.

It is interesting to note that greater than 60% of the clones analyzed when generating the mutant spectra for EMS were found to be GPI mutants and is a much

greater fraction than the ~16% found for mutants generated by radiation (6). This discrepancy may have several explanations; first, radiation causes large deletions which are of no consequence when they occur along chromosome 11, which for the most part is not essential for survival, while large deletions of *pigA* on the X chromosome would often be lethal. Secondly, we have reported that CD59⁻ cells that are likely GPI mutants increase from a small fraction to the majority of total CD59⁻ cells measured with the FCMA over several weeks (3). This increase could be caused by the importance of GPI linkage in the cell membrane for proper cell death signaling (25,26) allowing GPI mutants that would normally die to propagate.

We propose that generating mutant spectra by flow cytometry is not only much faster but can also be more accurate than PCR. Proper antibody binding requires both the presence of protein and correct folding compared to PCR, which can easily miss point mutations since only the presence of the two primer specific regions are necessary for positive results. Although sequencing of the genes of interest to generate a mutant spectrum would be more accurate than PCR or flow cytometry, it would not be time or cost effective for many clones, leaving flow cytometry as the best option, especially when studying novel agents.

When originally developing the FCMA, we defined the mutant region as 97% of unstained control cells which we later changed to 1% of the mean of the positive peak (2). Here we propose to set the standard mutant region for the FCMA at 10% of the mean of the CD59 positive peak. This change is supported by the results from sorting from the CD59⁻ regions and specifically the mutant spectra where nearly all of the clonal populations from regions 1-3 (Fig. 2) were negative for CD59. We have reported similar

results with mutants induced by ionizing radiation (11). Using this larger region for mutant detection with the FCMA will give a better estimate of the mutant yield and will be less sensitive to day to day fluctuations in antibody staining and detection.

Reference List

1. Ross CD, Lim CU, Fox MH. Assay to measure CD59 mutations in CHO A(L) cells using flow cytometry. *Cytometry A* 2005;66:85-90.
2. French CT, Ross CD, Keysar SB, Joshi DD, Lim CU, Fox MH. Comparison of the mutagenic potential of 17 physical and chemical agents analyzed by the flow cytometry mutation assay. *Mutat Res* 2006;602:14-25.
3. Keysar SB, Fox MH. Kinetics of CHO AL mutant expression after treatment with radiation, EMS and asbestos. *Cytometry A* 2009;
4. Waldren C, Jones C, Puck TT. Measurement of mutagenesis in mammalian cells. *Proc Natl Acad Sci U S A* 1979;76:1358-1362.
5. Waldren C, Correll L, Sognier MA, Puck TT. Measurement of low levels of x-ray mutagenesis in relation to human disease. *Proc Natl Acad Sci* 1986;83:4839-4843.
6. Ross CD, French CT, Keysar SB, Fox MH. Mutant spectra of irradiated CHO A(L) cells determined with multiple markers analyzed by flow cytometry. *Mutat Res* 2007;624:61-70.
7. Waldren CA, Ueno AM, Schaeffer BK, Wood SG, Sinclair PR, Doolittle DJ, Smith CJ, Harvey WF, Shibuya ML, Gustafson DL, Vannais DB, Puck TT, Sinclair JF. Mutant yields and mutational spectra of the heterocyclic amines MeIQ and PhIP at the S1 locus of human-hamster AL cells with activation by chick embryo liver (CELC) co-cultures. *Mutat Res* 1999;425:29-46.
8. Kraemer SM, Kronenberg A, Ueno A, Waldren CA. Measuring the spectrum of mutation induced by nitrogen ions and protons in the human-hamster hybrid cell line A(L)C. *Radiat Res* 2000;153:743-751.
9. Liber HL, Call KM, Little JB. Molecular and biochemical analyses of spontaneous and X-ray-induced mutants in human lymphoblastoid cells. *Mutation Research* 1987;178:143-153.
10. Ward JF. DNA damage produced by ionizing radiation in mammalian cells: identities, mechanisms of formation, and reparability. *Prog Nucleic Acid Res Mol Biol* 1988;35:95-125.
11. Ross CD, Fox MH. Multiparameter Analysis of CHO A(L) Mutant Populations Sorted on CD59 Expression after Gamma Irradiation. *Radiat Res* 2008;170:628-637.
12. Beranek DT. Distribution of methyl and ethyl adducts following alkylation with monofunctional alkylating agents. *Mutat Res* 1990;231:11-30.

13. Mientjes EJ, Luiten-Schuite A, van der WE, Borsboom Y, Bergmans A, Berends F, Lohman PH, Baan RA, van Delft JH. DNA adducts, mutant frequencies, and mutation spectra in various organs of lambda lacZ mice exposed to ethylating agents. *Environ Mol Mutagen* 1998;31:18-31.
14. Bodian DL, Davis SJ, Morgan BP, Rushmere NK. Mutational analysis of the active site and antibody epitopes of the complement-inhibitory glycoprotein, CD59. *The Journal of Experimental Medicine* 1997;185:507-516.
15. Nichols BJ, Kenworthy AK, Polishchuk RS, Lodge R, Roberts TH, Hirschberg K, Phair RD, Lippincott-Schwartz J. Rapid cycling of lipid raft markers between the cell surface and Golgi complex. *J Cell Biol* 2001;153:529-541.
16. Brodsky RA, Mukhina GL, Li S, Nelson KL, Chiurazzi PL, Buckley JT, Borowitz MJ. Improved detection and characterization of paroxysmal nocturnal hemoglobinuria using fluorescent aerolysin. *Am J Clin Pathol* 2000;114:459-466.
17. Miyata T, Takeda J, Iida Y, Yamada N, Inoue N, Takahashi M, Maeda K, Kitani T, Kinoshita T. The cloning of PIG-A, a component in the early step of GPI-anchor biosynthesis. *Science* 1993;259:1318-1320.
18. Clive D, Johnson KO, Spector JF, Batson AG, Brown MM. Validation and characterization of the L5178Y/TK+/- mouse lymphoma mutagen assay system. *Mutat Res* 1979;59:61-108.
19. Combes RD, Stopper H, Caspary WJ. The use of L5178Y mouse-lymphoma cells to assess the mutagenic, clastogenic and aneugenic properties of chemicals. *Mutagenesis* 1995;10:403-408.
20. Liber HL, Thilly WG. Mutation assay at the thymidine kinase locus in diploid human lymphoblasts. *Mutat Res* 1982;94:467-485.
21. Sankaranarayanan K. Ionizing radiation and genetic risks. III. Nature of spontaneous and radiation-induced mutations in mammalian in vitro systems and mechanisms of induction of mutations by radiation. *Mutat Res* 1991;258:75-97.
22. Waldren C, Correll L, Sognier MA, Puck TT. Measurement of low levels of x-ray mutagenesis in relation to human disease. *Proc Natl Acad Sci* 1986;83:4839-4843.
23. Kraemer SM, Waldren CA. Chromosomal mutations and chromosome loss measured in a new human-hamster hybrid cell line, ALC: studies with colcemid, ultraviolet irradiation, and ¹³⁷Cs gamma-rays. *Mutat Res* 1997;379:151-166.

24. Hong Y, Ohishi K, Inoue N, Kang JY, Shime H, Horiguchi Y, van der Goot FG, Sugimoto N, Kinoshita T. Requirement of N-glycan on GPI-anchored proteins for efficient binding of aerolysin but not Clostridium septicum alpha-toxin. EMBO J 2002;21:5047-5056.
25. Barcellini W, Fermo E, Guia IF, Zaninoni A, Bianchi P, Boschetti C, Zanella A. Increased resistance of PIG-A- bone marrow progenitors to tumor necrosis factor a and interferon gamma: possible implications for the in vivo dominance of paroxysmal nocturnal hemoglobinuria clones. Haematologica 2004;89:651-656.
26. Szpurka H, Schade AE, Jankowska AM, Maciejewski JP. Altered lipid raft composition and defective cell death signal transduction in glycosylphosphatidylinositol anchor-deficient PIG-A mutant cells. Br J Haematol 2008;

CHAPTER 4

Hypoxia induced mutations in mammalian cells detected by the flow cytometry mutation assay and characterized by mutant spectra

Abstract

It has been recognized for decades that oxygen interacts with free radicals induced by low LET radiation and “fixes” much of the resulting DNA damage, thus sensitizing the cells to radiation. Under hypoxic conditions, cells are more resistant to cell killing by a factor of 2.5 to 3, leading to detrimental consequences for the radiotherapy of tumors. Recently it has emerged that hypoxic conditions alone are sufficient to generate mutations *in vitro* and *in vivo*, likely due to the creation of reactive oxygen species (ROS) and a decrease in mismatch and homologous recombination DNA repair activity. These factors are known precursors to the onset of genetic instability and a reduced prognosis for cancer treatment. We have previously characterized the flow cytometry mutation assay (FCMA) and its sensitivity to detect significant mutant fractions induced by genotoxic agents that are not detected by other mammalian assays. Here we measure the mutant fraction induced by hypoxia. Cells cultured at $<0.1\%$ O_2 for 24 hr generated a significant mutant fraction of 141 ± 20 ($p < 0.01$) and had growth kinetics and survival characteristics similar to that obtained by other mutagens. We investigated the role of

ROS by treating cells with the radical scavenger DMSO, which significantly reduced hypoxia toxicity and mutagenesis. Single cells were sorted from the mutant region of both control and treated cells and the resulting clonal populations were stained for 5 antigens encoded by genes found along chromosome 11 to generate mutant spectra. There was no significant difference found between background and hypoxia-induced spectra. We have demonstrated that hypoxic conditions are sufficient to generate mutations in mammalian cells in culture and the spectrum of mutations is indistinguishable from background.

Introduction

The negative effects of the hypoxic tumor environment on cancer treatment and prognosis, specifically in the area of radiotherapy, have been discussed for nearly 80 years (1,2). Decreased oxygen in the environment significantly reduces cell killing by ionizing radiation, leading to an increased dose required to successfully treat the tumor (3). Recently, it has been reported that hypoxic stress itself can increase mutagenesis and genetic instability in cell lines, human tissues and tumors (4).

Several pathways for hypoxia-induced mutagenesis have been proposed, including DNA damage generated by reactive oxygen species (ROS) produced by reoxygenation (5) and leakage from mitochondria (6). DNA repair activity has also been reported to decrease in hypoxic cells and tissues, specifically in homologous recombination repair (HRR) (7,8) and mismatch repair (MMR) pathways (9). Hypoxia induced mutagenesis and suppressed repair can lead to genetic instability and more aggressive tumors (10,11). To date hypoxia-induced mutagenesis has not been quantified using traditional mammalian mutation assays.

The use of flow cytometry to detect mutations in the *CD59* gene of CHO A_L cells has been developed by several groups independently (12-14) and we have used the flow cytometry mutation assay (FCMA) to measure the mutagenic potential of a broad spectrum of physical and chemical agents (15). The CHO A_L cell line was traditionally used in the CHO A_L complement cytotoxicity assay (16-18), which is based on the loss of expression of the CD59 antigen encoded by the *CD59* gene found on the single copy of the incorporated human chromosome 11 (19). The FCMA scores mutants by the absence of fluorescence when stained with fluorochrome conjugated monoclonal antibodies specific for the CD59 surface protein, while the A_L assay utilizes CD59 specific antibodies and complement to kill CD59⁺ cells.

We also developed a method to generate mutant spectra for clonal populations sorted from the mutant region of cells after treatment by staining for 5 cell surface proteins that are expressed by genes located along the entire length of human chromosome 11 (20). Mutant spectra generated in this manner are more rapidly produced than those created using PCR (21) and when compared are equally accurate (20). Here we show that hypoxia induces significant mutant fractions as measured by the flow cytometry and CHO A_L mutation assays. The radical scavenger DMSO increases survival and decreases mutagenesis in cells cultured under severely hypoxic conditions. We also compare the mutant spectra for background and cells kept under hypoxic conditions.

Materials and Methods

Cell culture

CHO A_L(N) cells consist of a standard set of Chinese hamster ovary K1 chromosomes as well as a single copy of human chromosome 11, which contains a neomycin resistance gene that confers resistance to the antibiotic G418. By treating cells periodically with 800 µg/ml G418 antibiotic (Sigma-Aldrich, St. Louis, MO), spontaneous background mutants were reduced. Cells were cultured in Ham's F-12 medium supplemented with 10% FBS, penicillin/streptomycin (0.14 and 0.2 g/L, respectively) and 7.5% (w/v) sodium bicarbonate, pH 7.3. Medium used in the CHO A_L assay was supplemented in 3% FBS and 4% newborn calf serum. Cells were maintained in T75 tissue culture flasks at 37°C in a humidified 5% CO₂ incubator as described previously (15).

Hypoxia treatment

A Forma Scientific water jacketed incubator with thermal, CO₂ and oxygen control was used to obtain 2.5% to 0.1% oxygen environments. An incubator insert chamber C-274 PRO-OX Model 110 and PRO-CO₂ (BioSpherix, Redfield, NY) was used to obtain oxygen levels of 0.1%. For oxygen levels <0.1% a BBL™ GasPak™ Plus Anaerobic System (BD, Sparks, MD) was used and within 100 min of the start of the treatment oxygen levels decreased to <0.1%. The day prior to treatment 2.5x10⁵ to 4x10⁵ cells were seeded in 100 mm Petri dishes. Cells were plated with minimal medium to reduce the amount of diffused oxygen present at treatment. Petri dishes were placed in the hypoxic system for the desired period.

Certain samples were treated with the radical scavenger dimethyl sulfoxide (DMSO). Two hr prior to hypoxia treatment DMSO was diluted (0.5% v/v) in F-12

medium and added to culture plates. 12 hr after the end of hypoxia treatment medium containing DMSO was replaced with fresh medium.

CHO A_L complement cytotoxicity assay

After completion of hypoxia treatment cells were cultured for 10 days to allow for recovery of the temporary growth lag as described (16,22). Cells were then challenged with 2% rabbit serum as a complement (Covance Research Products Inc., Denver, PA), and 0.5% E7.1, a specific monoclonal antibody against the CD59 antigen. Surviving cells able to form colonies were counted as mutants. The mutant yield was adjusted for the plating efficiency and background mutants.

Antibody staining for FCMA

Cells (1×10^6) were trypsinized, centrifuged and the resulting pellets were suspended in 1 ml FACS buffer (1% BSA, 0.1% sodium azide in PBS). Cells were centrifuged a second time and stained with anti-CD59 monoclonal antibodies conjugated to phycoerythrin (PE) (Caltag Laboratories, Burlingame, CA) at a 1:40 dilution in FACS and were incubated at 37° C for 1 hour. One ml cold FACS was then added to the cells and they were again centrifuged, the supernatant was aspirated and cells were finally suspended in 0.5 ml cold FACS and filtered through 40 μ m mesh into flow cytometry sample tubes on ice prior to analysis.

Multicolor staining for mutant spectrum

Clonal populations were stained simultaneously for CD59, CD44 and CD90 and separately for CD151 and CD98 as previously reported (20). Cells (1×10^6) were stained with 1.25 μ l CD59-PE, 10 μ l CD90-Alexa 647, 10 μ l CD44-biotin and 28.75 μ l FACS buffer on ice for 30 min. After incubating, 1 ml FACS was added and cells were

centrifuged and the supernatant was aspirated. Samples were then stained with 1 μ l Alexa 488 Streptavidin and 99 μ l FACS and incubated on ice for 30 min. Other samples were similarly stained with 10 μ l CD98-FITC, 10 μ l CD151-PE and 30 μ l FACS for 30 min. on ice. After incubating 1 ml of buffer was added, samples were centrifuged and resuspended in 1 ml FACS and filtered into flow cytometry tubes.

Flow cytometry

A CyAn ADP flow cytometer with 488 and 635 nm lasers (Beckman Coulter, Fort Collins, CO) was used for quantification of mutant fractions and analysis of mutant clones. The CD59⁻ mutant regions were gated as 1% of the mean of the positive control peak on a log scale. For the mutation assay as well as clonal analysis, 1×10^5 cells from each sample were analyzed on the CyAn. Mutant regions for all other antigens were set as 97% of the negative unstained control peak and clones were scored negative for antigens if more than 80% of the clonal population fell within the region.

Mutant region sorting

Samples were stained for the presence of CD59 and single CD59 negative, positive or control cells were sorted into 96 well plates containing 200 μ l F12 medium 12 days after hypoxia treatment using a MoFlo High-Performance Cell Sorter (Beckman Coulter, Fort Collins, CO). Cells were allowed to form colonies in 96 well plates with one re-feeding. After 21 days clones were transferred to T25 plates and expanded until there were enough cells for flow cytometric analysis of the five antigens.

Clonogenic survival

From days 2 to 12 after hypoxia treatment cells were trypsinized, counted and plated for survival in 6-well plates. Three wells containing 4 ml medium were plated

with 300 to 500 treated cells depending on the time after treatment and three wells were plated with 300 control cells. Cells were grown for 7 to 8 days before they were stained with crystal violet for colony counting. Control wells were used to calculate plating efficiency (PE) and surviving fraction of treated cells was calculated by (colonies / (PE x cells plated)).

Results

Hypoxia mutant yield in the complement cytotoxicity CHO A_L assay

A survival curve was generated for cells cultured under severely hypoxic conditions (<0.1% oxygen) from 1 to 43 hr (not shown) and it was determined that the time required to achieve 50% survival was 24 hr. Using the CHO A_L complement cytotoxicity assay, mutant yields for cells cultured at oxygen levels of 2.5% (4 and 7 days), 1% (4 and 7 days) and 0.1% (4 days) were not significantly different when compare to background (Fig. 1). However, cells cultured at <0.1% oxygen for 24 hr demonstrated a significant ($p<0.05$) induction of mutations with 130 mutants per 1×10^5 cells.

FCMA hypoxia mutant yield

In order to verify these results from the cytotoxicity mutation assay, we treated cells with hypoxia and measured the mutant yield using the FCMA. After a 24 hr hypoxia treatment cells were cultured for 12 days, isolated and then stained with antibodies against CD59. After staining, cells were run on a flow cytometer and the mutant region was set at 1% of the CD59 positive peak (Fig. 2). The resulting mutant fractions are displayed in Fig. 3. The mutant fraction from hypoxia is significantly different from controls 141 ± 20 ($p<0.01$).

Effects of DMSO on survival and mutagenesis

We hypothesized that damage from ROS might be causing the mutations induced by hypoxia. To test this, we treated cells with DMSO, a free radical scavenger. DMSO had no toxicity on control cells but did increase the survival of cells cultured under hypoxic conditions (Fig. 6A). Cells treated concurrently with DMSO and hypoxia had reduced mutant yields in the FCMA than cells treated with hypoxia alone (Fig. 6B)

Mutant region survival

We have previously reported that the survival of cells sorted from the mutant regions on the peak day of mutant expression after treatment with EMS or gamma radiation was less than cells sorted from the CD59⁺ peak of the same population (23). The surviving fraction for the CD59⁻ region was significantly less than the treated positive peak with a p value of 0.02 (Fig. 5). Also, the surviving fractions of cells sorted from the CD59⁺ regions of hypoxia treated cells were lower than that of the positive peak of untreated stock cells. These results are similar to what has been found with other agents.

Daily clonogenic survival

We have previously shown that the return to control survival of treated cells is an indicator of the peak day of mutant expression after treatment with genotoxic agents (23). Cells were sorted from hypoxia treated and control populations from days 2-12 after treatment and grown into colonies for survival analysis. Two days after treatment, survival was only ~60% of controls but had returned to >90% by day 12 (Fig. 6) the peak day of mutant expression for hypoxia treated cells.

Mutant spectra

To determine if hypoxia generates mostly small intragenic mutations or large multi-locus mutations, individual cells were sorted for the mutant regions of hypoxia treated cells as well as untreated control cells and grown into clones. The resulting 23 control and 25 hypoxia treated stable clonal populations were then analyzed by flow cytometry for the presence of CD59, CD44, CD90, CD151 and CD98 on the cell surface to generate background and hypoxia-induced mutant spectra (Fig. 7).

All background mutants isolated from the mutant region of untreated control cells were negative for more than 1 surface protein; 17% were CD59⁻/CD90⁻, ~60% were CD59⁻/CD44⁻ and ~20% were negative for all antigens except for CD151. The mutant spectrum for clones isolated from the hypoxia treated population was similar to that of background mutants except for a higher proportion of cells missing all markers except CD151. Of the 25 hypoxia generated mutant clones, 4% were CD59⁻ only, 12% were CD59⁻/CD90⁻, 40% were CD59⁻/CD44⁻, 4% were CD59⁻/CD44⁻/CD98⁻ and 40% were negative for all antigens except for CD151.

Discussion

DNA damage and the resulting mutations are the known precursors to cellular transformation and tumorigenesis (24). The mutagenic and carcinogenic potential of many chemical and physical agents have been characterized using mammalian cell mutation assays (15,16,25). Hypoxia decreases the mutagenic potential of ionizing radiation since the presence of oxygen helps to “fix” (make permanent) DNA damage (3). Nevertheless it has been reported recently that hypoxic stress, both *in vivo* and *in vitro*, can generate DNA damage and mutations (6,10).

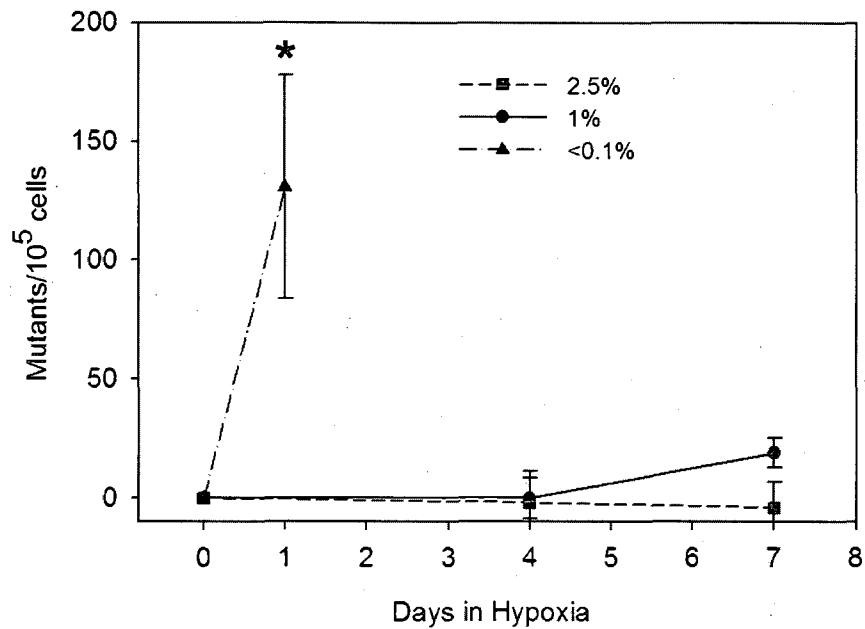


Figure 1. Mutant yield (mutants/1x10⁵ cells) using the CHO A_L complement cytotoxicity mutation assay for cells cultured under hypoxic conditions (<0.1% - 2.5% oxygen) for 1 to 7 days (minimum of three experiments run in triplicate). Mutant yield is corrected for background and the error bars represent the standard error of the mean. * significant at p<0.05.

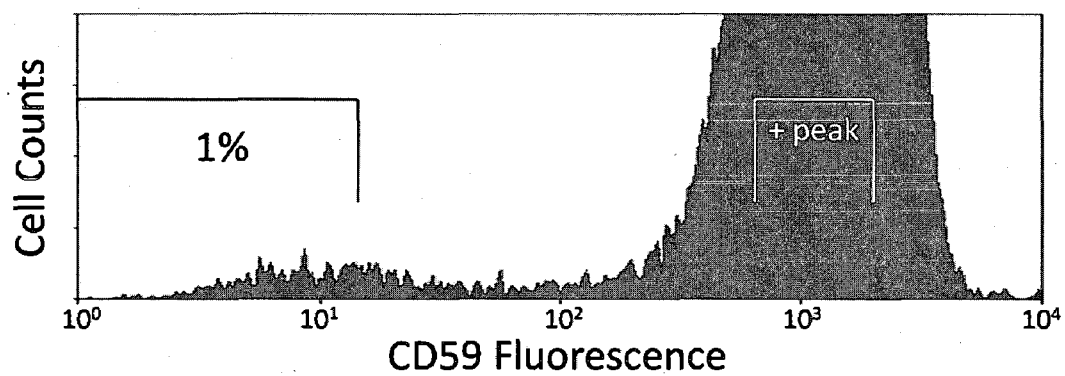


Figure 2. Example histogram of CHO A_L cells stained with PE conjugated monoclonal antibodies against CD59 12 days after a 24 hr $<0.1\%$ oxygen hypoxia treatment. Gating is set as 1% of the mean of the positive peak for hypoxia treated cells.

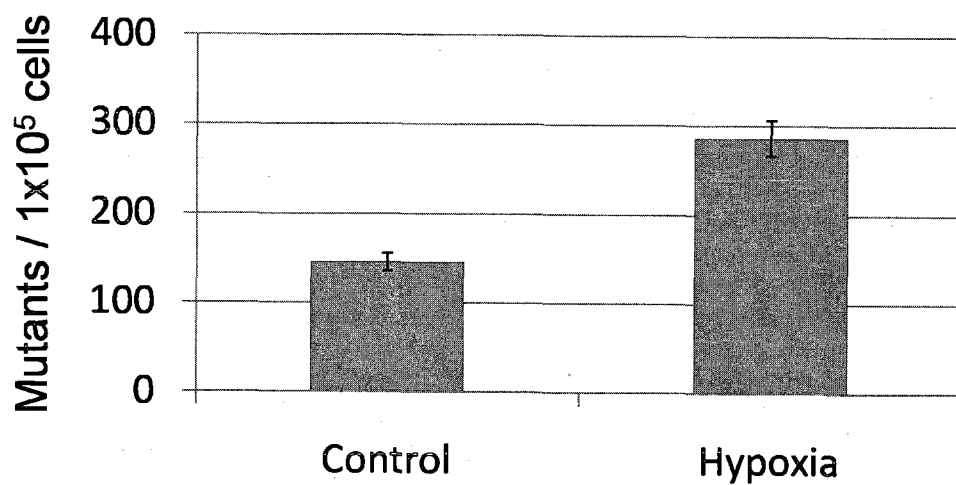


Figure 3. Mutant yield (mutants/1x10⁵ cells) for control and cells cultured at <0.1% oxygen for 24 hr. Results are from 3 experiments run in triplicate and error bars represent the standard error of the mean and results are significant at p<0.01.

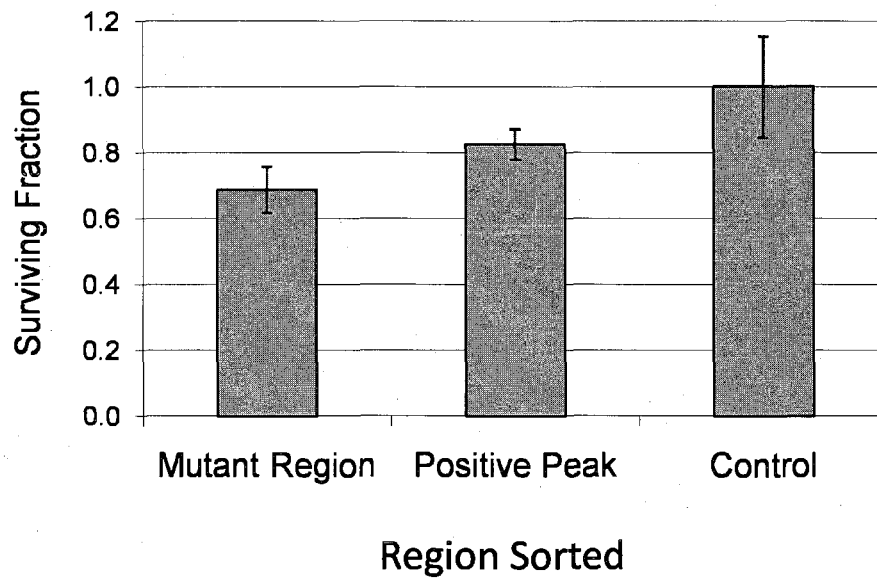


Figure 4. Clonogenic survival relative to control cells sorted from the 1% mutant region and positive peak 12 days after cells were cultured in hypoxic conditions (<0.1% oxygen) for 24 hr. Four replicates of 300 cells were sorted from each region and were cultured for 7-8 days to allow for colony formation. All error bars represent the standard deviation.

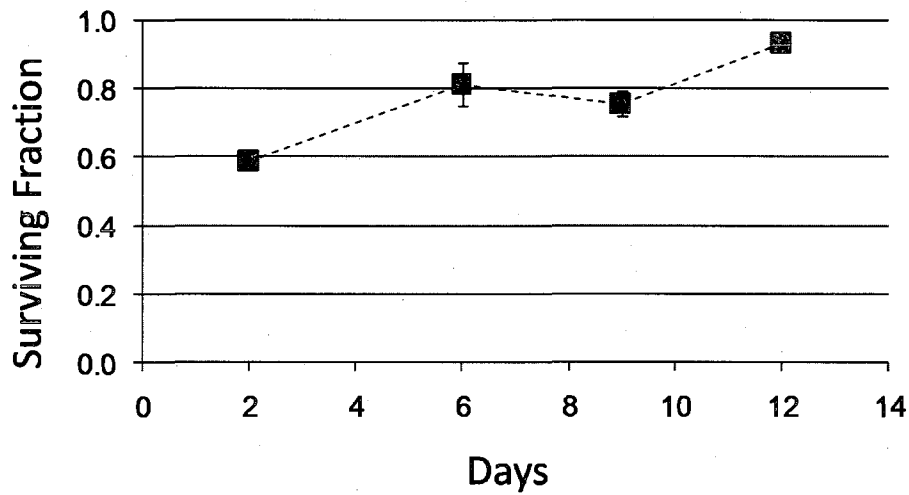


Figure 5. Clonogenic survival of CHO AL cells at time points (2-12 days) following treatment with hypoxia treatment (1 experiment run in triplicate). All error bars represent the standard deviation.

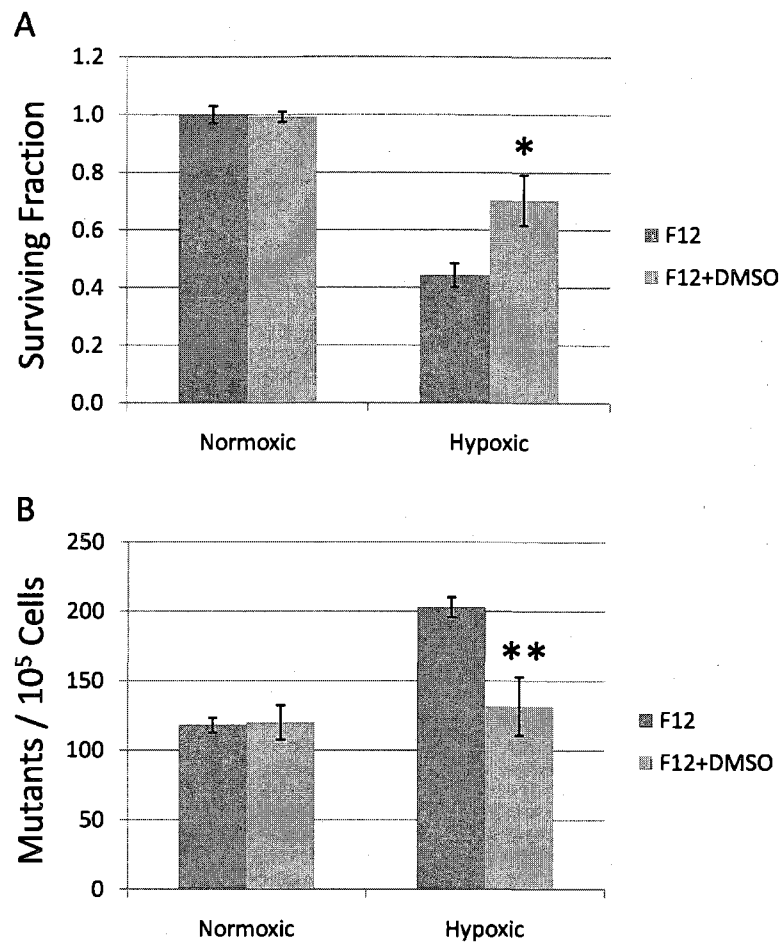


Figure 6. Effects of 0.5% DMSO in F12 media on (A) cell survival (2 experiments run in triplicate) and (B) mutant yield for untreated control cells and cells cultured for 24 hr at <0.1% oxygen (2 experiments run in quadruplicate). Error bars represent the standard error of the mean. * $p < 0.05$, ** $p < 0.01$.

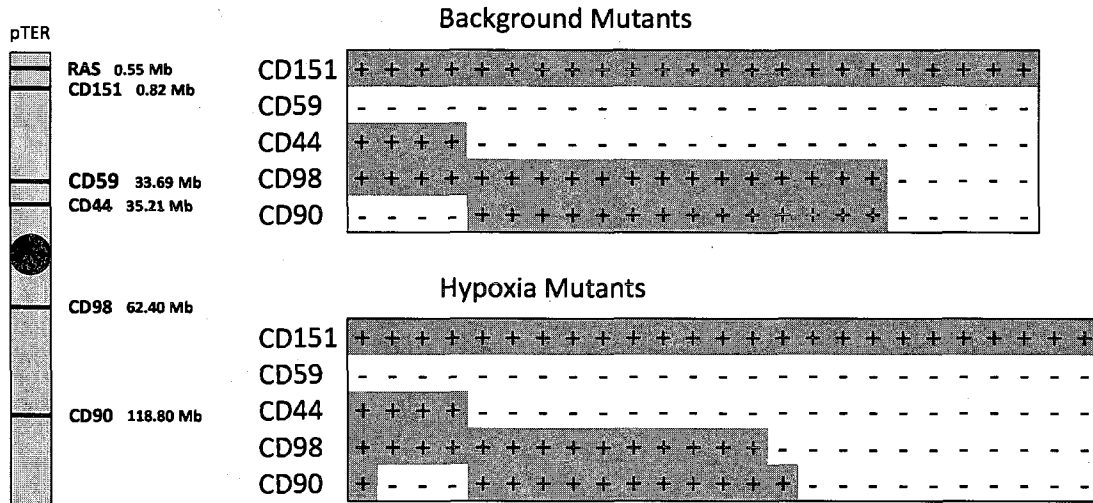


Figure 7. Mutant spectra of genes on chromosome 11 generated by flow cytometric analysis of 5 surface antigens for clones isolated 12 days after treatment from the 1% CD59 mutant region of **(Top)** control cells and **(Bottom)** hypoxia treated cells. Each column represents an individual mutant clone. Missing antigens are represented by negative marks while remaining antigens are marked by positive/shaded regions and measurements are relative to the terminus of the p-arm of chromosome 11.

Researchers have attempted to quantify the damage and resulting mutations generated by hypoxia. Hypoxia induced DNA damage has been detected throughout the bodies of individuals exercising at high altitude and has been attributed to ROS produced upon reoxygenation (5) or by stress induced leakage of ROS from mitochondria (6,26). Severe hypoxic conditions and the subsequent reoxygenation generate DNA damage in mammalian cells when measured using the comet assay (27). Also, hypoxia in the tumor environment decreases the activity of DNA repair mechanisms (7-9). Several groups have found up to a 4 fold increase in mutations of genes located on vectors in mammalian cells grown under hypoxic culture conditions as well as cells grown in hypoxic tumors (10,11,28).

We have demonstrated that culturing cells under hypoxic conditions for 24 hr generates a significant mutant yield as measured by the CHO A_L complement cytotoxicity assay. Using the same cell line we have also characterized the FMCA by testing its sensitivity with agents that were known low responders or false negatives with other mammalian cell assays (15). In order to evaluate the frequency and type of mutations that may be induced by hypoxia, we cultured CHO A_L cells for 24 hr in <0.1% oxygen and measured the mutant yield and spectrum of mutations. The results from both assays clearly demonstrate that hypoxia treatment alone is sufficient to generate a significant mutant yield.

An anaerobic chamber was used to generate hypoxic culture conditions and dry test strips indicated when oxygen levels dropped below <0.1%, which occurred within an hour. The culture medium and polystyrene culture dishes used during treatment contained absorbed oxygen, requiring time for the oxygen levels in the medium around

the cells to equilibrate to the chamber. A previous study of oxygen diffusion in polystyrene dishes demonstrated that the partial pressure of oxygen in medium (20 ml) held in 100 mm dishes reached the chamber levels within three hours and oxygen levels in dishes containing confluent mammalian cells dropped to 0% in under 90 min (29). From this we can be confident that oxygen levels in the medium during these experiments dropped below 0.1% in under 3 hr.

We have previously determined that the peak day of mutant expression falls between days 6 and 12 for 17 different mutagens tested (15). It is important to note that cells treated with hypoxia responded similarly in that the peak day of expression was day 12. We have reported that clonogenic survival of treated cells returns to control levels roughly the same time as the peak day of mutant expression (23). Hypoxia is no different given that the survival of treated cells was ~90% of control on day 12. The survival of mutants sorted from the CD59⁺ region on the peak day of expression was less than those cells sorted from the positive peak of the same population, which again holds true with studies using known mutagens (30).

An advantage of the FCMA is that mutant cells can easily be sorted and cloned to study the spectrum of mutations in different mutants. We have shown that mutants generated by gamma radiation are frequently large deletions (20) while those generated by EMS are small, frequently intragenic, mutations (31). We have previously compared the mutant spectrum obtained by detecting the presence or absence of CD surface proteins with the presence or absence of flanking genes obtained by PCR analysis and there is a perfect correlation (20). Thus we can confidently say that the mutant spectra shown here do represent actual genetic mutations. Here we showed that the mutants

generated by severe hypoxia were similar to spontaneous mutants isolated from control populations. Both mutant spectra consisted typically of large deletions encompassing two or more genes. Interestingly, the major difference between the spectra was that 40% of the hypoxia generated mutants were large deletions of all markers except for CD151 while only ~20% of the background mutants had this deletion. The spontaneous mutant background is ~0.05-0.15% for the 1% mutant region. Therefore, many more mutant clones would have to be analyzed to determine if hypoxia generates an abundance of a specific mutation.

It has been previously reported that hypoxic stress generates a wide range of mutations from C:G to A:T transversions to deletions (10). The base 8-oxoguanine generated by radicals upon reoxygenation is often mismatched with adenine leading to the C:G to A:T transversions (28). Also, hypoxia significantly increases DNA strand breaks that are likely responsible for the increase in deletions (27).

Using DMSO, we attempted to demonstrate that much of the damage generated by severe hypoxia and reoxygenation was caused by oxygen radicals. Many studies have demonstrated the ability of DMSO to reduce oxygen radical induced mutagenesis (32,33). DMSO increased cell survival of hypoxia treated cells by ~30% and decreased the mutant yield in the FCMA significantly. From our results we can conclude that oxygen radicals are a significant source of DNA damage induced by hypoxic stress.

Culturing cells in an extremely hypoxic environment may generate mutations caused by ROS leakage from mitochondria and ROS generated during reoxygenation. Hypoxia in tumors can suppress repair, leading to a hypermutable phenotype that can create an environment of genetic instability (34). Along with decreased DNA repair and

mutagenesis, hypoxia may no longer just be an indicator of poor prognosis for radiotherapy but may play a leading role in creating more aggressive metastases by inducing genetic instability (4).

Reference List

1. Moulder JE, Rockwell S. Tumor hypoxia: its impact on cancer therapy. *Cancer Metastasis Rev* 1987;5:313-341.
2. Brizel DM, Scully SP, Harrelson JM, Layfield LJ, Bean JM, Prosnitz LR, Dewhirst MW. Tumor oxygenation predicts for the likelihood of distant metastases in human soft tissue sarcoma. *Cancer Res* 1996;56:941-943.
3. Hall EJ: The Oxygen Effect and Reoxygenation. In: *Radiobiology for the Radiologist*, 5th ed. Edition, John J, Sutton P, and Marino D (eds). Lippincott Williams & Wilkins, Philadelphia, 2000, pp. 91-111.
4. Bristow RG, Hill RP. Hypoxia and metabolism. Hypoxia, DNA repair and genetic instability. *Nat Rev Cancer* 2008;8:180-192.
5. Risom L, Lundby C, Thomsen JJ, Mikkelsen L, Loft S, Friis G, Moller P. Acute hypoxia and reoxygenation-induced DNA oxidation in human mononuclear blood cells. *Mutat Res* 2007;625:125-133.
6. Moller P, Loft S, Lundby C, Olsen NV. Acute hypoxia and hypoxic exercise induce DNA strand breaks and oxidative DNA damage in humans. *FASEB J* 2001;15:1181-1186.
7. Bindra RS, Schaffer PJ, Meng A, Woo J, Maseide K, Roth ME, Lizardi P, Hedley DW, Bristow RG, Glazer PM. Down-regulation of Rad51 and decreased homologous recombination in hypoxic cancer cells. *Molecular and Cellular Biology* 2004;24:8504-8518.
8. Meng AX, Jalali F, Cuddihy A, Chan N, Bindra RS, Glazer PM, Bristow RG. Hypoxia down-regulates DNA double strand break repair gene expression in prostate cancer cells. *Radiother Oncol* 2005;76:168-176.
9. Rodriguez-Jimenez FJ, Moreno-Manzano V, Lucas-Dominguez R, Sanchez-Puelles JM. Hypoxia causes downregulation of mismatch repair system and genomic instability in stem cells. *Stem Cells* 2008;26:2052-2062.
10. Reynolds TY, Rockwell S, Glazer PM. Genetic instability induced by the tumor microenvironment. *Cancer Res* 1996;56:5754-5757.
11. Li CY, Little JB, Hu K, Zhang W, Zhang L, Dewhirst MW, Huang Q. Persistent genetic instability in cancer cells induced by non-DNA-damaging stress exposures. *Cancer Res* 2001;61:428-432.
12. Wedemeyer N, Greve B, Uthe D, Potter T, Denklau D, Severin E, Hacker-Klom U, Kohnlein W, Gohde W. Frequency of CD59 mutations induced in human-hamster hybrid A(L) cells by low-dose X-irradiation. *Mutat Res* 2001;473:73-84.

13. Ross CD, Lim CU, Fox MH. Assay to measure CD59 mutations in CHO A(L) cells using flow cytometry. *Cytometry A* 2005;66:85-90.
14. Zhou H, Xu A, Gillispie JA, Waldren CA, Hei TK. Quantification of CD59-mutants in human-hamster hybrid (AL) cells by flow cytometry. *Mutat Res* 2006;594:113-119.
15. French CT, Ross CD, Keysar SB, Joshi DD, Lim CU, Fox MH. Comparison of the mutagenic potential of 17 physical and chemical agents analyzed by the flow cytometry mutation assay. *Mutat Res* 2006;602:14-25.
16. Waldren C, Jones C, Puck TT. Measurement of mutagenesis in mammalian cells. *Proc Natl Acad Sci U S A* 1979;76:1358-1362.
17. Waldren C, Correll L, Sognier MA, Puck TT. Measurement of low levels of x-ray mutagenesis in relation to human disease. *Proc Natl Acad Sci* 1986;83:4839-4843.
18. Hei TK, Wu L, Liu S, Vannais DB, Waldren CA, Randers-Pehrson G. Mutagenic effects of a single and an exact number of alpha particles in mammalian cells. *Proc Natl Acad Sci* 1997;94:3765-3770.
19. Puck TT, Wuthier P, Jones C, Kao F. Genetics of Somatic Mammalian Cells: Lethal Antigens as Genetic Markers for Study of Human Linkage Groups. *Proc Natl Acad Sci* 1971;68:3102-3106.
20. Ross CD, French CT, Keysar SB, Fox MH. Mutant spectra of irradiated CHO A(L) cells determined with multiple markers analyzed by flow cytometry. *Mutat Res* 2007;624:61-70.
21. Waldren CA, Ueno AM, Schaeffer BK, Wood SG, Sinclair PR, Doolittle DJ, Smith CJ, Harvey WF, Shibuya ML, Gustafson DL, Vannais DB, Puck TT, Sinclair JF. Mutant yields and mutational spectra of the heterocyclic amines MeIQ and PhIP at the S1 locus of human-hamster AL cells with activation by chick embryo liver (CELC) co-cultures. *Mutat Res* 1999;425:29-46.
22. Waldren C, Correll L, Sognier MA, Puck TT. Measurement of low levels of x-ray mutagenesis in relation to human disease. *Proc Natl Acad Sci* 1986;83:4839-4843.
23. Keysar SB, Fox MH. Kinetics of CHO AL mutant expression after treatment with radiation, EMS and asbestos. *Cytometry A* 2009;
24. Waldren C, Correll L, Sognier MA, Puck TT. Measurement of low levels of x-ray mutagenesis in relation to human disease. *Proc Natl Acad Sci* 1986;83:4839-4843.

25. Chen T, Harrington-Brock K, Moore MM. Mutant frequency and mutational spectra in the Tk and Hprt genes of N-ethyl-N-nitrosourea-treated mouse lymphoma cells. *Environmental and Molecular Mutagenesis* 2002;39:296-305.
26. Bell EL, Chandel NS. Mitochondrial oxygen sensing: regulation of hypoxia-inducible factor by mitochondrial generated reactive oxygen species. *Essays Biochem* 2007;43:17-27.
27. Hammond EM, Dorie MJ, Giaccia AJ. ATR/ATM targets are phosphorylated by ATR in response to hypoxia and ATM in response to reoxygenation. *J Biol Chem* 2003;278:12207-12213.
28. Papp-Szabo E, Josephy PD, Coomber BL. Microenvironmental influences on mutagenesis in mammary epithelial cells. *Int J Cancer* 2005;116:679-685.
29. Allen CB, Schneider BK, White CW. Limitations to oxygen diffusion and equilibration in in vitro cell exposure systems in hyperoxia and hypoxia. *Am J Physiol Lung Cell Mol Physiol* 2001;281:L1021-L1027.
30. Ross CD, Fox MH. Multiparameter Analysis of CHO A(L) Mutant Populations Sorted on CD59 Expression after Gamma Irradiation. *Radiat Res* 2008;170:628-637.
31. Keysar SB, Fox MH. EMS mutant spectra generated by multi-parameter flow cytometry. Submitted for review 2009;
32. Hei TK, Liu SX, Waldren C. Mutagenicity of arsenic in mammalian cells: role of reactive oxygen species. *Proc Natl Acad Sci* 1998;95:8103-8107.
33. Xu A, Huang X, Lien YC, Bao L, Yu Z, Hei TK. Genotoxic mechanisms of asbestos fibers: role of extranuclear targets. *Chem Res Toxicol* 2007;20:724-733.
34. Coquelle A, Toledo F, Stern S, Bieth A, Debatisse M. A new role for hypoxia in tumor progression: induction of fragile site triggering genomic rearrangements and formation of complex DMs and HSRs. *Mol Cell* 1998;2:259-265.

CHAPTER 5

Variations in cell cycle and mutant induction in CHO A_L cells after suppression of DNA repair proteins

Abstract

The repair of DNA double-strand breaks (DSBs) is crucial for maintenance of the genome and the avoidance of carcinogenesis. Non-homologous end joining (NHEJ) and homologous recombination repair (HRR) are the foremost mechanisms for the repair of DSBs. Deficiencies in both mechanisms increase sensitivity to cell killing by genotoxic agents and affect mutagenesis. Here we used short interfering RNAs to silence the protein levels of Ku80 and Rad51C that play important roles in NHEJ and HRR respectively. We examined changes in cell survival, cell cycle and mutant induction after treatment with ionizing radiation (IR) and ethyl methanesulfonate (EMS). Mutagenesis was measured by the flow cytometry mutation assay, which uses the CHO A_L cell line to detect mutations in the *CD59* gene by lack of expression of CD59 cell surface protein. Knockdown of Rad51C or Ku80 caused a 3-fold increase in cell killing by IR while Rad51C knockdown caused a 4-fold increase in cell killing by EMS. Knockdown of Ku80 had no effect on cell killing by EMS. By measuring BrdU incorporation we determined that the knockdown of either protein slowed cell proliferation significantly

when compared to mock controls for untreated and treated cells alike. We measured the cell cycle distribution by staining with PI and found that silencing of Rad51C generated a buildup of G2 phase cells after treatment with EMS. Knockdown of Rad51C did not affect mutant yield after irradiation or EMS treatment; however, silencing of Ku80 decreased the mutant yield after EMS treatment. Increased cell killing after Rad51C silencing implies that significant alkylating damage generated by EMS is repaired by HRR. Also, reduced mutant yield after Ku80 knockdown suggests that damage generated by EMS during S phase is normally repaired by NHEJ.

Introduction

DNA repair is crucial for the proper maintenance of the genome, and deficiencies in its various mechanisms can have deleterious effects (1-3). DNA double-strand breaks (DSBs) are considered the most harmful type of lesion (4), and often result in mutations that play a key role in carcinogenesis. Homologous recombination repair (HRR) and non-homologous end joining (NHEJ) are the two prevailing repair mechanisms in mammalian cells that are responsible for repairing DNA DSBs.

HRR uses a homologous allele or region as a template for the repair of DSBs. If the region used is identical to the original sequence, a mutation is avoided (5,6). Rad51C, a Rad51 paralog, is involved in the recruitment of Rad51 to the DSB to form HRR foci (7,8). Rad51C forms at least two complexes with other Rad51 paralogs; these include the heterodimer Rad51C and XRCC3 and the heterotetramer Rad51B,C,D and XRCC2 (9). Previous reports have demonstrated that mammalian Rad51C mutants are up to 7-fold more sensitive to DNA crosslinking agents, 4-fold more sensitive to alkylating agents and

moderately sensitive to ionizing radiation (IR) (7,8,10,11). However, NHEJ is considered the predominant mechanism of DSB repair in mammals.

NHEJ is a process by which two broken DNA ends are brought together, resected and ligated (12). Unlike the high fidelity repair of HRR, end resection in NHEJ often results in small deletions, and the joining of two different chromosomes may result in translocations (13). The Ku70/80 heterodimer is proposed to be one of the first protein complexes to recognize the broken ends of chromosomes (14). Ku70 and Ku80 are constitutively expressed proteins, and the Ku70/Ku80 heterodimer is an abundant protein complex with an estimated 4×10^5 molecules per mammalian cell. Interestingly, the stability of each protein is dependent on dimerization with the other (15).

The binding of Ku70/80 attracts the catalytic subunit of DNA-dependent protein kinase (DNA-PK_{cs}) (16). NHEJ is regulated by the autophosphorylation of DNA-PK_{cs} (17), and the juxtaposition of the two broken ends only occurs when DNA-PK_{cs} is efficiently phosphorylated (18). This complex is vital for repair and genome maintenance. Ku80 heterozygosity leads to genomic instability (19), and gene silencing and mutated phenotypes increased sensitivity to IR (20,21).

We have developed the flow cytometry mutation assay (FCMA) using the CHO A_L cell line to measure mutations of the *CD59* gene. Mutants are scored by the absence of fluorescence when staining with fluorochrome conjugated antibodies against the CD59 surface protein (22). The mutagenic potentials of a broad range of chemical and physical agents have been determined and demonstrated the sensitivity and specificity of the assay (23).

To study the effects of DNA repair on mutagenesis, we have suppressed protein levels of the Rad51C and Ku80. These have important roles in HRR and NHEJ respectively. After transfection with Rad51C- or Ku80-specific short interfering RNAs (siRNA), cells were treated with the clastogen IR (4) or the alkylating agent ethyl methanesulfonate (EMS) (24). These agents were chosen due to their different genotoxic properties and their recent use in characterizing the kinetics of mutant expression in the FCMA (25). Here we demonstrate that knockdown of Rad51C significantly increases cell killing and cell cycle alterations following exposure to EMS. Knockdown of Ku80 also modestly sensitizes cells to both radiation and EMS and decreases the mutant yield after treatment with EMS.

Materials and Methods

Cell culture

The CHO A_L(N) cell line contains the entire Chinese hamster KI cell line genome with an incorporated copy of human chromosome 11 including a gene conferring resistance to the antibiotic G418 (Sigma-Aldrich, St. Louis, MO). By treating cells periodically with 800 µg/ml G418, spontaneous background mutants were reduced to ~300 mutants / 10⁵ cells. Cells were cultured in Ham's F12 medium supplemented with 10% FBS, penicillin/streptomycin (0.14 and 0.2 g/L, respectively) and 7.5% (w/v) sodium bicarbonate, pH 7.3. Cells were maintained in humidified 5% CO₂ incubators at 37° C as previously described (23).

siRNA transfection

Transfection was completed using target-specific small interfering RNAs (siRNAs) (21 nt) for hamster Ku80, hamster Rad51C and control non-target siRNA that

were purchased from Dharmacon (Lafayette, CO) as purified and annealed duplexes. The siRNA sequences used for knockdown (KD) in this study are, Ku80 GGAAGAAGUUUGAGAAGAAUU and Rad51C CAGCAAAGAAGUUGGGAUUAUU. Transfection of siRNAs was completed using Dharmafect-4 reagent (Dharmacon). Transfection efficiency was determined using transfection reagent and siGLO phycoerythrin conjugated RNAs (Dharmacon) analyzed by flow cytometry.

Cells (1×10^5) were plated in 60 mm dishes 24 hr prior to treatment in F12 medium. Before treatment cells were washed twice with PBS and 2.8 ml serum-free, antibiotic-free Opti-MEM medium was added. Dharmafect reagent and siRNA were incubated at room temperature for 5 min separately in a total of 100 μ l Opti-MEM. Transfection reagent (1.3 μ l/ml final concentration) and siRNA (100 nM final concentration) were mixed, incubated for 20 min at room temperature and finally added to cells. 24 hr after starting treatment 3 ml F12 (20% FBS) was added to the plates.

Irradiation and EMS treatment

All treatments occurred 48 hr after the beginning of siRNA knockdown. Prior to treatment cells were washed twice with PBS and fresh medium was added. EMS was diluted in F12 to a concentration of 8 mM and added to cells for 3 hr after which plates were washed twice with warm PBS and replaced with fresh F12. Irradiations were done at room temperature in a Mark I ^{137}Cs γ -irradiator (J.L. Shepherd and Associates, Glendale, CA) at a dose rate of 3.9 Gy/min.

Antibody staining

To stain for Ku80 or Rad51C, cells (1×10^6) were first fixed in 2 ml 1% paraformaldehyde in PBS at 4°C for 15 min, then 100% cold ethanol was added drop-

wise until reaching a final concentration of 80%. Cells were resuspended in permeabilization buffer (0.25% Triton X-100 in PBS) for 30 min on ice. The cells were resuspended in anti-Ku80 (1:400) or Rad51C (1:300) primary antibodies (US Biological, Swampscott, MA) in TBFP (0.5% Tween 20, 1% BSA, and 1% FBS in PBS) and incubated for 2 hr at room temperature. Cells were then incubated for 30 min on ice in 100 μ l Alexa Fluor 488 goat anti-rabbit IgG (Molecular Probes, Eugene, OR) with 1:500 dilution in TBFP. The stained cells were analyzed by flow cytometry.

To stain for CD59, 1×10^6 cells were suspended in 1 ml FACS buffer (1% BSA, 0.1% sodium azide in PBS). Samples were centrifuged and stained with anti-CD59 monoclonal antibodies conjugated to phycoerythrin (PE) (Caltag Laboratories, Burlingame, CA) at a 1:40 dilution in FACS and were incubated at 37° C for 1 hr. One ml cold FACS was then added to the cells and they were again centrifuged, the supernatant was aspirated and cells were finally suspended in 0.5 ml cold FACS and filtered through 40 μ m mesh into flow cytometry sample tubes which were kept on ice prior to analysis.

Cell survival

Six hours after treatment cells were trypsinized and counted. Cells were serially diluted to get a final concentration of ~500 cells/ml. Cells were then plated in six well plates and allowed to grow for 7 days before colonies were stained with crystal violet and counted. The surviving fraction was calculated by standard methods.

Cell cycle analysis

Immediately after treatment cells were labeled by adding 10 μ M bromodeoxyuridine (BrdU) directly to the culture medium. After 6 or 18 hr, cells were

trypsinized, counted and 5×10^5 cells were transferred to 15 ml conical tubes for processing. Samples were centrifuged for 3 min at 1500 rpm to pellet cells. The supernatant was aspirated and the cells were resuspended in 2 ml cold PBS. The samples were then fixed by adding 5 ml cold 100% ethanol (70% final concentration) drop wise while vortexing gently. Samples were kept on ice for at least 30 min prior to denaturation and staining.

After 30 min, samples were resuspended in 0.1 ml PBS followed by 2 ml of pepsin/HCl (0.2 mg/ml in 2 N HCl) while gently vortexing and samples were incubated at 37° C for 20 min. Pepsin hydrolysis was terminated by adding 3 ml of 1 M Tris. Cells were washed with 2 ml PBS and were resuspended in 100 μ l of a 1:30 dilution of the primary mouse anti-BrdU antibody (Dako, Denmark) in TBFP buffer (0.5% Tween 20, 1% BSA, 1% FBS in PBS). Samples were incubated for 25 min at room temperature and then rinsed with 5 ml PBS. Next, 200 μ l of a 1:200 dilution of the secondary antibody goat anti-mouse IgG conjugated to Alexa Fluor® 488 (Molecular Probes, Eugene, OR) in deionized water was added to samples which were incubated for 25 min at room temperature in the dark. Samples were washed with 5 ml PBS and resuspended in 1 ml of propidium iodide (10 μ g/ml in PBS) containing RNase (40 KU/ml). Samples were incubated at room temperature for 20 min prior to flow cytometry analysis.

Flow cytometry

A Dako CyAn™ flow cytometer with a 488 nm laser (Dako, Fort Collins, CO) was used for quantification of mutant fractions. The CD59 mutant region was gated as 10% of the mean of the positive peak on a log scale. For the mutation assay 1×10^5 cells from each sample were analyzed on the CyAn.

As previously described (25), an EPICS V (Beckman Coulter, Miami, FL) flow cytometer was used for cell cycle experiments using bromodeoxyuridine (BrdU) and propidium iodide (PI). Briefly, gating of forward scatter and integral red fluorescence versus peak red fluorescence was used to select for whole cells with incorporated PI and largely avoid clumped cells. Histograms of PI alone and PI versus log integral green fluorescence (LIGFL) for BrDU incorporation were collected for each sample (50,000 cells). Histograms were analyzed using MultiCycle and Multi2D software (Phoenix Flow Systems).

Results

siRNA transfection and gene silencing

Successful transfection of fluorochrome conjugated RNAs was measured by flow cytometry. By treating cells with 1 μ l/ml Dharmafect-4 reagent and 40 nM siGLO RNA we consistently achieved a transfection efficiency of >90% (Fig. 1). Cell samples collected 48 hr after siRNA treatment were fixed and stained for either Ku80 or Rad51C. Quantified decreases in staining for both proteins are displayed in Figure 2, but due to non-specific binding a percent knockdown is difficult to calculate.

Cell proliferation and survival

Cell growth was measured to determine the negative effects of siRNA transfection. Total cell number after a 48 hr treatment with non-target siRNAs was ~20% less than for mock-transfected controls. Transfection with Ku80 and Rad51 siRNAs both decreased total cell number by ~30% (Fig. 3A).

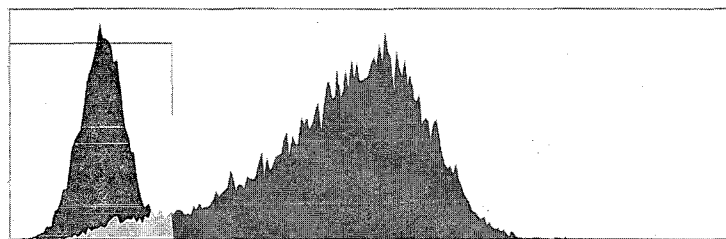
Cell survival of untreated Rad51C or Ku80 transfected cells was 0.78 or 0.86 respectively, compared to mock control. There was no toxicity from non-target siRNA

transfection (data not shown). Survival of mock-transfected cells after 4 Gy γ -rays (0.20) was further decreased by similar proportions after Ku80 (0.08) or Rad51C (0.06) knockdown (KD). Survival after 8 mM EMS treatment was reduced nearly 5-fold ($p < 0.01$) from mock for Rad51C KD, with no significant change in Ku80 KD cells (Fig. 3B).

DNA repair and cell cycle

To determine the effects of repair protein knockdowns, we analyzed cell cycle characteristics of cells isolated 6 and 18 hr after treatment with 4 Gy γ -rays and 8 mM EMS. By 6 hr after treatment, uptake of BrdU (Fig.4) had occurred in 95% of untreated stock cells but only 90% and 86% of Ku80 and Rad51C knockdown cells respectively. Similar patterns held true for irradiated and EMS-treated cells. BrdU uptake in mock, Ku80 knockdown and Rad51C knockdown was 84%, 81% and 77% respectively after irradiation and 77%, 71% and 67% respectively after treatment with EMS (Fig. 5). Untreated mock and KD cells all had significant populations of BrdU positive G1 phase cells (Fig. 4) while all cells treated with IR and EMS did not.

Univariate PI histograms were analyzed to measure changes in the proportion of cells in the different phases of the cell cycle. Representative DNA histograms are displayed in Figure 6 and detailed analyses are presented in Figure 7. Untreated Ku80 and Rad51C knockdown cells had slightly increased G2 populations when compared to controls. At 6 hr after treatment with 4 Gy control, Ku80 and Rad51C cells all had $>35\%$ of the populations in G2 phase. All three groups showed slight G2 increases after treatment with EMS. Cells were also analyzed 18 hr after treatment and there were no significant differences in the G2 population of Ku80 KD cells after irradiation but the



siGLO-PE

Figure 1. Transfection of CHO A_L cells with PE conjugated RNAs (siGLO) and Dharmafect-4 reagent. Gating region set as 99% of the mock transfected control (black) and positive cells are gray.

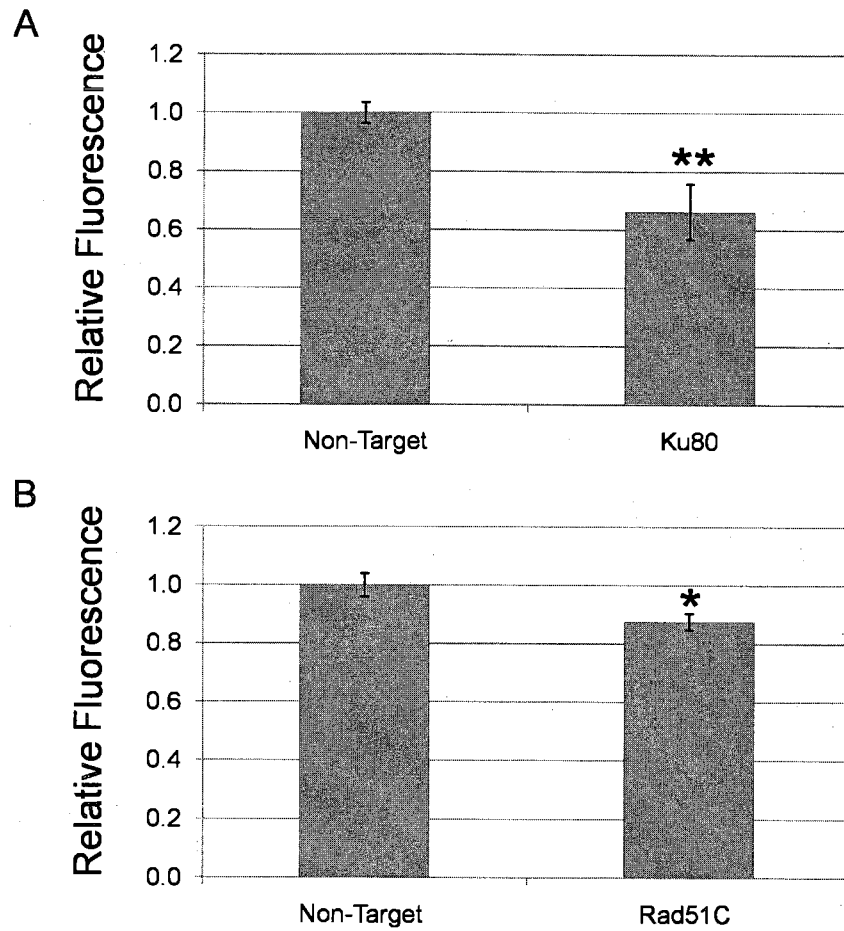


Figure 2. Relative fluorescence of cells after (A) Non-Target siRNA (control) and Ku80 knockdown; cells stained with antibodies against the Ku80 protein and (B) Rad51C knockdown; cells stained with antibodies against the Rad51C protein 48 hr after transfection. Results based on one experiment run in quadruplicate with error bars representing the standard deviation. * $p=0.013$, ** $p<0.01$.

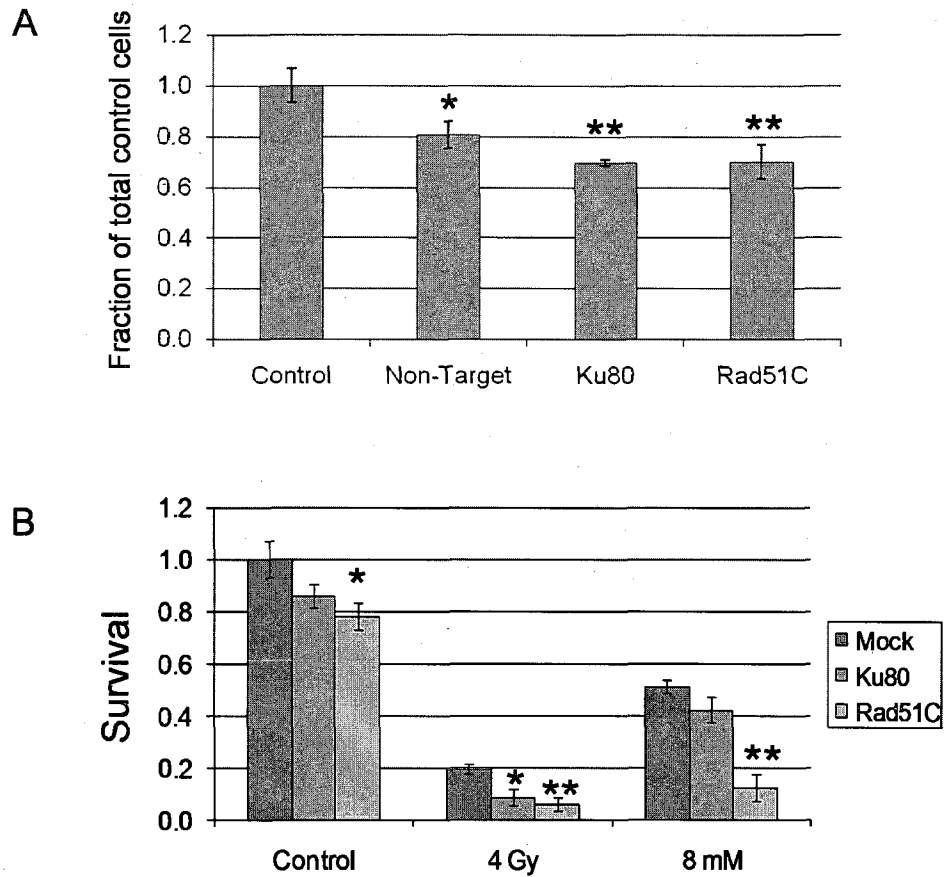


Figure 3. (A) Fraction of total cell number compared to mock transfected control for cells transfected with non-target, Ku80 or Rad51C specific siRNAs after 1×10^5 cells were originally plated and grown for 24 hr, followed by a 48hr siRNA transfection. (B) Survival of transfected cells after irradiation and EMS treatment. Both experiments are based on one experiment run in triplicate. * $p < 0.05$, ** $p < 0.01$ and error bars represent the standard deviation.

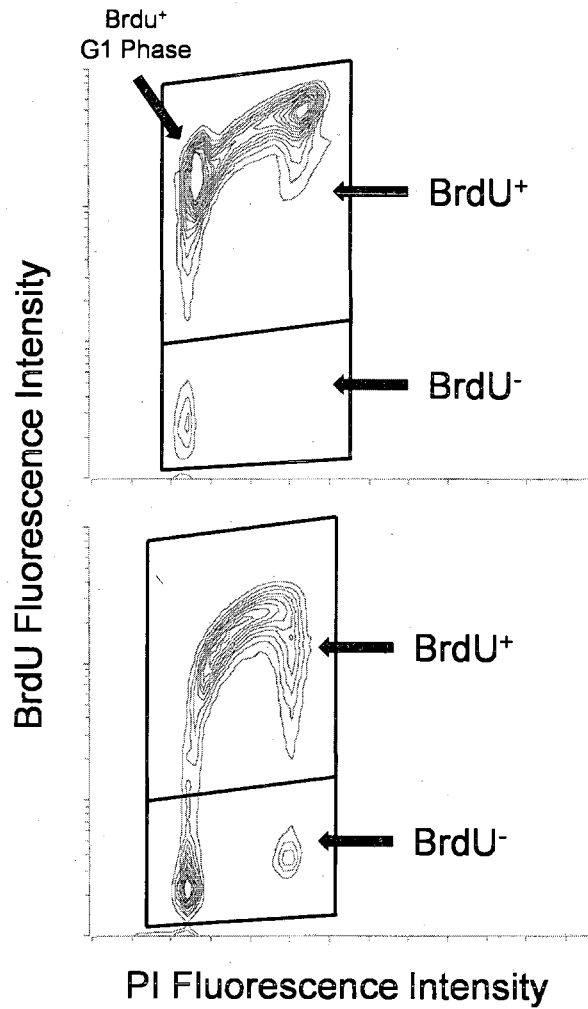


Figure 4. Bivariate histograms for (top) untreated control and (bottom) EMS treated cells measuring DNA content (PI) and incorporation of BrdU (6 hours treatment) during DNA replication. Control cells have a clear population that have incorporated BrdU and divided (G1 phase).

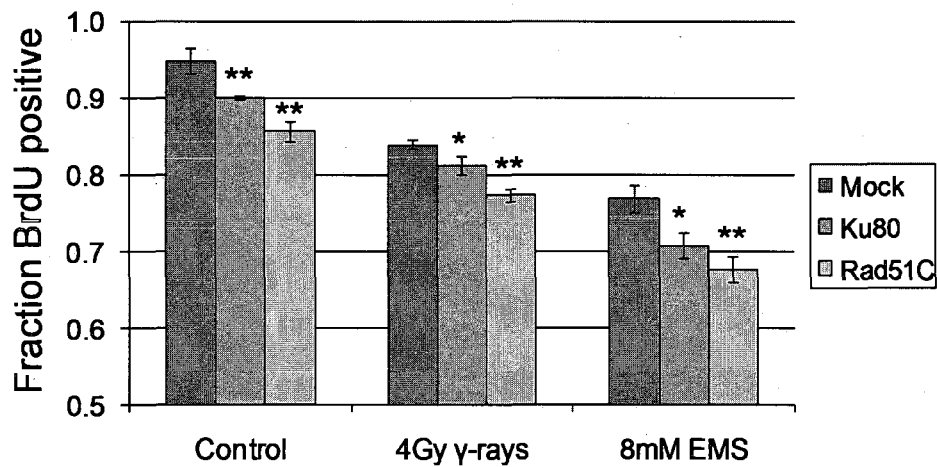


Figure 5. Cell cycle analysis 6 hr after treatment with 4 Gy γ -rays or 8 mM EMS for cells with reduced Ku80 or Rad51C protein levels measured by the fraction of total cells that have incorporated BrdU during DNA replication. Error bars represent the standard deviation of three experiments run in triplicate. * $p < 0.05$, ** $p < 0.01$.

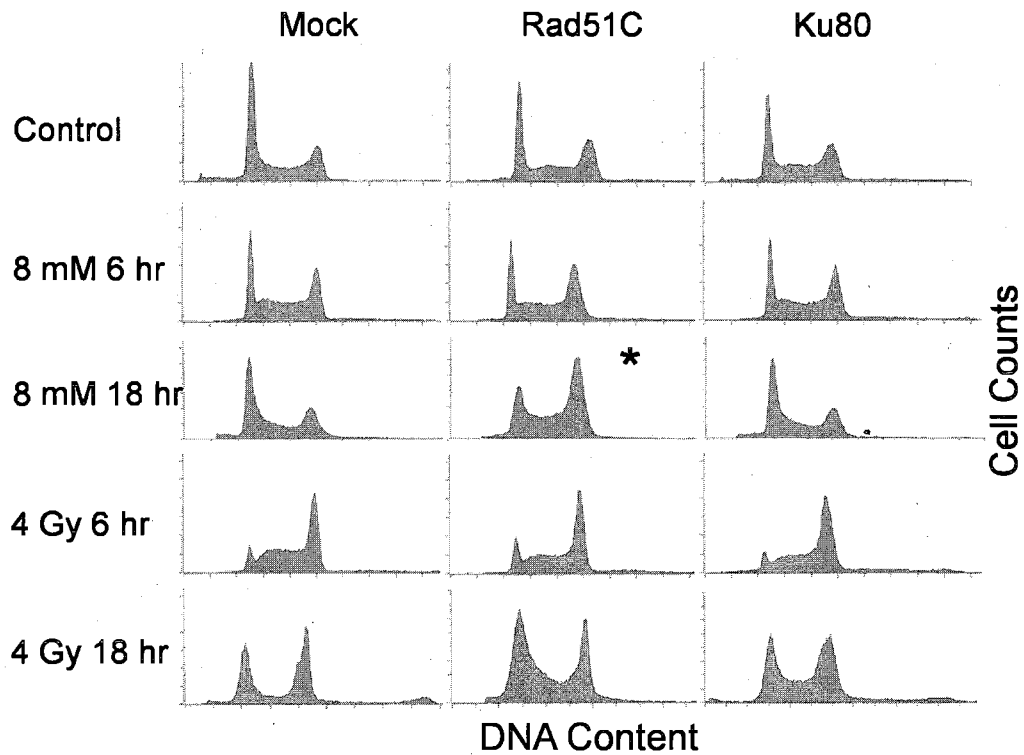


Figure 6. Representative DNA content histograms for Mock, Ku80 siRNA and Rad51C siRNA transfected cells 6 and 18 hours following 4 Gy γ -rays and 8 mM EMS treatments. * Buildup of G2 phase cells in the Rad51C KD population 18 hr after treatment with 8 mM EMS.

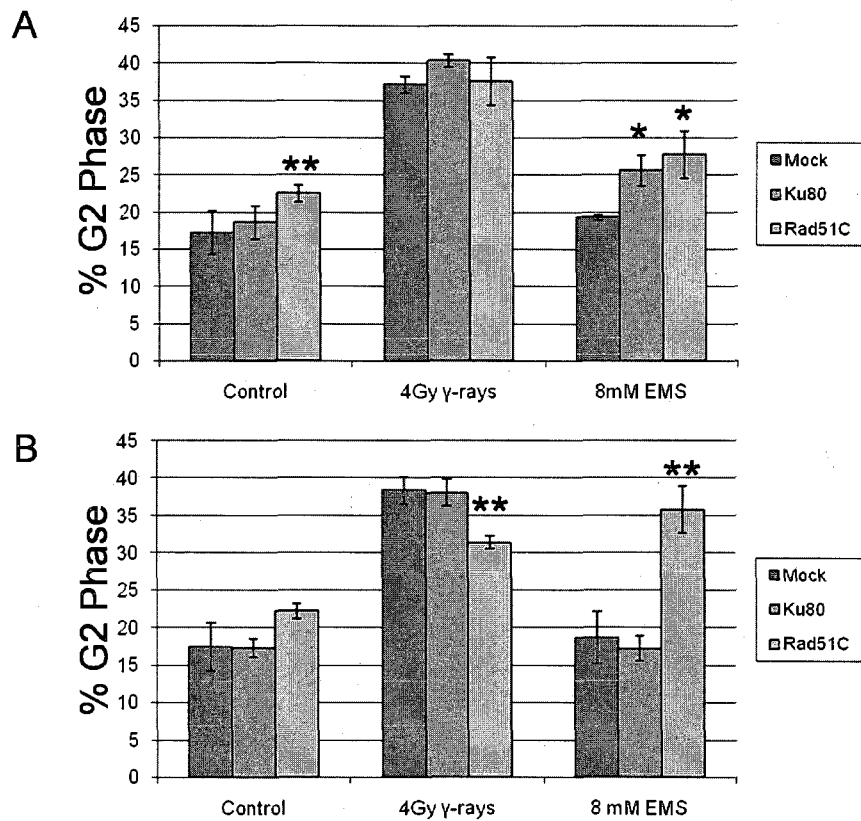


Figure 7. Effects of Ku80 and Rad51C knockdown on the percentage of cells in G2 phase at (A) 6 hr and (one experiment run in triplicate) (B) 18 hr (2 experiments run in triplicate) after 4 Gy irradiation or 8 mM EMS treatment. Error bars represent the standard deviation. Significant at * $p < 0.05$, ** $p < 0.01$ when compared to mock treatment.

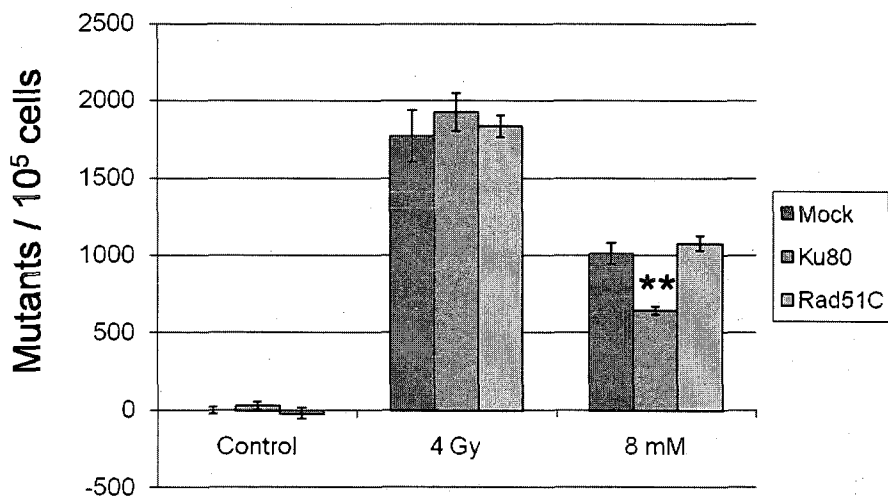


Figure 8. Effects of Ku80 or Rad51C knockdown on mutant fraction (mutants/ 10^5 cells) in CHO A_L cells measured by the FCMA for control, 6 days after 4 Gy γ -irradiation and 9 days after 8 mM EMS treatment. Results are from a minimum of 3 experiments run in triplicate with error bars representing the standard error of the mean. ** $p < 0.01$

percentage of cells in G2 decreased slightly for Rad51C KD cells. Also, there was a significant increase ($p < 0.01$) for EMS treated Rad51C knockdown cells (Fig. 7).

DNA repair and mutagenesis

Cells were transfected with siRNAs specific for Ku80 or Rad51C 48 hr prior to treatment with radiation or EMS. Suppression of protein levels did not significantly increase background mutations. The knockdown of Ku80 and Rad51C did not affect mutant induction after 4 Gy γ -rays. However, knockdown of Ku80 decreased the mutant fraction of cells treated with 8 mM EMS by 40% (Fig. 8).

Discussion

The repair of DNA double-strand breaks is crucial for the prevention of carcinogenesis. HRR is a high fidelity repair mechanism that uses homologous alleles on sister chromatids or homologous chromosomes as a template for repair (5,13). However, NHEJ is the mechanism predominantly used in mammalian cells to repair breaks (12). Here we have investigated the effects on cell cycle, survival and mutagenesis after knockdown by RNA interference of Ku80 and Rad51C proteins. These play important roles in NHEJ and HRR respectively. The direct calculation of protein knockdown was not possible for Rad51C since there was not a significant separation between knockdown and control. This is likely due to the non-specific binding of the polyclonal antibodies that were used for quantification. However, the effects on cell cycle and survival serve as a secondary confirmation of knockdown efficiency.

Previous studies of Rad51C deficient cells have found significantly increased sensitivity to the crosslinking agent mitomycin C, moderate sensitivity to methyl methanesulfonate, and slight sensitivity to IR (7,11,26). Sensitivity to IR was observed

specifically in S and G2 phases (8). Rad51 expression increases during S phase and peaks around the G2/M transition along with HRR activity (27). Here we demonstrate that decreasing the levels of Rad51C increased cell killing 3-fold by ionizing radiation and increased sensitivity to EMS by nearly 4-fold compared to mock cells. This suggests that HRR plays an important role in the repair of damage generated by EMS that is known to consist predominantly of base adducts and single strand breaks (24,28).

Similar to decreased survival caused by knockdown of Rad51C, knockdown of Ku80 sensitized cells to killing by ionizing radiation. However, Ku80 appears to have no significant effect on killing induced by EMS. These results were expected since the role of Ku80 in NHEJ is to recognize and recruit repair proteins to DSBs (14), and unlike radiation, EMS does not commonly generate DSBs. This is supported by previous reports finding that IR increased apoptosis and decreased survival in Ku80 silenced and mutated cells (20,21,29).

Next we investigated the effects of DNA repair protein gene silencing on the cell cycle after treatment with IR or EMS. By measuring BrdU incorporation, we found that knockdown of Rad51C altered cell cycle characteristics in CHO A_L cells after treatment with EMS and radiation by slowing progression through the cell cycle. Knockdown of Rad51C slightly decreased the proportion of cells in G2 phase 18 hours after irradiation. Knockdown of Rad51C followed by EMS treatment increased the percentage of cells in G2 phase by 6 hours and doubled that of control treated cells by 18 hours. We have previously investigated the effects of EMS treatment on cell cycle in CHO cells and found slowed proliferation but an increase in G2 phase cells (25). This “buildup” is likely due to damage that is usually reversed by HRR activating cell cycle checkpoints,

specifically the G2/M checkpoint (30,31). Since Rad51 expression and HRR activity increase during S phase and peak at the G2/M transition (8) and Rad51 foci formation decreases with knockdown of Rad51C (11), damage induced by EMS during late S and G2 phase would likely not be sufficiently repaired, leading to a transient G2 block. The rate of incorporation of BrdU was also reduced with Rad51C knockdown followed by either radiation or EMS. This suggests that the S phase checkpoint is also activated due to unrepaired damage (30,32). It should also be noted that these cell cycle results represent a snapshot at particular times. The fraction of cells in G2 phase at a particular time is affected both by a transient cell cycle block and slowed progression through S phase.

Silencing of Ku80 decreased the uptake of BrdU during DNA replication but did not significantly affect the fraction of cells in G2 phase in untreated or irradiated cells when compared to mock controls. Others have also recently reported that Ku80 silencing suppresses DNA replication (33). Previously, we reported that ionizing radiation generates a significant G2 block in CHO A_L cells (25) but Ku80 knockdown did not increase this effect (20). Ku80 knockdown slightly increased the percentage of cells in G2 phase 6 hours after treatment with EMS, but the G2 fraction returned to control levels by 18 hours. This modest increase may only be due to the increased stress of transfection, but could point to EMS damage during replication that resulted in DSBs. The latter is likely since the induction of γ -H2AX foci formation (34) by alkylating agents has been found predominantly in BrdU labeled cells (35). Alkylating damage, when not repaired prior to DNA synthesis, can stall replication and in turn lead to DSBs (36-38).

The relationship between DNA repair and mutagenesis was explored. HRR of chromosome 11 would only be expected to occur during late S or G2 phase in CHO A_L cells because a sister chromatid would be required for a homology search due to the lack of a homologous chromosome. Rad51C deficient cells have been reported to increase sensitivity to IR in S and G2 phases when compared to G1 phase (8) and decrease repair (HRR) of the oxidative stress induced by the bystander effect (39). Here we found that silencing of Rad51C had no significant effect on background mutants or mutant yield after irradiation or EMS treatment. Since EMS generates significant killing in Rad51C knockdown cells, we can be confident that HRR is crucial in the repair of alkylating damage that leads to cell death. The high fidelity of HRR and the increase in killing after knockdown of Rad51C could lead to potential mutants being killed, which might be the reason behind the lack of a change in mutant yield. In the future it would be interesting to study mutations at hamster loci, possibly *hprt*, to measure a possible difference between the activities of HRR on the hamster genome when compared to chromosome 11.

Previous studies have reported decreased mutagenesis and chromosomal rearrangements in *LacZ* reporter genes isolated from Ku80 null mice, suggesting that without NHEJ, HRR accurately repairs damage and unrepaired DSBs are lost by apoptosis (29). Conversely, increases in aberrations have been found by other groups (19,40). The increase in cell cycle checkpoints and apoptosis was dependent on the presence of WT p53 (41), hence the presence of p53 in Ku80 deficient cells may keep mutation rates low. We found that knockdown of Ku80 did not alter the mutant yield after irradiation and since CHO A_L cells do not express p53, mutation rates would not be expected to decrease. Furthermore, an increased killing of cells that are normally

repaired by NHEJ may have inhibited a significant increase. However, the mutant yield after EMS treatment was significantly reduced in Ku80 knockdown cells. EMS damage may generate DSBs during DNA replication that are later repaired by NHEJ. In turn, mutations would ultimately decrease in Ku80 deficient cells due to cell killing (35).

We have demonstrated that silencing proteins with important roles in NHEJ (Ku80) and HRR (Rad51C) both sensitize CHO A_L cells to killing. Interestingly, suppression of the Rad51 paralog Rad51C increases cell killing 5-fold and generates significant buildup of G2 phase cells after EMS treatment, but it does not alter the mutant yield after either EMS or IR treatment. However, silencing of Ku80 reduces the mutant yield in the FCMA after treatment with EMS, suggesting NHEJ repairs DSBs induced by alkylation damage during replication.

Reference List

1. Zhang Y, Zhou J, Held KD, Redmond RW, Prise KM, Liber HL. Deficiencies of double-strand break repair factors and effects on mutagenesis in directly gamma-irradiated and medium-mediated bystander human lymphoblastoid cells. *Radiat Res* 2008;169:197-206.
2. Wang J, Pluth JM, Cooper PK, Cowan MJ, Chen DJ, Yannone SM. Artemis deficiency confers a DNA double-strand break repair defect and Artemis phosphorylation status is altered by DNA damage and cell cycle progression. *DNA Repair (Amst)* 2005;4:556-570.
3. Errami A, Smider V, Rathmell WK, He DM, Hendrickson EA, Zdzienicka MZ, Chu G. Ku86 defines the genetic defect and restores X-ray resistance and V(D)J recombination to complementation group 5 hamster cell mutants. *Mol Cell Biol* 1996;16:1519-1526.
4. Ward JF. DNA damage produced by ionizing radiation in mammalian cells: identities, mechanisms of formation, and reparability. *Prog Nucleic Acid Res Mol Biol* 1988;35:95-125.
5. Pardo B, Gomez-Gonzalez B, Aguilera A. DNA double-strand break repair: how to fix a broken relationship. *Cell Mol Life Sci* 2009;
6. Iliakis G, Wang H, Perrault AR, Boecker W, Rosidi B, Windhofer F, Wu W, Guan J, Terzoudi G, Pantelias G. Mechanisms of DNA double strand break repair and chromosome aberration formation. *Cytogenet Genome Res* 2004;104:14-20.
7. Takata M, Sasaki MS, Tachiiri S, Fukushima T, Sonoda E, Schild D, Thompson LH, Takeda S. Chromosome instability and defective recombinational repair in knockout mutants of the five Rad51 paralogs. *Molecular and Cellular Biology* 2001;21:2858-2866.
8. Lio YC, Schild D, Brenneman MA, Redpath JL, Chen DJ. Human Rad51C deficiency destabilizes XRCC3, impairs recombination, and radiosensitizes S/G2-phase cells. *Journal of Theoretical Biology* 2004;279:42313-43320.
9. Kawabata M, Kawabata T, Nishibori M. Role of recA/Rad51 family proteins in mammals. *Acta Medica Okayama* 2005;59:1-9.
10. Benson FE, Stasiak A, West SC. Purification and characterization of the human Rad51 protein, an analogue of E. coli RecA. *The EMBO Journal* 1994;13:5764-5771.
11. Godthelp BC, Wiegant WW, van Duijn-Goedhart A, Scharer OD, et.al.. Mammalian Rad51C contributes to DNA cross-link resistance, sister

chromatid cohesion and genomic stability. *Nucleic Acids Research* 2002;30:2172-2182.

12. van Gent DC, van der BM. Non-homologous end-joining, a sticky affair. *Oncogene* 2007;26:7731-7740.
13. Hoeijmakers JH. Genome maintenance mechanisms for preventing cancer. *Nature* 2001;411:366-374.
14. Weterings E, van Gent DC. The mechanism of non-homologous end-joining: a synopsis of synapsis. *DNA Repair (Amst)* 2004;3:1425-1435.
15. Walker JR, Corpina RA, Goldberg J. Structure of the Ku heterodimer bound to DNA and its implications for double-strand break repair. *Nature* 2001;412:607-614.
16. Smith GC, Jackson SP. The DNA-dependent protein kinase. *Genes Dev* 1999;13:916-934.
17. Chan DW, Chen BP, Prithivirajasingh S, Kurimasa A, Story MD, Qin J, Chen DJ. Autophosphorylation of the DNA-dependent protein kinase catalytic subunit is required for rejoining of DNA double-strand breaks. *Genes Dev* 2002;16:2333-2338.
18. Meek K, Douglas P, Cui X, Ding Q, Lees-Miller SP. trans Autophosphorylation at DNA-dependent protein kinase's two major autophosphorylation site clusters facilitates end processing but not end joining. *Mol Cell Biol* 2007;27:3881-3890.
19. Karanjawala ZE, Grawunder U, Hsieh CL, Lieber MR. The nonhomologous DNA end joining pathway is important for chromosome stability in primary fibroblasts. *Curr Biol* 1999;9:1501-1504.
20. Yang QS, Gu JL, Du LQ, Jia LL, Qin LL, Wang Y, Fan FY. ShRNA-mediated Ku80 gene silencing inhibits cell proliferation and sensitizes to gamma-radiation and mitomycin C-induced apoptosis in esophageal squamous cell carcinoma lines. *J Radiat Res (Tokyo)* 2008;49:399-407.
21. Nimura Y, Kawata T, Uzawa K, Okamura J, Liu C, Saito M, Shimada H, Seki N, Nakagawara A, Ito H, Ochiai T, Tanzawa H. Silencing Ku80 using small interfering RNA enhanced radiation sensitivity in vitro and in vivo. *Int J Oncol* 2007;30:1477-1484.
22. Ross CD, Lim CU, Fox MH. Assay to measure CD59 mutations in CHO A(L) cells using flow cytometry. *Cytometry A* 2005;66:85-90.

23. French CT, Ross CD, Keysar SB, Joshi DD, Lim CU, Fox MH. Comparison of the mutagenic potential of 17 physical and chemical agents analyzed by the flow cytometry mutation assay. *Mutat Res* 2006;602:14-25.
24. Sega GA. A review of the genetic effects of ethyl methanesulfonate. *Mutat Res* 1984;134:113-142.
25. Keysar SB, Fox MH. Kinetics of CHO AL mutant expression after treatment with radiation, EMS and asbestos. *Cytometry A* 2009;
26. French CA, Massons J, Griffin CS, O'Regan P, West SC, Thacker J. Role of mammalian RAD51L2 (RAD51C) in recombination and genetic stability. *The Journal of Biological Chemistry* 2002;277:19322-19330.
27. Chen F, Nastasi A, Shen Z, Brenneman M, Crissman H, Chen DJ. Cell cycle-dependent protein expression of mammalian homologs of yeast DNA double-strand break repair genes Rad51 and Rad52. *Mutat Res* 1997;384:205-211.
28. Abbondandolo A, Dogliotti E, Lohman PH, Berends F. Molecular dosimetry of DNA damage caused by alkylation. I. Single-strand breaks induced by ethylating agents in cultured mammalian cells in relation to survival. *Mutat Res* 1982;92:361-377.
29. Rockwood LD, Nussenzweig A, Janz S. Paradoxical decrease in mutant frequencies and chromosomal rearrangements in a transgenic lacZ reporter gene in Ku80 null mice deficient in DNA double strand break repair. *Mutat Res* 2003;529:51-58.
30. Zhou BB, Elledge SJ. The DNA damage response: putting checkpoints in perspective. *Nature* 2000;408:433-439.
31. Iliakis G, Wang Y, Guan J, Wang H. DNA damage checkpoint control in cells exposed to ionizing radiation. *Oncogene* 2003;22:5834-5847.
32. Tourriere H, Pasero P. Maintenance of fork integrity at damaged DNA and natural pause sites. *DNA Repair (Amst)* 2007;6:900-913.
33. Rampakakis E, Di Paola D, Zannis-Hadjopoulos M. Ku is involved in cell growth, DNA replication and G1-S transition. *J Cell Sci* 2008;121:590-600.
34. Rogakou EP, Pilch DR, Orr AH, Ivanova VS, Bonner WM. DNA double-stranded breaks induce histone H2AX phosphorylation on serine 139. *J Biol Chem* 1998;273:5858-5868.
35. Staszewski O, Nikolova T, Kaina B. Kinetics of gamma-H2AX focus formation upon treatment of cells with UV light and alkylating agents. *Environ Mol Mutagen* 2008;49:734-740.

36. Oph, V, Zdzienicka MZ, Vrieling H, Lohman PH, van Zeeland AA. Molecular analysis of ethyl methanesulfonate-induced mutations at the hprt gene in the ethyl methanesulfonate-sensitive Chinese hamster cell line EM-C11 and its parental line CHO9. *Cancer Res* 1994;54:3001-3006.
37. Kaina B, Fritz G, Coquerelle T. Contribution of O6-alkylguanine and N-alkylpurines to the formation of sister chromatid exchanges, chromosomal aberrations, and gene mutations: new insights gained from studies of genetically engineered mammalian cell lines. *Environ Mol Mutagen* 1993;22:283-292.
38. Kaina B. Critical steps in alkylation-induced aberration formation. *Mutat Res* 1998;404:119-124.
39. Nagasawa H, Wilson PF, Chen DJ, Thompson LH, Bedford JS, Little JB. Low doses of alpha particles do not induce sister chromatid exchanges in bystander Chinese hamster cells defective in homologous recombination. *DNA Repair (Amst)* 2008;7:515-522.
40. Ferguson DO, Sekiguchi JM, Chang S, Frank KM, Gao Y, DePinho RA, Alt FW. The nonhomologous end-joining pathway of DNA repair is required for genomic stability and the suppression of translocations. *Proc Natl Acad Sci U S A* 2000;97:6630-6633.
41. Difilippantonio MJ, Zhu J, Chen HT, Meffre E, Nussenzweig MC, Max EE, Ried T, Nussenzweig A. DNA repair protein Ku80 suppresses chromosomal aberrations and malignant transformation. *Nature* 2000;404:510-514.

CHAPTER 6

CONCLUSIONS

Research Overview

The major role of genetic mutations in the initiation and progression of cancer has been widely reported (1,2), placing great importance on quantifying the mutagenic potential of compounds to which the population is exposed (3,4). In Chapter 1 I described several traditional mutation assays that have been used to evaluate the genotoxicity of hundreds of physical and chemical agents. The capabilities of these assays to sensitively measure mutagenesis have not been limited to genotoxicity testing but have also been used in novel investigations into the adaptive response, the bystander effect and DNA repair (5-7).

The progression of mutation assays from bacteria to mammalian cells has improved the relationship between the measured genotoxicity and the response an agent will likely generate in humans. Ross *et al.* (8) adapted the CHO A_L cell line, previously used in the complement mediated cytotoxicity assay, to measure mutagenesis by flow cytometry. Other groups have independently developed similar flow based assays but have not investigated the kinetics of CD59 mutant expression or the definition of the

mutant region in depth (9-11). The FCMA decreased the amount of time needed to test the genotoxicity of an agent and measured significant mutant fractions generated by a wide range of compounds (12). We have also reported the ability to rapidly generate mutant spectra for γ -rays of mutations up to the size of a large deletion that encompasses nearly the entire length of chromosome 11 using multi-parameter flow cytometry (13). However, to fully characterize this ability, agents that generate different types of DNA damage also had to be assayed.

The speed and sensitivity of the FCMA makes it a great candidate for research in a variety of fields using mutagenesis as an endpoint. The kinetics of CD59 expression in CHO A_L cells has previously been investigated (14). However, the kinetics of mutant expression in the FCMA must be fully clarified prior to its use in novel studies. In Chapter 2 I investigated in detail the kinetics of the expression of mutated *CD59* after treatment with EMS, asbestos and radiation. In clonogenic mutation assays treated cells are consistently challenged on the same day and mutant fractions remain stable over time (15). In these respects the FMCA differs slightly in that mutant expression for all agents tested occurs maximally between days 6 and 12 (12), and after peak expression mutant fractions decreased to a stable plateau.

To investigate peak mutant expression, I analyzed variations in cell proliferation and cell survival. T_{pot} values for cells treated with EMS and asbestos and the percentage of cells in G2 phase after irradiation returned to control levels within three days post treatment. Since peak expression occurred no earlier than day 6 for all agents tested to date, cell cycle changes are not likely the foremost source for variation in mutant expression. However, clonogenic survival was found to return nearly to control levels by

the day of peak expression (EMS, asbestos, MNNG) or shortly thereafter (γ -rays). From this it can be concluded that the efficient measurement of *CD59*⁻ mutants requires a sufficient time for the optimal expression of the mutated *CD59* phenotype, as well as to allow for the loss of dying cells from the population.

Next, I examined the mechanisms that cause the mutant fraction in a treated population to decrease after the peak day of expression to a stable plateau. The working hypothesis was that *CD59*⁻ cells are preferentially lost from the population due to retarded growth and/or cell death. After treatment with EMS and radiation, the surviving fraction of cells sorted from the mutant region on the peak day of expression was ~50% of cells sorted from the positive peak of the same population. Interestingly, there was no difference in survival between mutants and non-mutants one month after treatment, implying that many *CD59*⁻ cells on the peak day of expression are actually dead or in the process of dying. Also, when EMS generated *CD59*⁻ clonal cells were mixed with *CD59*⁺ cells the *CD59* mutants were exponentially lost from population. Therefore, the decrease in mutant fraction after the peak day of expression can be attributed to a combination of the inclusion on the peak day of expression of clonogenically dead *CD59*⁻ cells and slowed mutant growth. Slow mutant growth has been observed in other assays (16), but since most of chromosome 11 is not essential for growth or survival, this was not expected to occur in the CHO A_L cells while selecting for mutations in *CD59*. With the current information on mutant expression kinetics it is completely reasonable to report all *CD59*⁻ cells on the peak day of mutant expression as the mutant fraction. Though all cells are not clonogenically viable we do measure DNA damage resulting in the loss of the *CD59* surface protein, which is also a result of the genotoxicity of an agent.

In Chapter 3 I generated mutant spectra for EMS and simultaneously attempted to clarify the definition of the gating region of mutants in the FCMA. Clonal populations were sorted from CD59 mutant regions following EMS treatment, and the stability of CD59 fluorescence over time was measured. This was done to determine whether cells scored as mutants were truly negative for CD59 or in a transient stage of expression. Fluorescence, including intermediate levels, remained stable with repeated analysis over several weeks, with fluorescence intensity closely related to the sorting region. This contradicts results for clonal populations sorted from CD59⁻ negative regions after irradiation; these clones initially had intermediate CD59 fluorescence but were consistently positive or negative when stained at a later date (14). The differing results were not surprising because radiation often generates large deletions that would result in the complete loss of *CD59*; in contrast EMS would be expected to generate point mutations and intragenic deletions, allowing for expression of a mutated protein and intermediate staining. For example, point mutations and small intragenic deletions could result in conformational changes in the CD59 protein and in turn the affinity of the antibodies used for detection.

We have previously used flow cytometry to generate mutant spectra for CHO A_L cells treated with ionizing radiation (13), which was validated by simultaneously using a standard PCR method (6,17). As expected, radiation predominantly induced large deletions ranging from several Mb to nearly the entire length of chromosome 11 (~150 Mb). I generated mutant spectra following EMS treatment by analyzing clonal populations sorted from 3 regions that had intermediate levels of CD59 expression. Most sorted cells were determined to be negative for CD59, but a significant fraction appeared

to be mutated in a GPI linkage gene as determined by analysis with FLAER (18). The lack of GPI is likely caused by a single mutation of the X-linked *pigA* gene that encodes an essential biosynthesis protein (19). In comparison to radiation, EMS generates small mutations, and a much larger fraction of the total mutants are GPI negative. This is easily explained by the observation that large deletions of *pigA* may encompass essential hamster genes while smaller intragenic mutations would have little to no effect. Finally, we confirmed that the 1% mutant region was a conservative estimate (14,20) and that a 10% mutant region should be used in the future, in order to include a greater proportion of the mutants.

In Chapter 4 I used the FCMA to study the induction of mutations by culturing cells under severely hypoxic conditions. Previous studies have determined that the stress induced from hypoxia and the subsequent reoxygenation can generate DNA damage and mutations (21,22). The increase in mutagenesis has been attributed to the production of ROS (23,24) and the suppression of DNA repair pathways in cells under hypoxic stress (25,26). A 24 hr hypoxic treatment generated significant mutant fractions in both the CHO A_L complement mediated assay and the FCMA. Survival characteristics of cells treated with hypoxia were similar to those treated with other known mutagens, as described in Chapter 2. Survival of the treated population did not return to control levels until the peak day of expression, and survival of cells sorted from the mutant region on the peak day was significantly less than the cells sorted from the positive peak of the same population.

Mutant spectra were generated for background and hypoxia treated cells using the same flow cytometry method as Chapter 3. Hypoxia mutations were not significantly

different from background and consisted primarily of large deletions encompassing at least two markers. Hypoxic stress would be expected to generate large quantities of oxidative damage resulting in point mutations up to deletions (22). Reducing background levels prior to treatment and increasing the number of mutant clones analyzed would result in a better picture of the lesions predominantly generated in CHO A_L cells by hypoxia.

The radical scavenger DMSO was used to investigate the probable link between hypoxia induced ROS and mutations (21). The presence of low levels of DMSO during and after treatment was found to significantly increase cell survival and decrease mutagenesis using the FCMA. These results strongly support the mechanism that hypoxia induced DNA damage is at least partially a consequence of ROS interactions. However, future studies will have to be conducted to determine the manner in which the radicals are produced.

In Chapter 5 I discussed the relationship between DNA repair proteins, the induction of mutations, consequent changes to the cell cycle and the effects of these on the proliferation of CHO cells. I used short interfering RNAs (siRNA) to significantly decrease the protein levels of Ku80 and Rad51C at the time of treatment with radiation or EMS. These proteins were chosen for their significant roles in NHEJ and HRR respectively. EMS and γ -rays were chosen for this study due to the differences in the types of DNA damage they generate and because they have previously been studied in depth.

Both knockdowns resulted in increased sensitivity to IR and Rad51C silencing resulted in nearly a fivefold increase in cell killing after EMS treatment while Ku80 KD

had little effect, which has been observed by several groups previously (27-30). In Chapter 2 I investigated the cell cycle kinetics of CHO A_L cells after irradiation and EMS treatment and in Chapter 5 I found that following knockdown of Ku80, cell cycle characteristics are not significantly altered in cells treated with radiation or EMS. Interestingly, EMS generated a significant build-up of G2 phase cells by six hours after treatment and further increased by 18 hours. These results suggest that Rad51C plays an important role in the repair of the DNA damage generated by EMS that has previously been determined to be predominantly alkylations and single-strand breaks. Next I investigated silencing of these proteins and the effects on mutant yield in the FCMA. Knockdown of Rad51C did not alter the mutant yield generated by these agents. HRR is not predominantly used to repair radiation damage and increased killing by EMS may have negated any net change in the mutant yield. However, silencing of Ku80 significantly reduced the mutant yield after treatment with EMS, which may be due to DSBs generated by alkylation damage during replication being repaired by high fidelity HRR rather than NHEJ. Finally, these results demonstrate the ability of the FCMA to be used outside conventional genotoxicity testing.

Strengths and Limitations of the FCMA

We have found that mutagens often generate larger mutant yields in the FCMA when compared to other mammalian assays, most interestingly the CHO A_L complement mediated cytotoxicity assay (20). However, many of the CD59⁻ cells measured on the peak day of mutant expression would likely not form colonies in the complement cytotoxicity assay meaning the FCMA is measuring mutations encompassing the *CD59* gene, but damage to the cells is too severe for clonogenic survival (colonies >50 cells)

(31,32). When using the assay alone to assess genotoxicity the complication of the variation of peak expression can be overcome by analyzing treated cells on days 6, 9 and 12 to get within a day or two of the peak day.

The variation in peak expression and the subsequent loss of *CD59* mutants contribute to the complexity of using the FCMA as an endpoint in novel studies, such as DNA repair. For example, by treating cells with siRNAs to knockdown expression of DNA repair proteins prior to genotoxic insult, the ability of the cells to express mutated *CD59* proteins may be altered, in turn changing the peak day of mutant expression. If necessary this can also be compensated for by analyzing cells a day prior to and after the expected peak day.

By analyzing clonal populations sorted from *CD59*⁻ regions after treatment with EMS I have confirmed previous results that support setting the mutant gating region of the FCMA at 10% of the positive peak (Fig. 1). By using the 10% region the variation of mutant expression between experiments is reduced. Also, the 10% region reduces the effect of variation in background mutants over time on the mutant fraction, especially in the case of low responders like asbestos. However, even using the conservative estimate of 1%, the mutant yield in the FCMA (>600 mutants / 10⁵ cells, 8 mM) (12) is greater than 12 fold higher than the *hprt* assay (~50 mutants / 10⁵ cells) at a higher dose (10 mM) (33). Significantly lower responses have also been found in the MLA, TK6 and *LacZ* phage assays (34-36).

I have also confirmed that a portion of *CD59* negative cells are actually mutated in an X-linked GPI biosynthesis gene rather than the *CD59* gene. Since two separate mutations can lead to the same phenotype this makes the FCMA slightly more complex.

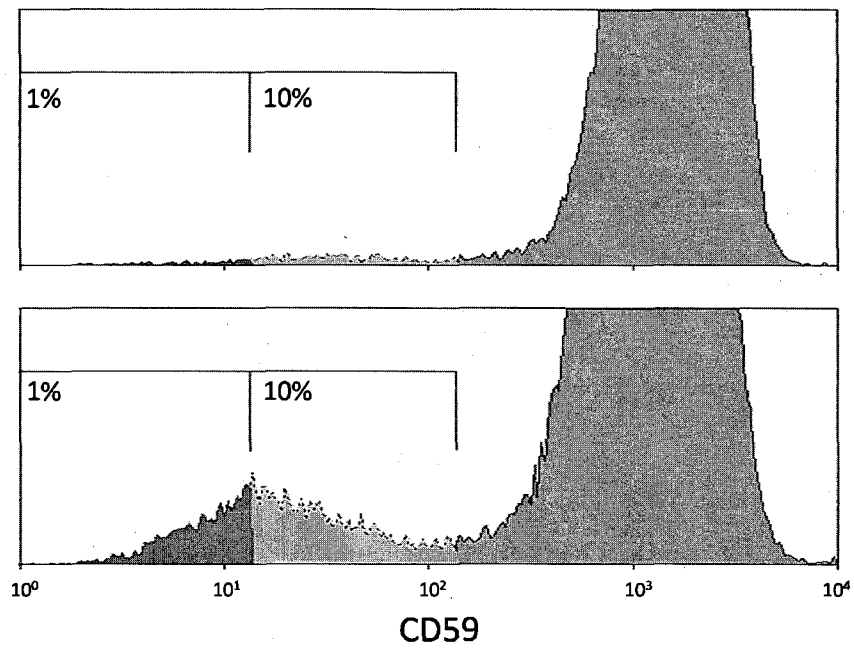


Figure 1. Example histograms defining the 1% and 10% gating regions used in the FCMA for (Top) untreated control cells and (Bottom) cells 9 days after treatment with 8 mM EMS

However, it is interesting to note that the ratio between *CD59* mutations and GPI mutations could be investigated for different genotoxic agents. We have already determined that GPI mutants are rare after treatment with IR but make up a large percentage of EMS generated *CD59*⁻ cells since large deletions of hamster chromosomes would be fatal but small intragenic mutations would have no effect.

Future Directions

To further investigate the use of the CHO A_L cell line in the FCMA it would be interesting to look in depth into why some cells mutated in the *CD59* gene grow slower than WT cells. Also, it would be important to explore any relationship between the size/type of mutation and the numerical difference between the mutant fraction on the peak day of expression and the mutant fraction at the following plateau phase. In Chapter 2, we show that the ratio of peak MF:plateau MF is ~3:1 and 5:1 for EMS and radiation respectively. Future research may result in a relationship between the amount of DNA damage, or non-clonogenically viable *CD59*⁻ cells, and stable mutations induced by different agents. If the plateau consists of normally growing stable *CD59* negative cells the FCMA could be calibrated to the CHO A_L clonogenic assay by setting the mutant region at the same mutant yield as the complement assay.

Reference List

1. Hoeijmakers JH. Genome maintenance mechanisms for preventing cancer. *Nature* 2001;411:366-374.
2. Hall EJ: Radiation Carcinogenesis. In: *Radiobiology for the Radiologist*, 5th ed. Edition, John J, Sutton P, and Marino D (eds). Lippincott, Williams & Wilkins, Philadelphia, 2000, pp. 144-165.
3. Thybaud V, Aardema M, Clements J, Dearfield K, Galloway S, Hayashi M, Jacobson-Kram D, Kirkland D, MacGregor JT, Marzin D, Ohyama W, Schuler M, Suzuki H, Zeiger E. Strategy for genotoxicity testing: hazard identification and risk assessment in relation to in vitro testing. *Mutat Res* 2007;627:41-58.
4. Kirkland D, Aardema M, Henderson L, Muller L. Evaluation of the ability of a battery of three in vitro genotoxicity tests to discriminate rodent carcinogens and non-carcinogens I. Sensitivity, specificity and relative predictivity. *Mutation Research* 2005;584:1-256.
5. Zhang Y, Lim CU, Williams ES, Zhou J, Zhang Q, Fox MH, Bailey SM, Liber HL. NBS1 knockdown by small interfering RNA increases ionizing radiation mutagenesis and telomere association in human cells. *Cancer Res* 2005;65:5544-5553.
6. Zhou H, Randers-Pehrson G, Waldren CA, Vannais DB, Hall EJ, Hei TK. Induction of a bystander mutagenic effect of alpha particles in mammalian cells. *Proc Natl Acad Sci* 2000;97:2099-2104.
7. Waldren CA. Adaptive response induced by low levels of radiation. Summary and comments. *Hum Exp Toxicol* 1999;18:452-453.
8. Ross CD, Lim CU, Fox MH. Assay to measure CD59 mutations in CHO A(L) cells using flow cytometry. *Cytometry A* 2005;66:85-90.
9. Wedemeyer N, Greve B, Uthe D, Potter T, Denklau D, Severin E, Hacker-Klom U, Kohnlein W, Gohde W. Frequency of CD59 mutations induced in human-hamster hybrid A(L) cells by low-dose X-irradiation. *Mutat Res* 2001;473:73-84.
10. Zhou H, Xu A, Gillispie JA, Waldren CA, Hei TK. Quantification of CD59-mutants in human-hamster hybrid (AL) cells by flow cytometry. *Mutat Res* 2006;594:113-119.
11. Göhde W, Uthe D, Wedemeyer N, Severin E, Greif K, Schlegel D, Brede HJ, Kohnlein W. Mutagenic effect of low energy neutrons on human chromosome 11. *International Journal of Radiation Biology* 2005;79:911-918.

12. French CT, Ross CD, Keysar SB, Joshi DD, Lim CU, Fox MH. Comparison of the mutagenic potential of 17 physical and chemical agents analyzed by the flow cytometry mutation assay. *Mutat Res* 2006;602:14-25.
13. Ross CD, French CT, Keysar SB, Fox MH. Mutant spectra of irradiated CHO A(L) cells determined with multiple markers analyzed by flow cytometry. *Mutat Res* 2007;624:61-70.
14. Ross CD, Fox MH. Multiparameter Analysis of CHO A(L) Mutant Populations Sorted on CD59 Expression after Gamma Irradiation. *Radiat Res* 2008;170:628-637.
15. Liber HL, Thilly WG. Mutation assay at the thymidine kinase locus in diploid human lymphoblasts. *Mutat Res* 1982;94:467-485.
16. Moore MM, Clive D, Hozier JC, Howard BE, Batson AG, Turner NT, Sawyer J. Analysis of trifluorothymidine-resistant (TFTr) mutants of L5178Y/TK+/- mouse lymphoma cells. *Mutat Res* 1985;151:161-174.
17. Kraemer SM, Kronenberg A, Ueno A, Waldren CA. Measuring the spectrum of mutation induced by nitrogen ions and protons in the human-hamster hybrid cell line A(L)C. *Radiat Res* 2000;153:743-751.
18. Brodsky RA, Mukhina GL, Li S, Nelson KL, Chiurazzi PL, Buckley JT, Borowitz MJ. Improved detection and characterization of paroxysmal nocturnal hemoglobinuria using fluorescent aerolysin. *Am J Clin Pathol* 2000;114:459-466.
19. Miyata T, Takeda J, Iida Y, Yamada N, Inoue N, Takahashi M, Maeda K, Kitani T, Kinoshita T. The cloning of PIG-A, a component in the early step of GPI-anchor biosynthesis. *Science* 1993;259:1318-1320.
20. Ross, C. D. Development of a mammalian cell mutation assay based on flow cytometry and its use in analyzing mutations induced by ionizing radiation and chemicals. 2006. Colorado State University.
21. Bristow RG, Hill RP. Hypoxia and metabolism. Hypoxia, DNA repair and genetic instability. *Nat Rev Cancer* 2008;8:180-192.
22. Reynolds TY, Rockwell S, Glazer PM. Genetic instability induced by the tumor microenvironment. *Cancer Res* 1996;56:5754-5757.
23. Moller P, Loft S, Lundby C, Olsen NV. Acute hypoxia and hypoxic exercise induce DNA strand breaks and oxidative DNA damage in humans. *FASEB J* 2001;15:1181-1186.

24. Risom L, Lundby C, Thomsen JJ, Mikkelsen L, Loft S, Friis G, Moller P. Acute hypoxia and reoxygenation-induced DNA oxidation in human mononuclear blood cells. *Mutat Res* 2007;625:125-133.
25. Bindra RS, Schaffer PJ, Meng A, Woo J, Maseide K, Roth ME, Lizardi P, Hedley DW, Bristow RG, Glazer PM. Down-regulation of Rad51 and decreased homologous recombination in hypoxic cancer cells. *Molecular and Cellular Biology* 2004;24:8504-8518.
26. Meng AX, Jalali F, Cuddihy A, Chan N, Bindra RS, Glazer PM, Bristow RG. Hypoxia down-regulates DNA double strand break repair gene expression in prostate cancer cells. *Radiother Oncol* 2005;76:168-176.
27. Nimura Y, Kawata T, Uzawa K, Okamura J, Liu C, Saito M, Shimada H, Seki N, Nakagawara A, Ito H, Ochiai T, Tanzawa H. Silencing Ku80 using small interfering RNA enhanced radiation sensitivity in vitro and in vivo. *Int J Oncol* 2007;30:1477-1484.
28. Yang QS, Gu JL, Du LQ, Jia LL, Qin LL, Wang Y, Fan FY. ShRNA-mediated Ku80 gene silencing inhibits cell proliferation and sensitizes to gamma-radiation and mitomycin C-induced apoptosis in esophageal squamous cell carcinoma lines. *J Radiat Res (Tokyo)* 2008;49:399-407.
29. Takata M, Sasaki MS, Tachiiri S, Fukushima T, Sonoda E, Schild D, Thompson LH, Takeda S. Chromosome instability and defective recombinational repair in knockout mutants of the five Rad51 paralogs. *Molecular and Cellular Biology* 2001;21:2858-2866.
30. Godthelp BC, Wiegant WW, van Duijn-Goedhart A, Scharer OD, et.al.. Mammalian Rad51C contributes to DNA cross-link resistance, sister chromatid cohesion and genomic stability. *Nucleic Acids Research* 2002;30:2172-2182.
31. Waldren C, Jones C, Puck TT. Measurement of mutagenesis in mammalian cells. *Proc Natl Acad Sci U S A* 1979;76:1358-1362.
32. Hei TK, Wu L, Liu S, Vannais DB, Waldren CA, Randers-Pehrson G. Mutagenic effects of a single and an exact number of alpha particles in mammalian cells. *Proc Natl Acad Sci* 1997;94:3765-3770.
33. Op h, V, Zdzienicka MZ, Vrieling H, Lohman PH, van Zeeland AA. Molecular analysis of ethyl methanesulfonate-induced mutations at the hprt gene in the ethyl methanesulfonate-sensitive Chinese hamster cell line EM-C11 and its parental line CHO9. *Cancer Res* 1994;54:3001-3006.
34. Davies MJ, Phillips BJ, Rumsby PC. Molecular analysis of mutations at the tk locus of L5178Y mouse-lymphoma cells induced by ethyl

methanesulphonate and mitomycin C. *Mutation Research* 1993;290:145-153.

35. Amundson SA, Liber HL. A comparison of induced mutation at homologous alleles of the tk locus in human cells. *Mutat Res* 1991;247:19-27.
36. Mientjes EJ, Luiten-Schuite A, van der WE, Borsboom Y, Bergmans A, Berends F, Lohman PH, Baan RA, van Delft JH. DNA adducts, mutant frequencies, and mutation spectra in various organs of lambda lacZ mice exposed to ethylating agents. *Environ Mol Mutagen* 1998;31:18-31.